A BEAM STEERING, BROADBAND MICROSTRIP ANTENNA FOR NON-CONTACT VITAL SIGN RADAR DETECTION

By

ZIVIN PARK

A DISSERTATION PRESENTED TO THE GRADUATE SCHOOL
OF THE UNIVERSITY OF FLORIDA IN PARTIAL FULFILLMENT
OF THE REQUIREMENTS FOR THE DEGREE OF
DOCTOR OF PHILOSOPHY

UNIVERSITY OF FLORIDA

2011

To my father, mother, and grandmother, for their support and encouragement

ACKNOWLEDGMENTS

I would like to express my sincere gratitude to my advisor Dr. Jenshan Lin for his advice, encouragement, and mentoring throughout my PhD study. I would also like to thank Dr. Sheng Li, Dr. Huikai Xie, Dr. Changzhi Li, and Dr. Paul Holloway for their time and for being on my committee. I am also thankful to Dr. Lance Covert for his unconditional help when I first started antenna research and for his sincere friendship. Also, I am thankful to Dr. Changzhi Li, who is now one of my committee members, for showing me the epitome of being excellent in research, diligence, and his sincere friendship. I am also thankful to Dongha Shim for the technical advices, equipment, and his sincere friendship. I am thankful to all of the RFSOC group members for their technical support, guidance, and friendship. The antenna measurements performed by Yazid Yusuf under Dr. Xun Gong's research group at the University of Central Florida are greatly appreciated. I would like to thank my parents for their encouragement and unconditional support.

TABLE OF CONTENTS

page

LIST OF TABLES

LIST OF FIGURES

Abstract of Dissertation Presented to the Graduate School
of the University of Florida in Partial Fulfillment of the
Requirements for the Degree of Doctor of Philosophy

A BEAM STEERING, BROADBAND MICROSTRIP ANTENNA FOR NON-CONTACT VITAL SIGN RADAR DETECTION

By

Zivin Park

May 2011

Chair: Jenshan Lin
Major: Electrical and Computer Engineering

The non-contact vital sign radar detection system requires a development of the high gain, broadband, and beam steering patch antenna. The proposed design approach combines the advantages of the wideband antenna, the advantage of the parasitic patch, and the advantage of beam steering antennas within a single microstrip patch antenna. As a result, a 2.8–4.8 GHz beam steering broadband microstrip antenna was designed, fabricated, and measured. The proposed antenna can steer beam in broadband range (sampled at 3, 3.5, 4, and 4.5 GHz) by switching PIN diodes that connect stubs and a partial ground plane. Its broadband beam steering is suitable for a vital sign radar. The proposed antenna requires no array for beam steering but requires only two additional diodes. The wide frequency tuning range allows the radar system to be tuned for an optimum transmission frequency. In addition, effects of modifying the proposed antenna on the antenna characteristics such as reflection coefficient, radiation pattern, gain, or beam steering capability are investigated.

CHAPTER 1
MOTIVATION AND BACKGROUND INFORMATION

1.1 Motivation

Microwave Doppler radar has been used for detecting physiological movements. The radar transmits a radio frequency (RF), single-tone continuous-wave (CW) signal, which is reflected off a target and then demodulated in the receiver. This technique enables non-contact detection of vital signs of humans or animals from a distance away, without any sensor attached to the body [Li1].

A non-contact solution is desired for several reasons. First, unlike methods using electrodes, it does not cause discomfort in the subjects. Second, the reliability can be increased since the subject is unaware of the measurement. Last, the detector can be ideal for long-term, continuous-monitoring applications. Compared to either infrared or visible light, microwave has a greater penetration capability through the building materials [Li1]. Therefore, an antenna transmitting an RF signal can be used with the Microwave Doppler radar. In particular, a microstrip patch antenna is desired because of its easy integration with the sensor, i.e., integration on a same substrate.

Microstrip patch antennas are low profile, conformable to planar and non-planar surfaces, simple, and inexpensive to manufacture using modern printed-circuit technology. It is mechanically robust when mounted on rigid surfaces, compatible with Monolithic Microwave Integrated Circuits (MMIC) designs, and when the particular patch shape and mode are selected, they are very versatile in terms of resonant frequency, polarization, pattern, and impedance. In addition, by adding loads between the patch and the ground plane, such as pins and varactor diodes, impedance, polarization, and pattern can be designed [Balanis].

For the specific application such as the aforementioned non-contact detection of vital signs, a microstrip patch antenna to be integrated with the sensor needs to have a high gain, broad bandwidth and a size within a limited area.

1.2 Requirements

The main criteria of the antenna design for this vital sign detector application can be summarized as follows. First, the patch antenna should cover the frequency range of 4.4-6.7 GHz, which is the full operating range of the portable radar designed [Li2]. The optimal carrier frequency could be as high as in the lower region of Ka-band (26.5-40 GHz) for people with weak physiological movement. However, the operating frequency can be limited by the radar, which uses low-cost components. Also, lower broadband range can be desired because of larger penetration depth, better vital sign detection when the subject has large physiological movement, and a smaller FR-4 loss. Second, the patch antenna must have a high directivity. Third, the isolation between the transmitting and receiving antennas should be good. Fourth, the patch antenna should fit within an area of 3 inch by 3 inch. Last, broadband beam steering is desired because of its use for radar application.

1.3 Background Information

1.3.1 Yagi Dipole Antenna

Figure 1-1 shows a layout of a Yagi dipole antenna. The basic Yagi–Uda array consists of a parallel set of linear dipole radiators. The left-most element is typically slightly larger than resonant length and is called a reflector. The next element is a dipole element with a feed line. The right-most elements are typically slightly less than resonant length and are called directors. Spacing between elements is typically 0.2–0.3 λ. In this way, it is rather easy to achieve gains ranging 10–20 dB. This is in contrast to

a single dipole element, having a gain of 2.2 dB. The gain of the array increases with the number of directors that are used. Adding more reflector elements to the left of the feed has little effect on the array, since radiation is predominantly along the director elements [Pozar1].

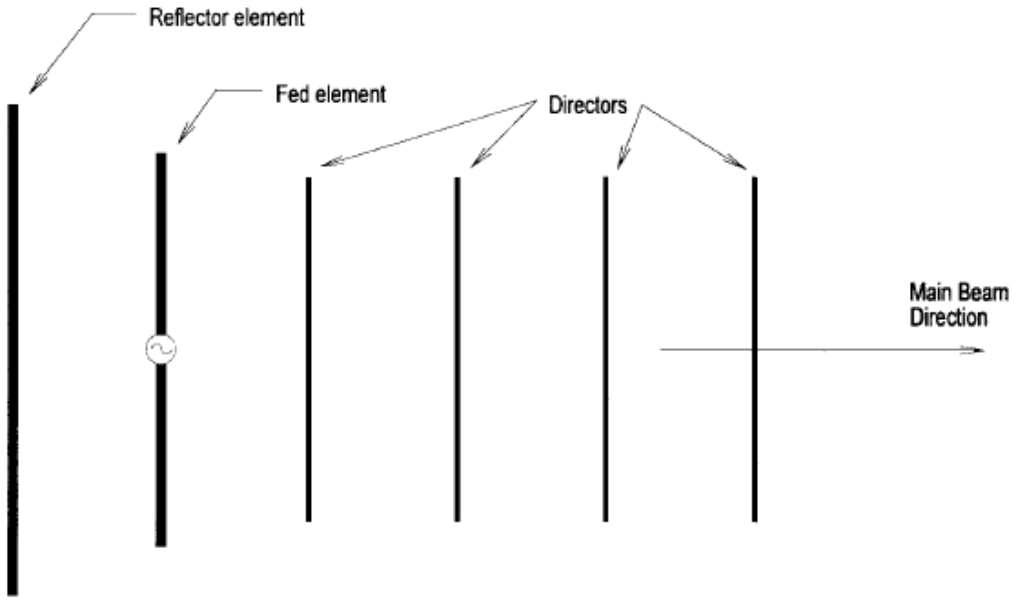

Figure 1-1. Geometry of the Yagi–Uda dipole array antenna [Pozar1]

An increase in the number of directors increases the directivity of the array, although this increase reaches the point of diminishing returns after about 10–15 director elements.

1.3.2 Coupling Mechanism of Patch Antenna

Mutual coupling is primarily attributed to the fields that exist along the air-dielectric interface. The fields can be expressed as Equation 1-1:

Fields = Space waves (~ 1/r) + Higher order waves (~ $1/(r^2)$) +

Surface wave (~ $1/(\sqrt{r})$) + Leaky waves (~ exp (-λ•r) / ($\sqrt{r}$)) (1-1)

Space waves and higher order waves are dominant for small spacing and surface wave is dominant for large spacing [Balanis].

In addition, a theoretical investigation of the rectangular microstrip antenna element regarding mutual conductance between two microstrip patches was reported. The mutual conductance between two patches can be expressed as Equation 1-2 [Derneryd]:

$$G_{12} = \frac{1}{\pi} \bullet \sqrt{\frac{e}{\mu}} \int_0^{\pi} \frac{\sin^2\left(\frac{\pi\omega}{\lambda} \bullet \cos\theta\right)}{\cos^2\theta} \bullet \sin^3\theta \bullet \left\{ \begin{array}{l} 2 \bullet J_0\left(\frac{\chi}{\lambda} \bullet 2\pi \bullet \sin\theta\right) + J_0\left(\frac{\chi + L}{\lambda} \bullet 2\pi \bullet \sin\theta\right) \\ + J_0\left(\frac{\chi - L}{\lambda} \bullet 2\pi \bullet \sin\theta\right) \end{array} \right\} d\theta \quad (1\text{-}2)$$

The χ represents a center to center separation between patches and J is Bessel function. This equation is shown as graph in Figure 1-2.

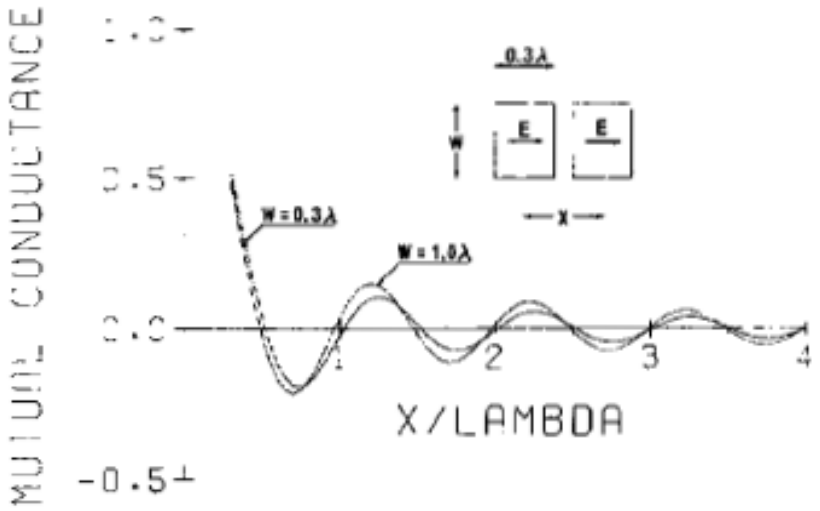

Figure 1-2. Mutual conductance between two parasitic patches [Derneryd]

As shown in Figure 1-2, the mutual conductance between the patches decreases as the spacing between the patches increases.

The mutual conductance between elements can be seen as composed of conductances between the ends of one element and both ends of the other element. Calculations showed that the mutual conductance is higher along the E-plane than along the H-plane as shown in Figure 1-3 [Pozar2].

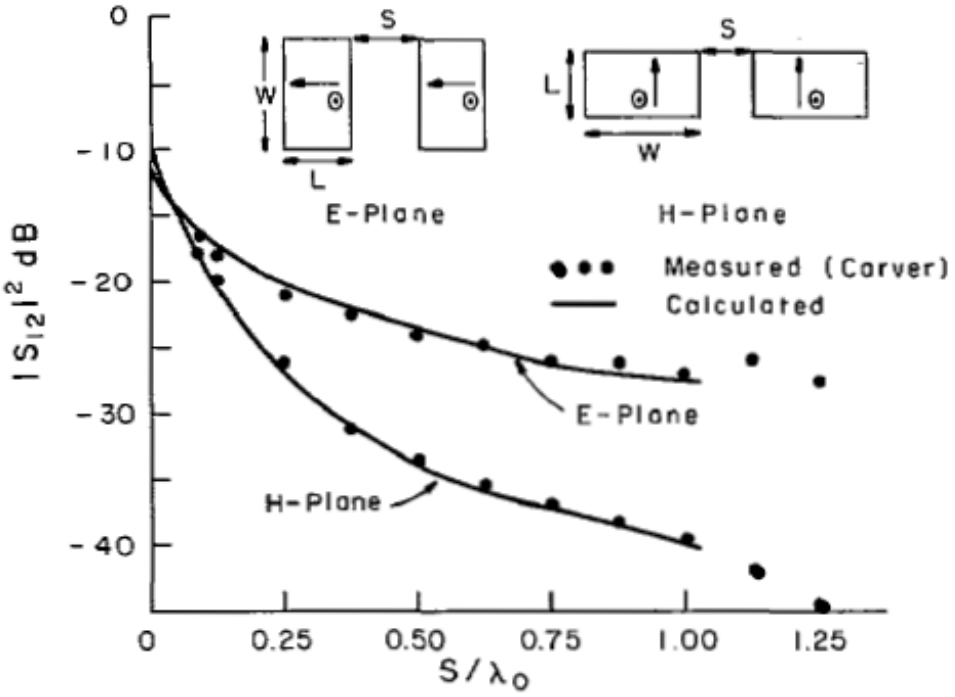

Figure 1-3. Mutual coupling between two coax fed microstrip antennas, for both E-plane and H-plane coupling [Pozar2]

In addition, for the coupling to occur, the dielectric constant of the substrate material can neither be too low nor too high. The width and length of a rectangular patch is inversely proportional to a square root of a dielectric constant of a substrate [Covert]. If the relative dielectric constant is very low (less than 1.5), the patch size becomes larger than 0.35 free-space wavelength and consequently the separation distance that is required can no longer be held. On the other hand, if the relative dielectric constant is

too high (more than 5), the patches will be very small and the gaps between patches become large in order to hold the required element separation [Huang2].

1.4 Summary

Motivations and requirements for the proposed antenna are discussed. As background information, Yagi dipole antenna and coupling mechanisms of microstrip patches are discussed.

CHAPTER 2
PROPOSED APPROACHES VS. EXISTING APPROACHES

2.1 Wideband Microstrip Antennas with a Partial Ground Plane

There have been many design approaches for wideband antennas using partial ground planes. A wideband patch antenna consisting of a rectangular patch with two steps, a single slot on the patch, and a partial ground plane was reported [Choi1]. A further modification of partial ground plane patch antenna was introduced by adding a bent stub on the radiating patch and stepping the ground plane. By inserting an inverted-U shaped slot on the circular patch, the antenna showed a band-rejection characteristic [Choi2]. The effects of ground plane dimensions on antenna performance such as gain, bandwidth and radiation pattern were investigated [Curto]. These wideband patch antennas operated approximately from 3 GHz to 12 GHz.

In detail, Figure 2-1 shows a layout of the wideband antenna example using a partial ground plane. This antenna shows a 3.2–12-GHz frequency range for VSWR < 2 with a maximum gain value of about 5dB [Choi1]. Figure 2-2 shows another example of wideband antenna using a partial ground plane [Choi2].

As seen in Figure 2-2, a bent slot and a bent stub are added to the radiating patch, and the ground plane is modified to have a stepped shape. These modifications gave additional characteristics to the basic wideband characteristics. This antenna shows a bandwidth ranging from 2.9 to 12.1 GHz for a VSWR < 2 with a maximum gain less than 4 dB [Choi2]. As a last example of the wideband antennas using a partial ground plane, Figure 2-3 is shown. In this example, by removing the substrate surrounding the radiating patch, impedance bandwidth was increased at the higher end to be 3.1 ~ 11.2

GHz. It was discovered that this antenna's bandwidth is dependent on the ground plane size.

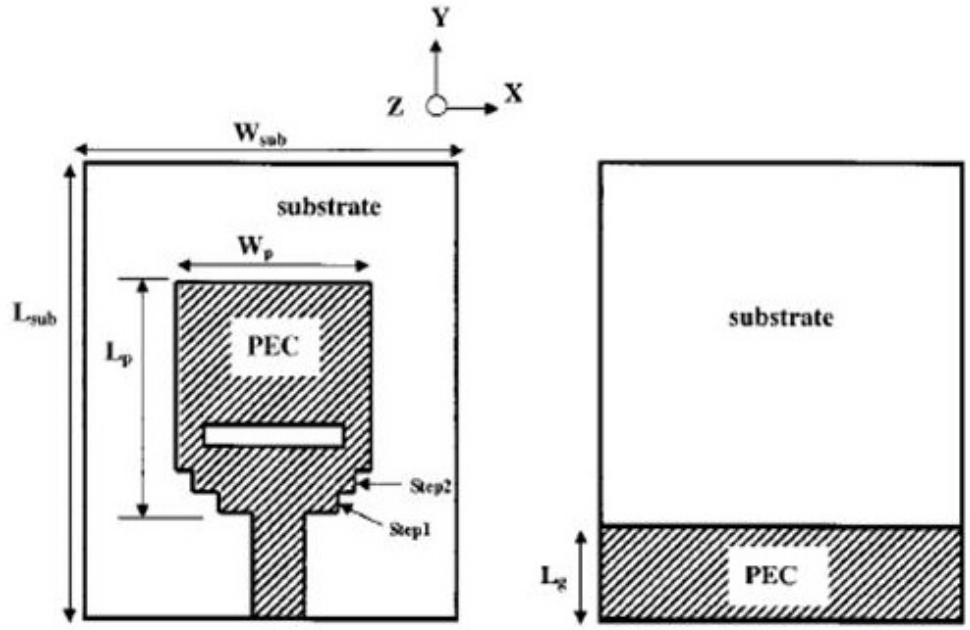

A B

Figure 2-1. An example of a wideband microstrip antenna with a partial ground plane: (A) front view (B) back view [Choi1]

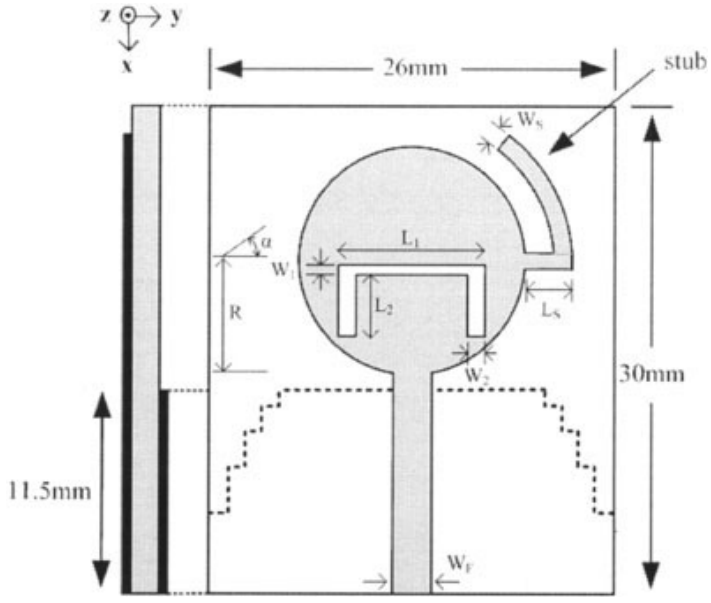

Figure 2-2. Another example of a wideband microstrip antenna with a partial ground plane [Choi2]

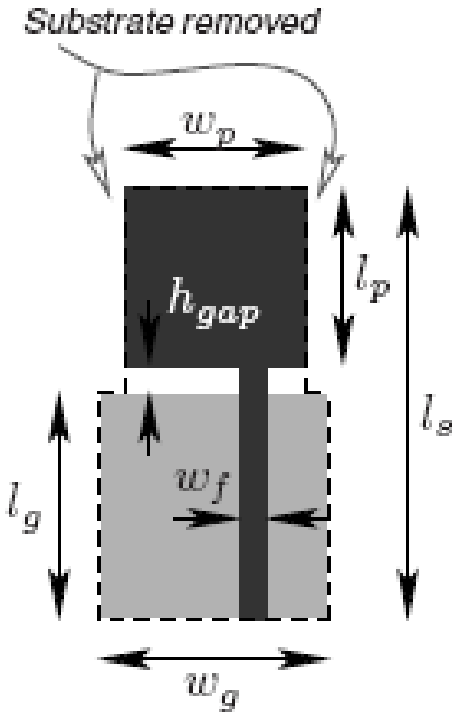

Figure 2-3. Yet another example of wideband microstrip antenna with a partial ground plane [Curto]

In particular, wide bandwidth is lost for a very narrow ground plane. In this case, the maximum gain remains below 5dB [Curto].

One common characteristic in all of these wideband antenna examples showed above is that they all demonstrate wideband characteristics by using the partial ground plane. Another characteristic common to all of these wideband patch antennas is that there is still room for improvement in directivity or gain value.

2.2 Microstrip Antennas using Parasitic Patches

There have been design approaches using parasitic patches to control the peak directivity or improve the bandwidth of microstrip antennas. The Yagi-antenna [Pozar1] concept was introduced to control the peak directivity. With parasitic director and reflector patches located on the same plane of the driven element, the peak directivity,

by the effect of mutual coupling, was tilted toward the end fire direction with peak gain of 8 dB [Huang1]. The antenna was later used in an array for mobile satellite applications [Huang2]. Figure 2-4 shows a microstrip antenna, which adopted the Yagi concept [Huang1].

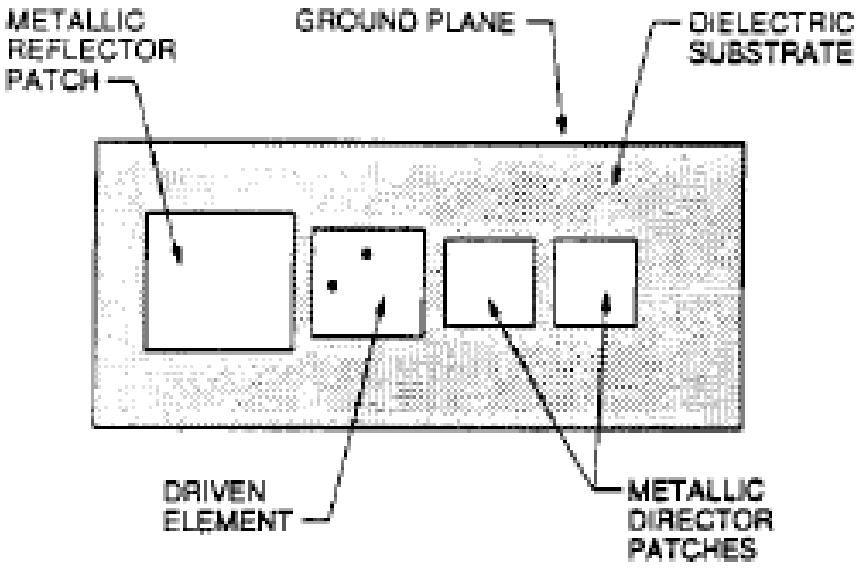

Figure 2-4. Geometry of the microstrip Yagi array antenna [Huang1]

It was shown that parasitic patches could be placed around a driven element to increase the gain of this single, driven element by several dBs. The configuration of the planar, microstrip, Yagi array was similar to that of a conventional dipole Yagi array. The dimensions and spacings between the microstrip driven element and reflectors were all designed based on the Yagi dipole array's design. Depending on the substrate thickness and dielectric constant, the dimension ratio of the reflector to the driven element was found experimentally to be between 1.1 and 1.3. The dimension ratio between the director and the driven element should be from 0.8 to 0.9. The distance between the centers of the reflector and the driven element is about 0.35 wavelengths, and the separation should be approximately 0.3 wavelengths between the director and

driven element. The driven element was coax fed. Three Yagi arrays having different dielectric constant and dimensions were experimented for operation at 6.9 GHz and 1.58 GHz. As a result, the peak directivity of the Yagi array was directed at 40 degrees from the broadside direction, and about 2.5 dB of higher peak directivity was achieved by the Yagi than the single patch [Huang1].

Four rows of the same microstrip Yagi antenna were used to achieve the MSAT (mobile satellite) required gain of 10 dB within the angular region between 20 ° and 60 ° elevations, as configured in Figure 2-5 [Huang2]. Antenna gain was measured at various elevation angles at 1552 MHz and 1654 MHz. The rows of Yagi antennas were however, mechanically steered.

One common characteristic found in the patch antennas with parasitic patches mentioned above is that all of the antennas show increased gain with tilted directivity using the parasitic patches. Another common characteristic is that both of the antennas operate over a very narrow band.

Parasitic patches were not only used for increasing gain, but also were used for increasing bandwidth. To improve the bandwidth, parasitic patches on all four edges including non-radiating edges were used to increase the impedance-matching bandwidth to 815 MHz [Kumar]. Figure 2-6 shows the improvement in bandwidth using multiple, gap-coupled patches. However, the maximum bandwidth still remained less than 1 GHz.

2.3 Beam Steering Patch Antennas

Beam-steerable antennas are widely used in areas such as radar and satellite communications. The beam steering can be performed by mechanical means or

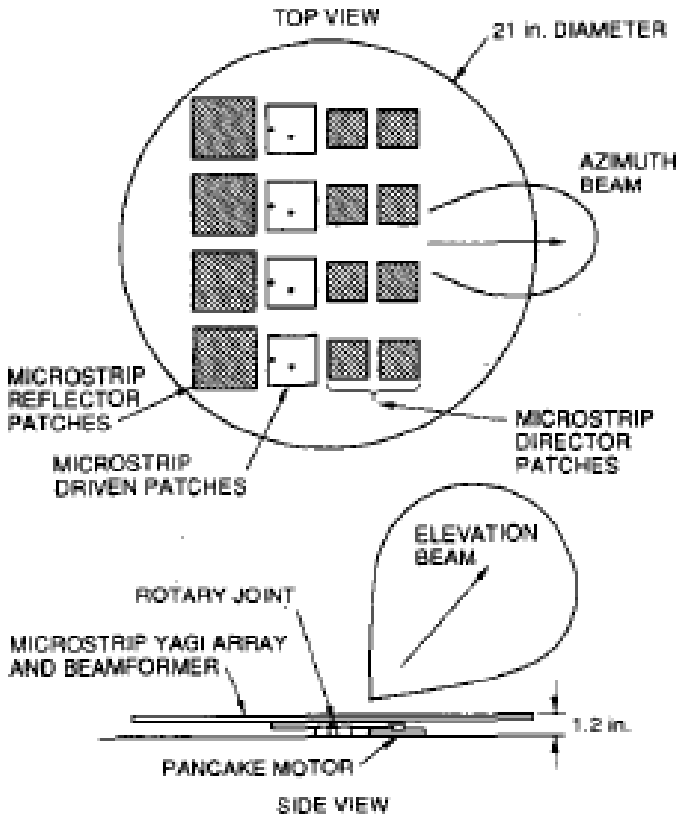

Figure 2-5. Microstrip Yagi array concept for MSAT application [Huang2]

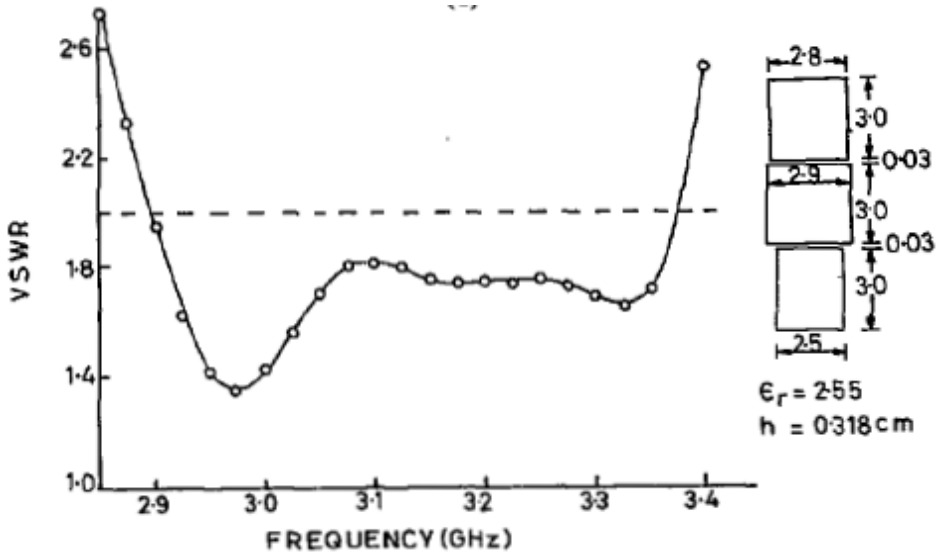

Figure 2-6. Improved bandwidth using parasitic patches [Kumar]

electronic means. As an example of the mechanical beam-steering antenna, four Yagi patch arrays were placed on a mechanically rotating platform which accomplishes

the functions of azimuth rotation by a thin pancake motor whose motion is controlled by a monopulse signal [Huang2]. The rotating platform was required to track a satellite. As another example of the mechanical beam-steering antenna, a mechanical reflect-array, which uses rotating circular disks immersed in a circularly polarized field was reported [Fusco]. However, in general, the electronic beam steering is preferred over the mechanical beam steering because the mechanical beam steering has disadvantages such as a complex and large mechanical structure, high power requirements, and slow orientation speed.

One of many examples of the patch antennas with electronic beam-steering capability is microstrip patch array with varactor-diode-based phase shifters between the elements [Andersson]. The phase shifters were adopted to give a fast response time. As another example of the patch antenna with electronic beam-steering capability, Ka-band microstrip patch antenna arrays with twelve elements were designed and feeding structures were used to radiate dual beams [Rodenbeck].

For the electronic beam steering, phased array has been the primary type. However, the phased array requires many elements such as additional circuit components including power dividers and phase shifters. Consequently, there have been approaches to minimize the complexity required for electronic beam steering. Recently, a concept termed electronically steerable passive array radiator (ESPAR) has been reported for achieving beam steering without the need of phase shifters. In ESPAR, passive radiators can be excited by a driven antenna through a mutual coupling between the passive radiators and the driven antenna. As an example, an antenna array, which uses one driven element surrounded by a number of parasitic

elements operating near resonance was reported [Preston]. Three-element phased array, where the center (driven) antenna is fed by an RF source and the two neighboring (passive) antennas are excited through the mutual coupling from the center antenna is reported [Yusuf1]. By adjusting the capacitors' value, the beam was tilted from –20 degree to +20 degree. However, this antenna requires array of antennas for steering beam and operates at narrow band (at 3 GHz).

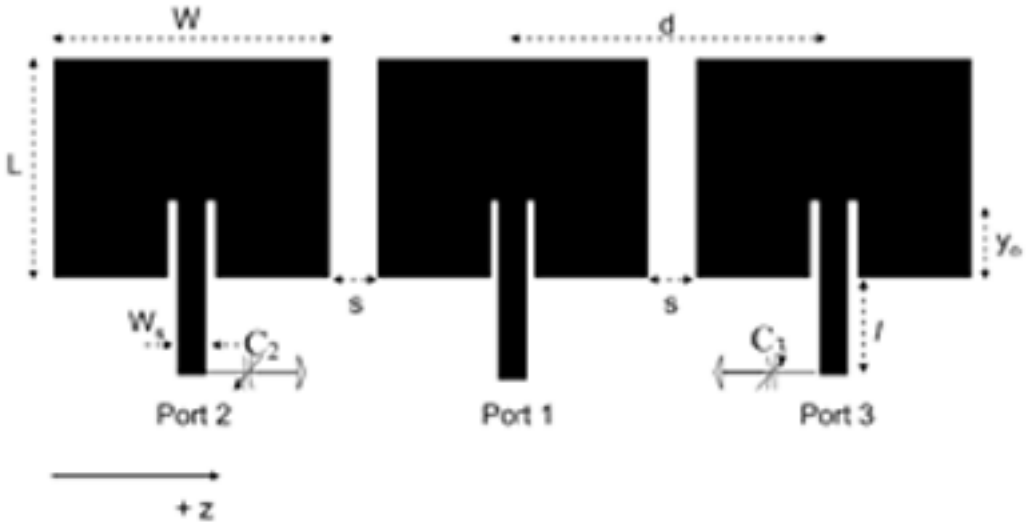

Figure 2-7. Three-element array for beam steering [Yusuf1]

The patch antenna phased array was demonstrated with analog beam steering without using phase shifters, therefore reducing the cost of a phased-array system. Another example of the ESPAR antenna array used parasitically coupled and reactively loaded patch antenna array to achieve beam steering in an analog manner [Yusuf2]. The parasitic coupling between closely spaced patch antennas was used to form a phased array with a single driven element. The phase shift between the array elements was adjustable by changing the reactive loading on the parasitic patch antenna. However, most of the examples of the antennas require an array of antennas for

electronically steering the beam instead of a single antenna. Therefore there is a room for further simplification because not all applications require the complexity of phase array, and for some applications, an alternative, simpler system is desired.

2.4 Patch Antennas using Diodes

Many patch antennas that use diodes have been reported. One example is a reconfigurable, dual-frequency, slot-loaded patch antenna controlled by PIN diodes. A PIN diode was placed at the extended slot arm to change the electrical length of the slot and thus shifted the two resonant frequencies considerably in different states of the diode. For example, when the diode is switched off, the currents have to flow through a capacitor, with an increased current path, resulting in the shifting of resonant frequencies [Shynu]. Another example is a reconfigurable ground-slotted patch antenna using PIN-diode switching. A dual-frequency operation was achieved by controlling PIN diode conduction [Byun]. A patch antenna consisting of a square radiating patch, a parasitic patch, and PIN-diodes, which connect the radiating patch and the parasitic patch was reported. By controlling the DC bias voltage applied to the diodes, surface current distributions changed, thus, dual-frequency operation was achieved [Lee]. As shown in Figure 2-8, when diodes are turned on, the current flows to the parasitic patch and the antenna operates at WCDMA (2110 ~ 2170 MHz). When the diodes are turned off the current does not flow to the parasitic patch and the antenna operates at DMB (2630 ~ 2655 MHz). As another example, an annular slot antenna using two PIN diodes that are placed on front and back were reported. This antenna was reconfigurable in both frequency and radiation pattern [Nikolaou]. As yet another example, a reconfigurable, spiral antenna array was designed for pattern diversity.

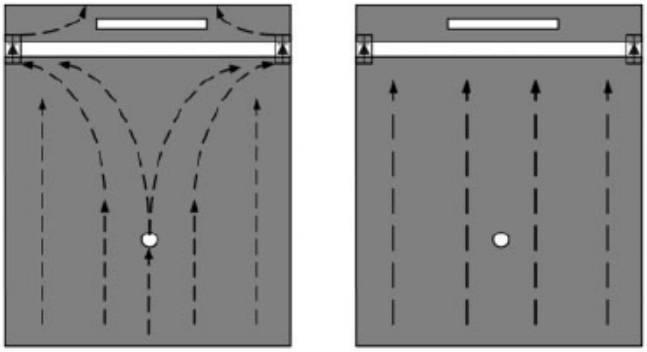

Figure 2-8. Reconfigurable antenna for dual frequency operation [Lee]

It utilizes the fact that the single-arm, Archimedean spiral can produce tilted beams by changing its arm length. The arm length was reconfigured in length using PIN diode switches [Mookiah]. As the last example, a reconfigurable Hilbert antenna using high-speed PIN diodes was reported [Caverly]. The PIN diodes were used to reconfigure the fractal pattern and the antenna exhibited two resonant frequency bands. Figure 2-9 shows the antenna. By changing the ON/OFF status of the two diodes, the antenna operated at dual frequency.

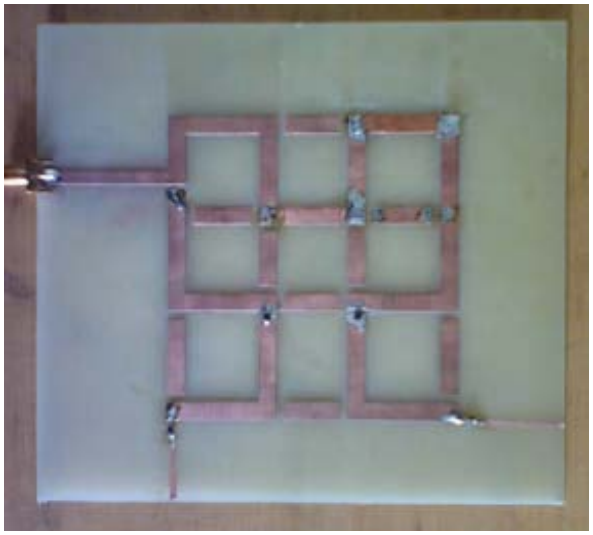

Figure 2-9. Reconfigurable antenna for dual frequency operation [Caverly]

2.5 Proposed Design Approaches

Figure 2-10 shows a layout of the proposed antenna with two diodes connecting the gap between the stubs and the partial ground plane.

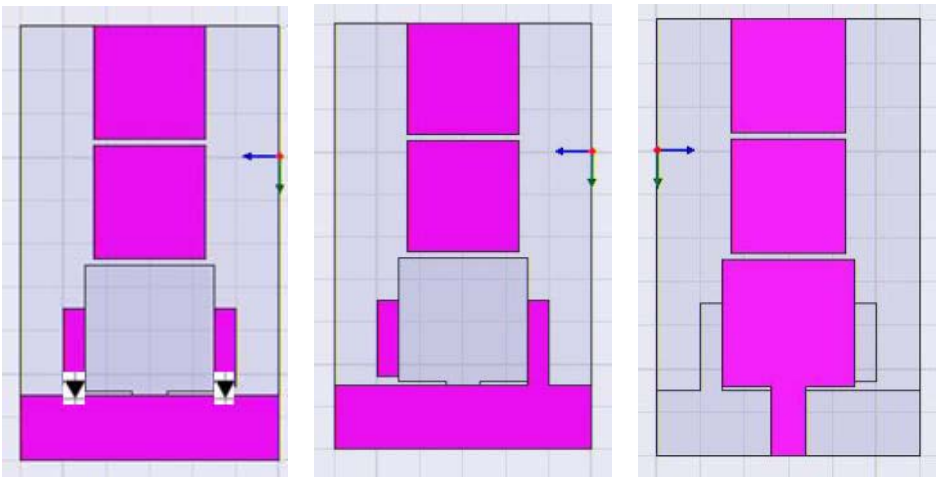

Figure 2-10. HFSS layout of antenna; Left: bottom layer with diodes; Middle: bottom layer for simulating one of the diodes being turned on; Right: top layer

Design procedures that lead into the above proposed antenna are described as follows. In the beginning of the design procedure, in order to meet the requirements stated in 1.2, a reference broadband antenna with a partial ground plane was designed. Ansoft HFSS was used for the design and optimization. The dimensions of the reference broadband antenna are shown in Figure 2-11.

The FR4 lamination with a thickness of 1.6 mm and a dielectric constant of 4.4 was used as the substrate. The front trace layer consists of a square patch with dimensions of 15 mm × 15 mm and a feed line with dimensions of 8 mm × 4 mm. The partial ground with a dimension of 7.5 mm × 30 mm was placed underneath the substrate (30 mm (W) × 35 mm (L)). After achieving its bandwidth requirement (4.4-6.7 GHz) in the first design stage through the reference antenna, meeting the second criterion, (i.e., increasing gain) was necessary because it was found that

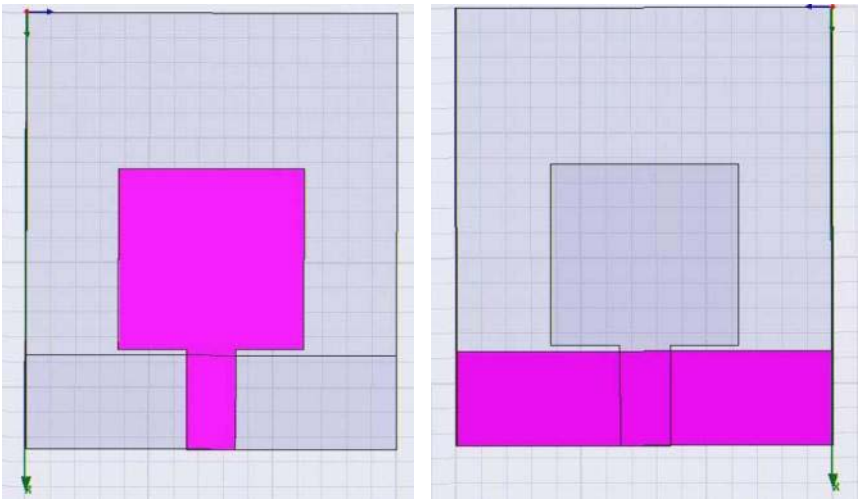

Figure 2-11. Layouts of conventional broadband antenna as a reference antenna; Left: Top layer, Right: Bottom layer

this reference antenna or traditional single patch partial ground plane broadband antenna does not work well with the broadband transceiver because of insufficient gain and directivity, as well as poor isolation between the transmitting and receiving antennas.

To meet the second criterion, numerous design approaches were performed. Using an array of antennas is one of the most common methods to increase gain. Therefore, at first, arrays of antennas were simulated. For example, two, three, or four element arrays of the reference antennas were simulated to improve gain towards the broadside direction of the antennas. Figure 2-12 shows the layouts of the examples of the arrays.

As seen in the Figure 2-12, each of the array antennas consists of a different number of reference antennas with varying shape of the partial ground plane, and all of them use coax feed. However, in most of the cases, the reflection coefficient or the first criterion of the requirements, was destroyed by failing to maintain its original broadband characteristics.

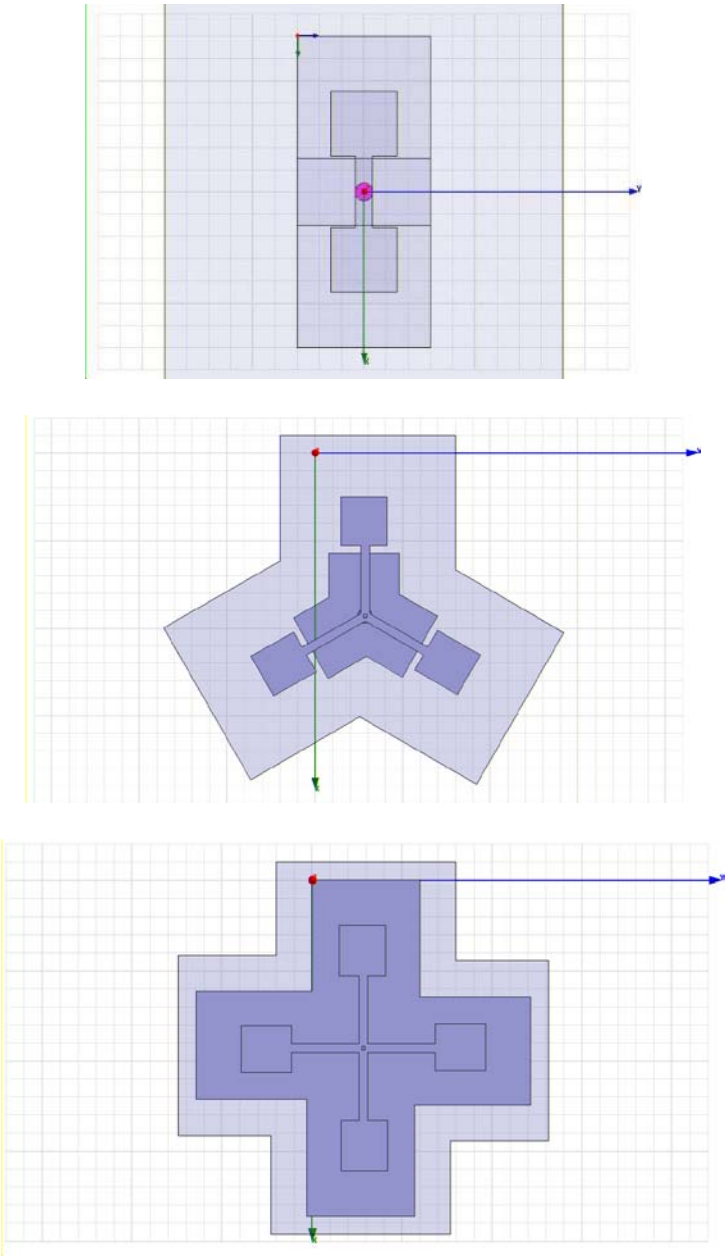

Figure 2-12. The examples of layouts of the arrays of the reference antennas; (Top) Two-antenna array (Middle) Three-antenna array (Bottom) Four-antenna array

Thus, the array approach for boosting gain was discarded from design consideration. After further research of previous work, instead of using an array, it was found out that a microstrip Yagi array antenna having a reflector, driven element, directors as seen in Figure 2-4 could be a better approach to increase gain. Figure 2-13

shows some of the early examples adopting the microstrip yagi concept to the reference antenna. In Figure 2-13, it is shown that the reference antennas use coax feed and have the ground plane with different dimensions. For the antenna (A), which has a short partial ground plane, the reflector has a dimension of 17mm X 17mm, or 1.13 times the length of the side of the driven element. For the antenna (B), which has a long partial ground plane, the reflector has a dimension of 24mm X 24mm or 1.2 times the length of the side of the driven element.

In this approach, the reflection coefficient was substantially maintained. However, the size became quite large, and this time reducing the size became a concern, i.e., meeting the third criterion of the requirements. Thus, additional modifications were performed.

After several design considerations, an edge feed was selected and the reflector was eliminated. Removing the reflector and using the edge feed are beneficial in antenna size reduction and fabrication. In addition, simulations showed that having both the reflector and the partial ground plane was not necessary because the partial ground plane alone can function as the reflector, which will be discussed further in the following chapter. Removing the redundant reflector does not have a negative effect on S11, radiation pattern, or gain. Therefore, a successful design which meets all of the requirements, i.e., bandwidth, gain, and size is created. The layout is shown in Figure 2-14 [Park].

The ratio of directors/driven element size was 0.9. In detail, the two parasitic patches with dimensions of 13mm X 13 mm are placed on top with 0.8mm gap from the

front trace layer and from each other. As seen in Figure 2-14, in addition to the microstrip Yagi array antenna having a reflector, driven element, directors on front

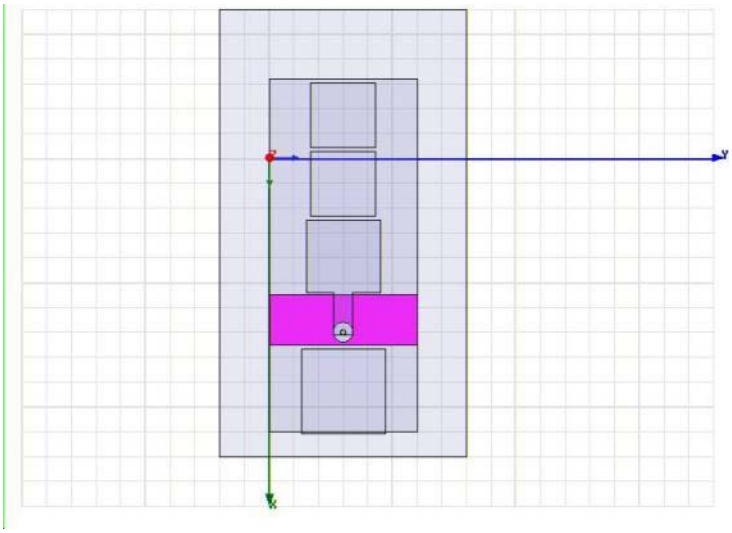

A

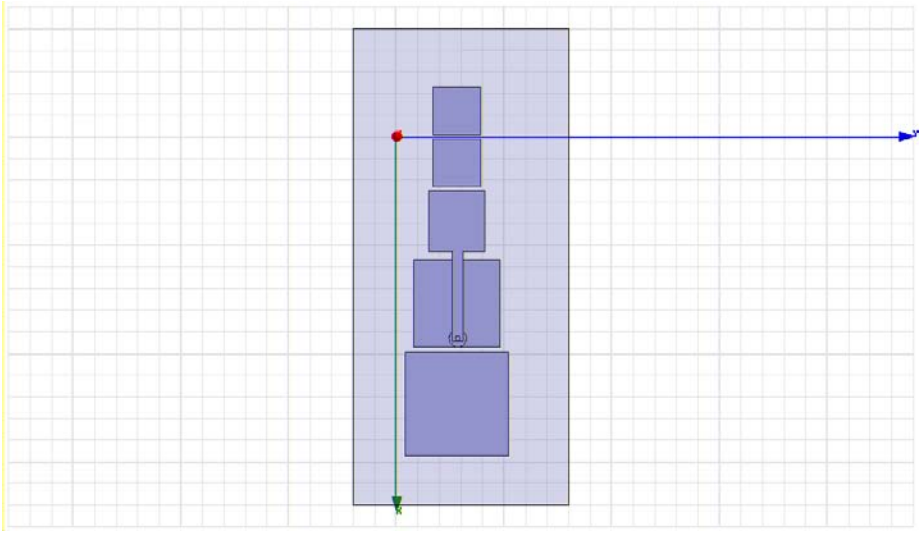

B

Figure 2-13. Examples of the reference antenna adopting microstrip Yagi array (A) short partial ground plane (B) long partial ground plane

layer as seen in Figure 2-14, additional two directors were placed on bottom of the substrate to maximize the improvement of gain. It is known that electromagnetic energy is coupled from the driven patch to the parasitic patches through both space waves and

surface waves [Huang2]. By placing additional parasitic patches on the bottom of substrate, more energy can be coupled through surface waves in the substrate.

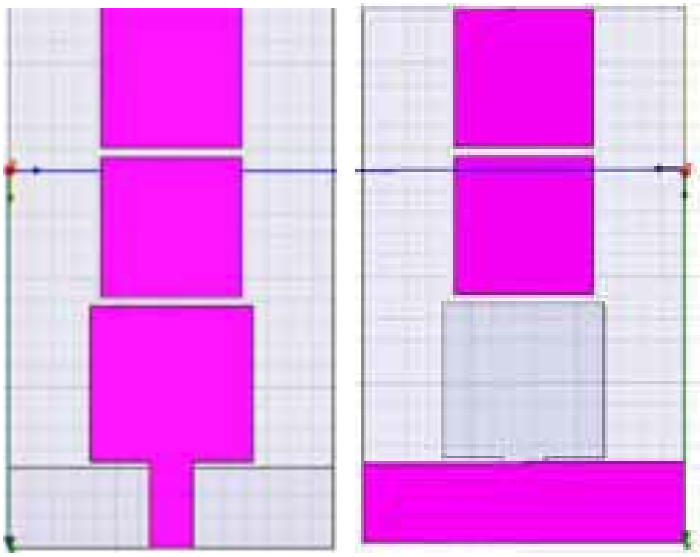

Figure 2-14. Layouts of broadband directional microstrip antenna; Left: Top layer, Right: Bottom layer [Park]

Simulation showed that the antenna with both top and bottom patches can increase gain about 0.3 dB at 4.5 GHz and 0.2 dB at 6.5 GHz when compared to an antenna with only top patches. Note that the driven element and the ground plane of the broadband directional microstrip antenna have the same dimension as those of the reference antenna. The partial ground plane improves broadband characteristics and the parasitic patches improve the gain. Also, note that a simple form of main trace layer that is same as the reference antenna is used, instead of the highly-modified trace layer designs as shown in [Choi2] for simplicity.

Through this design approach, many variations of the broadband directional microstrip antenna were simulated, such as broadband directional microstrip antenna with a short partial ground plane or a long partial ground plane, broadband directional microstrip antenna with one director or three directors, broadband directional microstrip

antenna having different spacing between elements. Among the variations, the broadband directional microstrip antenna having a long partial ground plane did not show a gain that is as high as the broadband directional microstrip antenna with short ground plane as shown in Figure 2-14, thus the broadband directional microstrip antenna having a long partial ground plane was discarded from design consideration.

The difference between Figure 2-11 and Figure 2-14 is basically the additional parasitic patches. It may seem simple to design the broadband directional microstrip antenna from the reference antenna. However, as described above, adopting the Yagi concept to the reference antenna and meeting the requirements required many simulations and optimization.

In the non-contact vital sign radar detection application, broadband beam steering is desired because of its use for radar application. Unlike the patch antennas that use array for beam steering, the proposed antenna requires no array for beam steering but has single antenna and a pair of diodes attached to the single antenna. The diodes can be switched on and off to modify the electrical length of stubs of the single antenna.

Numerous simulations to optimize the stub shape attached to the ground plane and the locations of the stub have been performed for realizing electronic beam steering while maintaining broadband characteristic. The result of optimized layout is shown again in Figure 2-15.

In detail, Figure 2-15 shows two stubs added on the bottom of the substrate to the partial ground plane. The stubs are the only change made to the broadband directional microstrip antenna. Thus, the driven element and the ground plane of the proposed antenna have the same dimension as those of the broadband directional microstrip

antenna. There are lots of possible design combinations such as changing gap distances between elements and size and/or shape of each element.

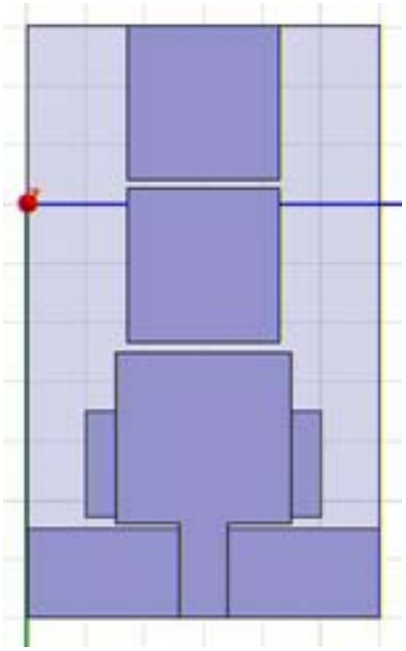

Figure 2-15. A layout of the proposed antenna or electronic beam steering broadband single microstrip antenna

However, due to a limited time for design optimization, not all of the possible combinations were simulated. Some of the design considerations will be discussed in the following chapters. Among the many design considerations, discovering that the partial ground plane can function as a reflector is one of the most important facts found, which will be discussed in the following chapters.

2.6 Summary

Examples of microstip antennas using a partial ground plane to give wideband characteristics are shown; however, there is still a room for improvement in gain and directivity. In addition, microstip antennas using parasitic patches to give increased gain are shown; however, all of these kinds of antennas operate over a very narrow band. Neither case of the antenna is ideal for the specific application of the non-contact

detection of vital signs, where a microstrip patch antenna needs to have a high gain and broad bandwidth at the same time.

In addition, examples of antennas for beam steering and patch antenna examples using diodes are shown; however, those antennas operate at narrow band.

Proposed design approach combines the advantages of the cited references of each category. In detail, the proposed antenna combines the advantage of the wideband antenna, the advantage of the parasitic patch, and the advantage of beam steering antennas. The proposed antenna requires no array for beam steering but requires only two additional diodes.

CHAPTER 3
BROADBAND DIRECTIONAL MICROSTRIP ANTENNA

3.1 Fabricated Broadband Directional Microstrip Antenna

After performing simulations in Ansoft HFSS, the broadband directional microstrip antenna was fabricated on a low-cost FR4 substrate, which was pre-sensitized with photoresist. This allows for simple pattern application via photolithography and subsequent copper etching with ferric chloride. Figure 3-1 shows the fabricated broadband directional microstrip antenna. Also shown in Figure 3-1 is the edge-mounted, standard-polarity SMA connector.

Figure 3-1. Layouts of fabricated broadband directional microstrip antenna; Left: front layer. Right: bottom layer

3.2 Input Reflection Coefficient (S11)

The one-port scattering parameters (input reflection coefficients) of the reference antenna and the broadband directional microstrip antenna were measured using an

Agilent E8361A 10 MHz to 67 GHz PNA series network analyzer as shown in Figure 3-2. To accompany the measurements, each antenna was simulated using HFSS.

Figure 3-2. Agilent Vector Network Analyzer (Courtesy of Agilent Technologies, Inc.)

The reflection coefficient (S11) of the broadband directional microstrip antenna was compared with the reference broadband antenna as shown in Figure 3-3. The measurement results show that parasitic patches affected the broadband characteristics of the partial ground plane antenna in the lower frequency. In particular, the measured first resonant frequency of the broadband directional microstrip antenna shifted about 400 MHz up from that of the reference broadband antenna simulation. The discrepancy can be caused by one or more of the following reasons. First, the fabricated antenna may have different line width and different patch size than the values used in simulation model because of the around 0.3 mm resolution of lithography. Second, the actual dielectric constant of FR4 substrate at frequencies above 6 GHz might be different and the actual dielectric constant might vary from board to board. Further modifications such as modifying ground plane and patch shape may improve the broadband characteristics [Choi1]. Nevertheless, the measurement result confirms that the broadband directional microstrip antenna has met the design requirement of impedance matching bandwidth.

3.3 Far-Field Radiation Patterns

The radiation patterns were measured in an anechoic chamber at the Electromagnetic Wave Measurement Center in Seoul, South Korea. For this broadband antenna, it would be ideal to measure the radiation patterns at frequencies with small interval between them, but instead, the radiation patterns were measured at 4.5, 5, 5.5, 6, and 6.5 GHz due to practical reasons.

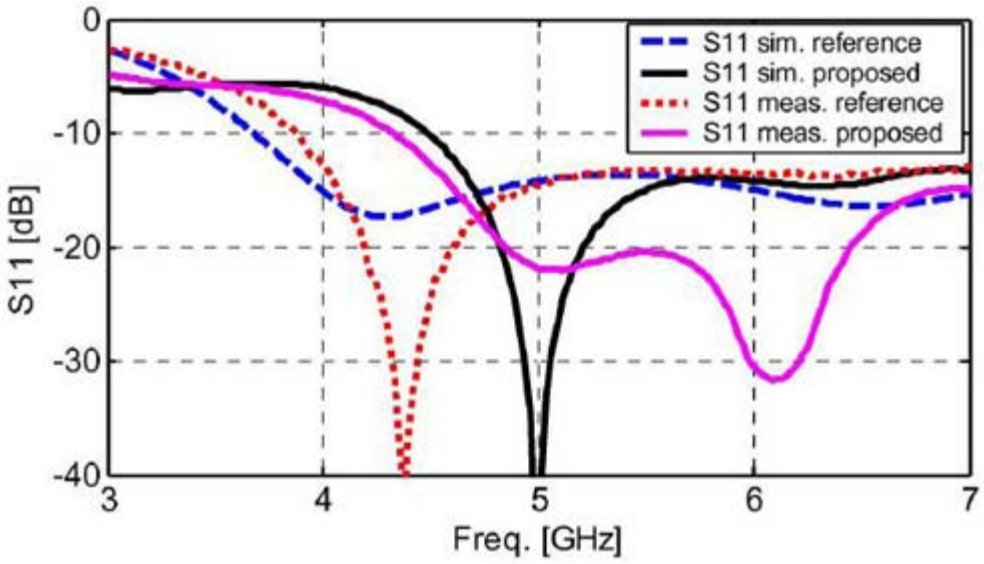

Figure 3-3. Input reflection coefficients of the reference antenna and broadband directional microstrip antenna

At each of the frequencies, E-plane and H-plane cuts were measured. For the E-plane measurement, an E-plane that is vertical to the substrate (E1) and another E-plane that is horizontal to the substrate (E2) were measured. Also, at each of the frequency, co-polarization and cross-polarization of the E-planes and H plane were measured as well. Figure 3-4 shows inside of the anechoic chamber. The Standard Gain Antenna is shown on the left, and the antenna under test (AUT) mounted is shown on the right. Figure 3-5 shows one of the ways of how the AUT was mounted. After the AUT is securely mounted, it is rotated for the radiation pattern measurement. The

measured data are shown on a computer screen, which is located outside of the chamber as in Figure 3-6. Also, the radiation patterns were simulated using HFSS.

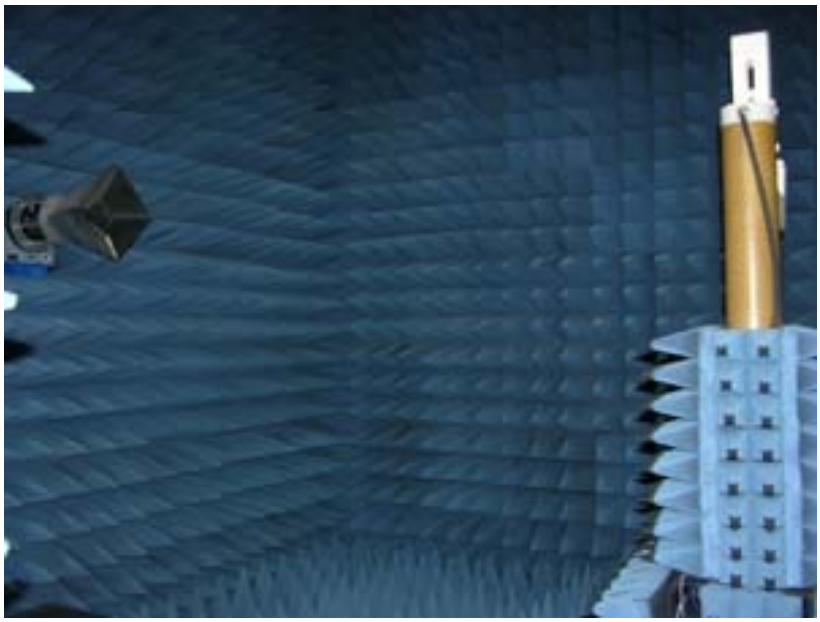

Figure 3-4. Inside of an anechoic chamber for the radiation pattern measurement

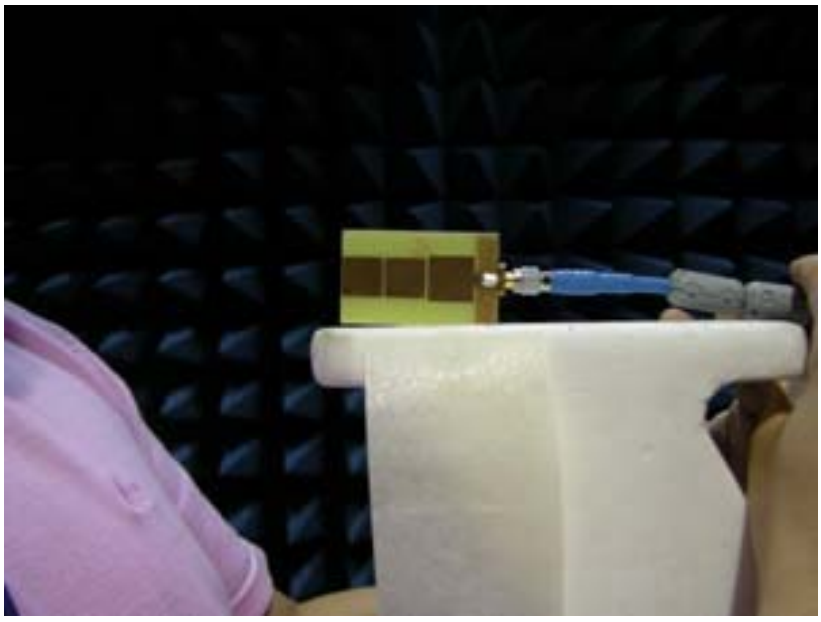

Figure 3-5. One of the configurations of mounted AUT

These radiation patterns of the reference antenna and the broadband directional microstrip antenna are reported in Figure 3-7. In particular, E-plane co-polarization and

cross-polarization radiation patterns measured at frequencies of 4.5 GHz, 5.5 GHz, and 6.5 GHz are compared with simulations.

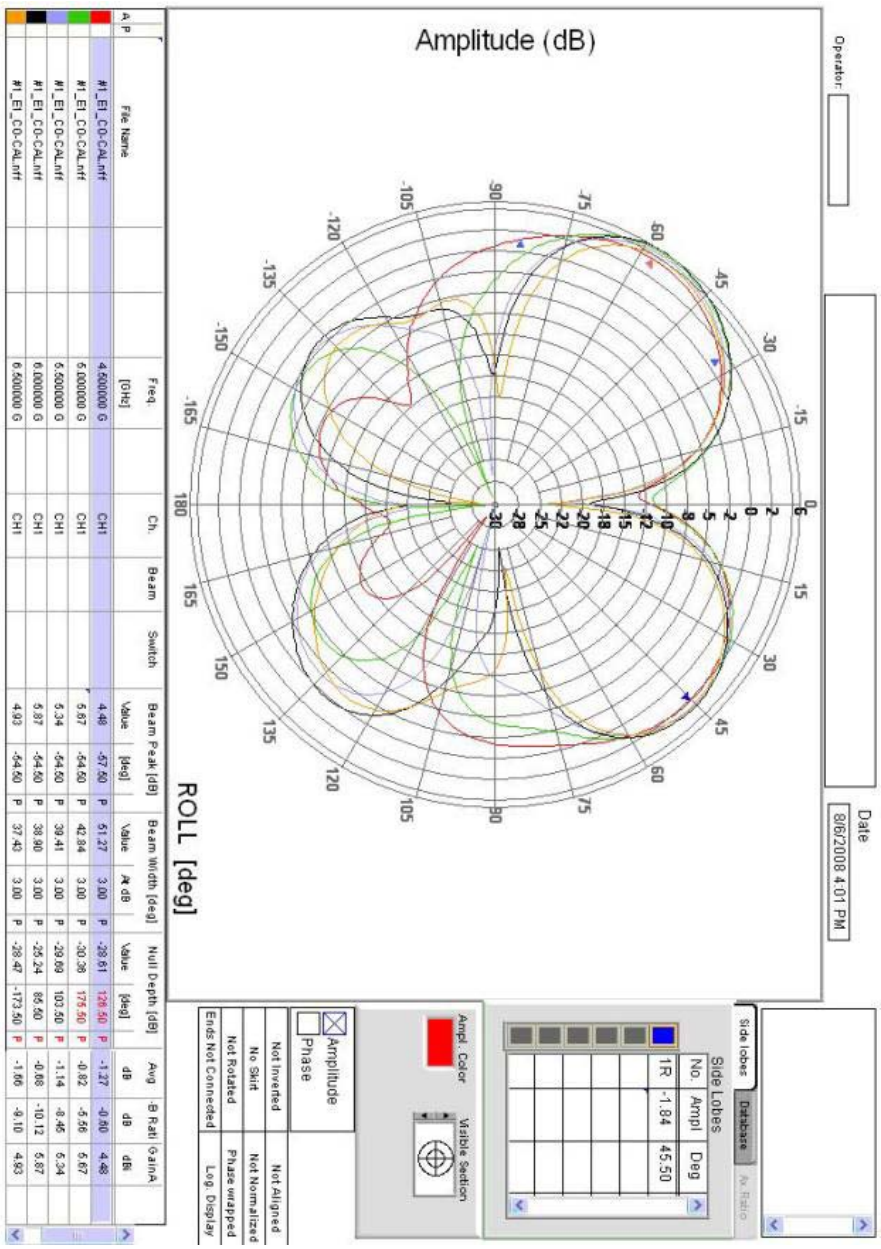

Figure 3-6. Radiation pattern measurement shown on a computer screen outside of the chamber

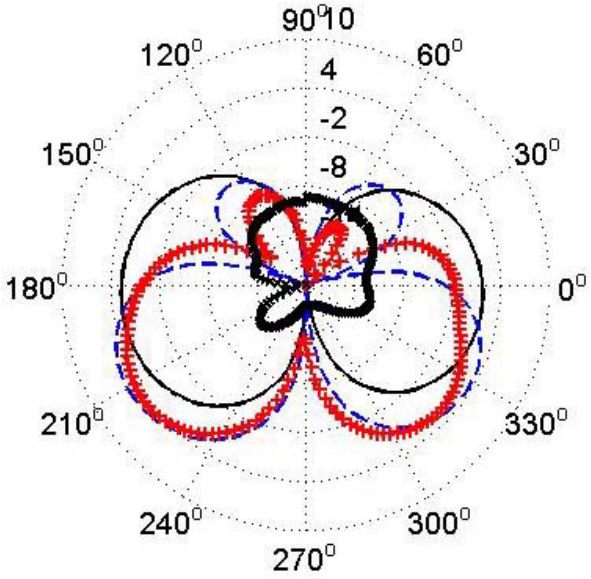

A

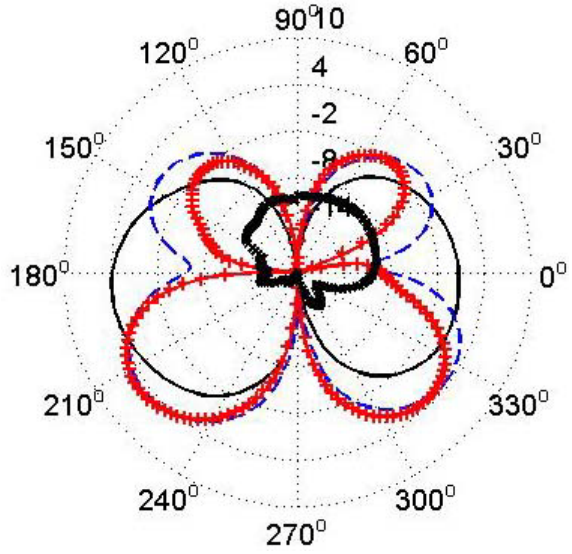

B

Figure 3-7. Comparison of simulated/measured radiation patterns of the broadband directional microstrip antenna and the reference antenna (Solid black: Reference, Dashed blue: broadband directional microstrip antenna - simulated, “++” red: broadband directional microstrip antenna - measured, “x” black: broadband directional microstrip antenna – measured cross-polarization) along Phi =0˚ plane. Radiation patterns at frequencies of 4.5 GHz (A), 5.5 GHz (B), and 6.5 GHz (C) are plotted. Antenna configuration with axes is shown in (D).

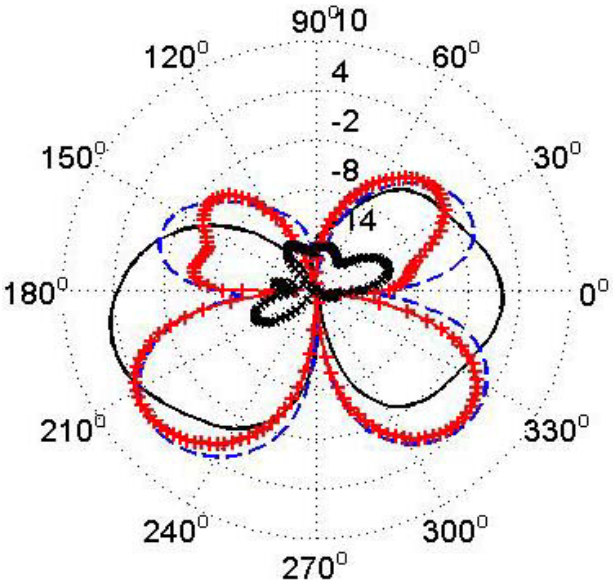

C

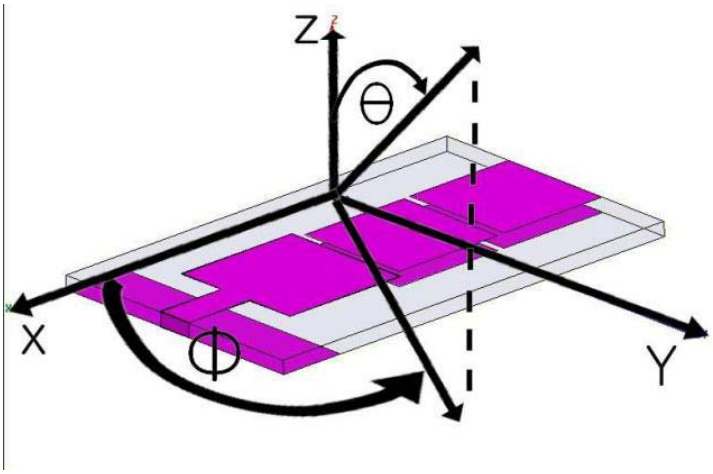

D

Figure 3-7. Continued

It can be seen in Figure 3-7 that the measured and simulated radiation patterns for the broadband directional microstrip antenna are in good agreement with each other. In addition, it can be seen that the actual measured side lobes of the broadband directional microstrip antenna are smaller than that of the simulated pattern. Figure 3-7 (D) shows the antenna configuration used in HFSS simulation.

Also shown in Figure 3-7 is that the peak directivity was tilted by about 35° from the broadside toward the end fire direction, which is caused by the effect of mutual coupling. A 35° of peak directivity angle is chosen because it is an appropriate angle for installation on the ceiling at a corner location. If the angle is tilted too close to end-fire direction, the beam will be almost parallel to the ceiling. If the angle is close to 0, i.e., broadside direction, the radar detection will be limited to a spot just below where the antenna is installed. Neither case is desired for the intended application. The designed radiation pattern of the antenna makes it possible to be mounted on the ceiling at the corner of a room or a hallway for human vita sign detection.

The maximum gains of these two antennas are compared in Figure 3-8. In addition, half-power beam width (HPBW) is found to be about 43°. Simulation shows that adding more than two directors does not change the angle of main beam. It is because the amount of energy that couples into the second director is significantly reduced after most of the energy coupled into the first director has been radiated [Huang2]. Specifically, when only a single director is used, the peak directivity angle is tilted only 14° from broadside. However, the angle remains at 35° even after the third director is added. The tilted angle is also known to be a function of dielectric constant, substrate thickness, patch separation, and sizes of the parasitic patches [Huang2].

Therefore, the tilted angle can be modified by varying the above parameters and the number of patches. Figure 3-9 shows two of the broadband directional microstrip antennas mounted on the broadband Doppler radar for non-contact vital sign detection and Figure 3-10 shows the installation diagram.

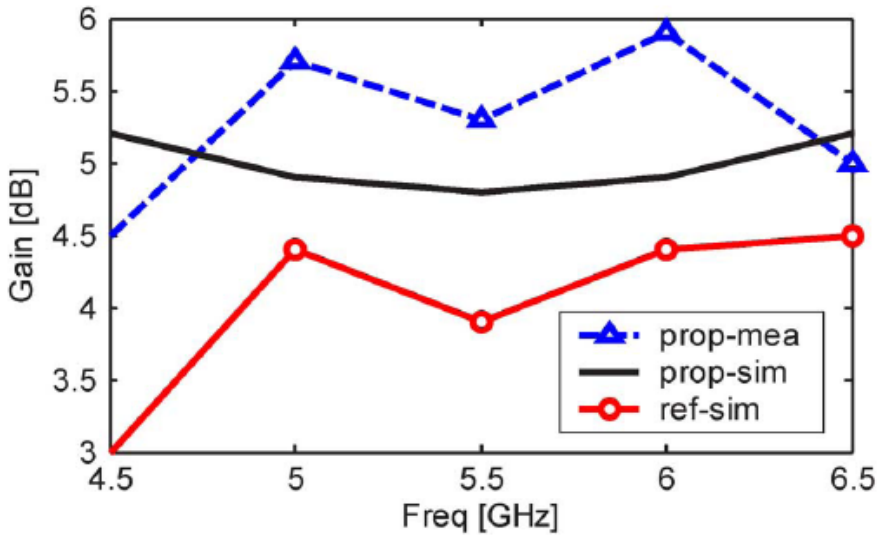

Figure 3-8. Antenna gain comparison between the broadband directional microstrip antenna and the reference antenna

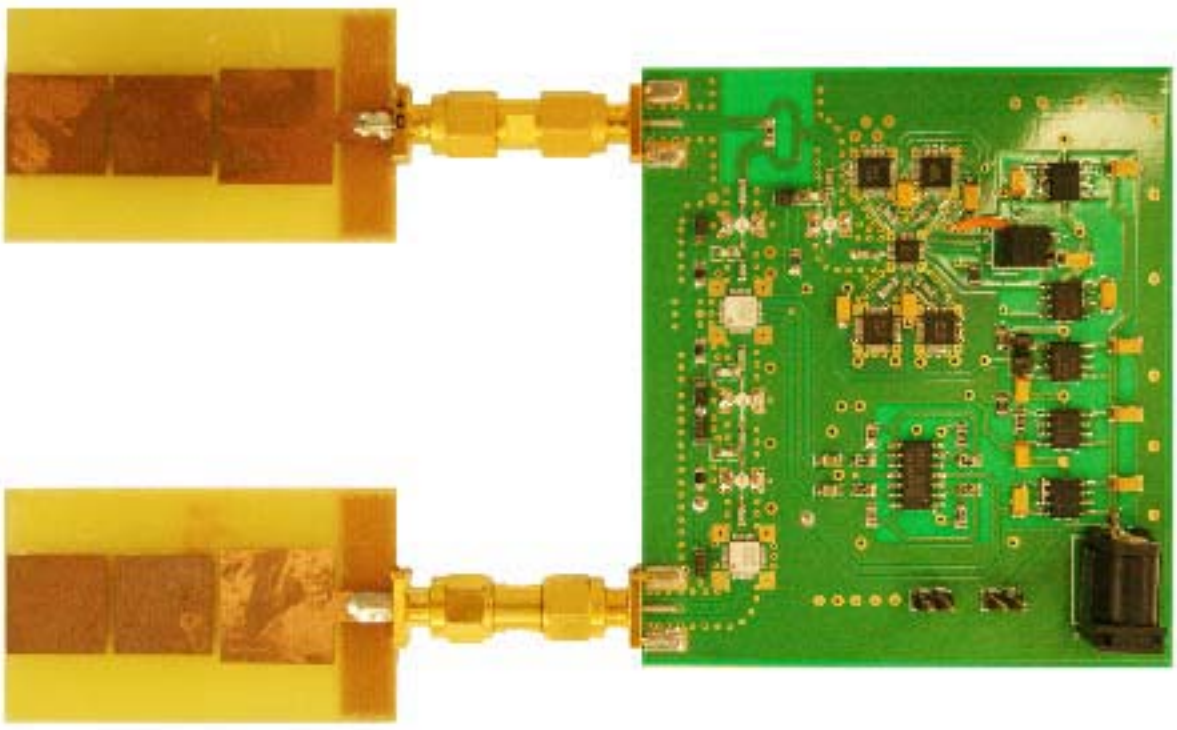

Figure 3-9. Antennas implemented in the radar

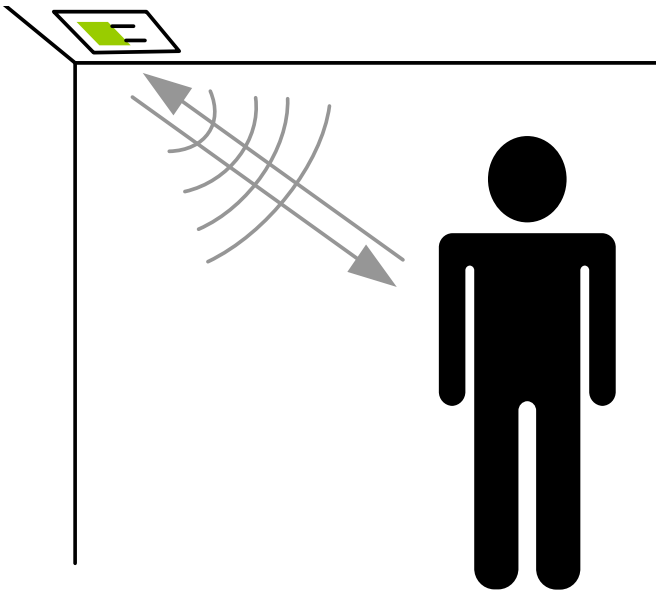

Figure 3-10. Illustration of the antenna and the radar installation

3.4 Isolation

Figure 3-11 shows measured isolations or S12 between the transmitting and receiving antennas mounted on the radar for both the broadband directional microstrip antenna and the reference antenna. The distance between the two antennas' feeds were 60mm because it is the actual distance between the feeds of the transmitting and receiving antennas when installed in radar. It shows the broadband directional microstrip antenna have better isolation than the reference antennas in most of the frequency band. Therefore, in addition to meeting the bandwidth and gain requirements, the broadband directional microstrip antenna shows also good isolation between the transmitting and receiving antennas.

3.5 Vital Sign Detection Performance

The broadband directional microstrip antenna and the reference antenna were tested in the system using the same vital sign radar transceiver and the measurement results were compared.

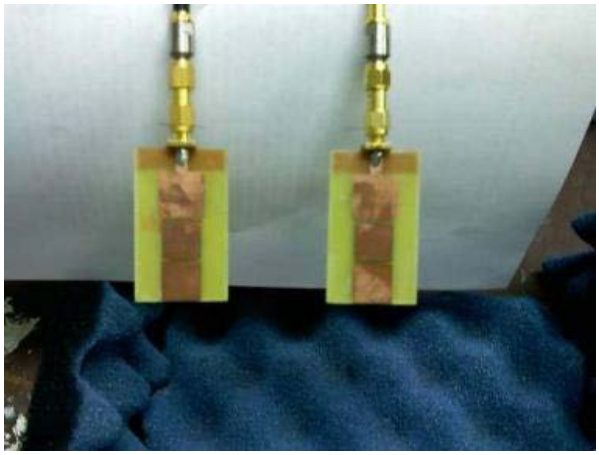

A

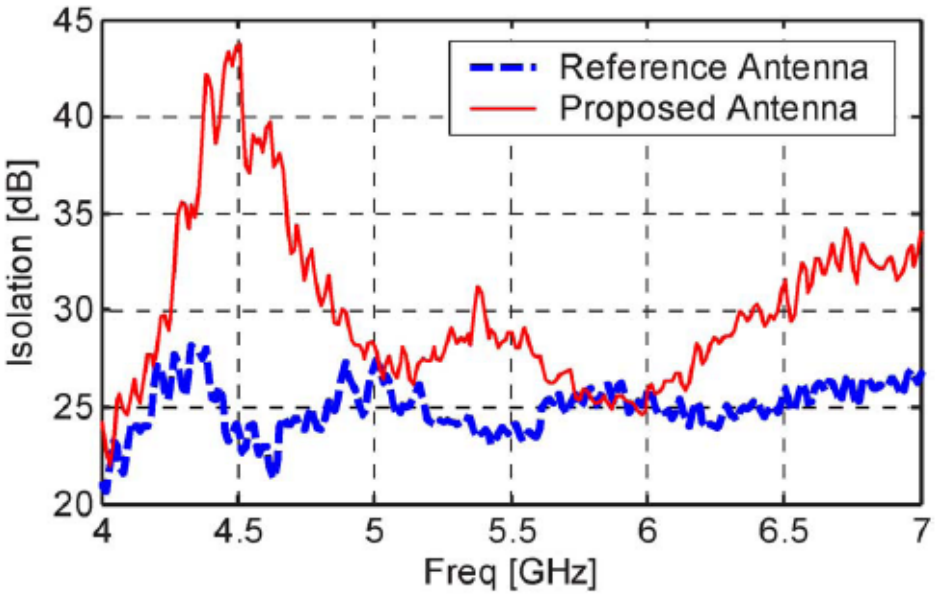

B

Figure 3-11. Measured isolation between a pair of the broadband directional microstrip antennas and a pair of reference antenna (A) measurement configuration (B) result

The pair of broadband directional microstrip antenna and the pair of reference antenna were mounted in the same configuration as in Figure 3-9.The baseband outputs measured with the two types of antennas are plotted in Figure 3-12. It is clearly shown in the measurement results that the broadband directional microstrip antenna

produced much larger signal amplitude with clearer peaks and periodic pattern because of the improved gain. As the frequency increases, increase in signal amplitude becomes less significant due to less improvement in gain at high frequency end of the band as shown in Figure 3-8. Overall, the vital sign detection performance is improved by the broadband directional microstrip antenna.

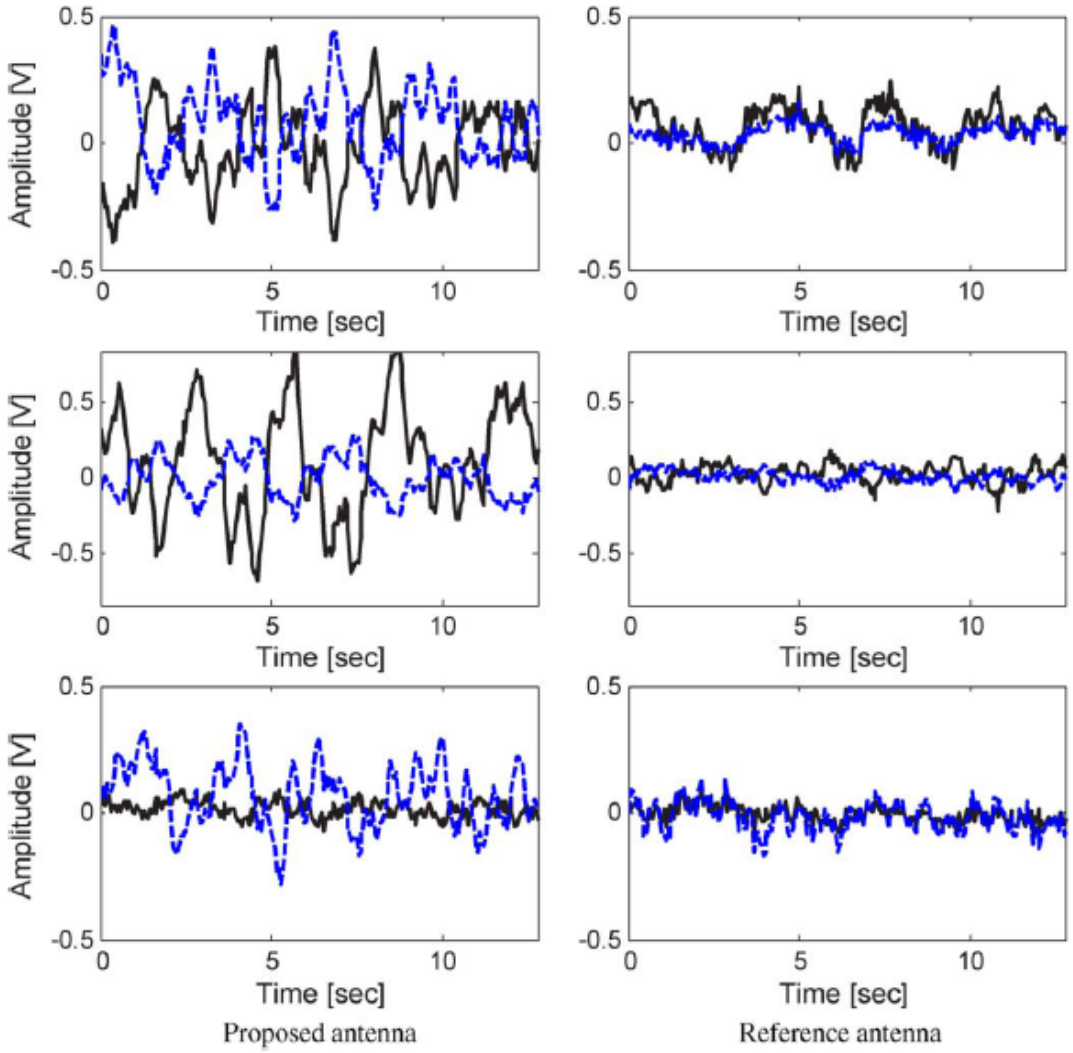

Figure 3-12. Comparison of the I- (dashed blue) and Q- (solid black) channel signals received by the two types of antennas at the frequencies of: 4.58 GHz (top figures), 5.15 GHz (middle figures), and 5.57 GHz (bottom figures)

3.6 Summary

A new design combining the partial ground plane and parasitic patches is presented. The partial ground plane improves broadband characteristics and the parasitic patches improve the gain. As a result, a 4.3–7 GHz broadband antenna with improved gain was designed and fabricated. Compared to a partial-ground-plane, single-patch, reference antenna, this broadband directional microstrip antenna shows desired directivity and improved gain performance. Its radiation pattern was designed for a vital sign radar detector mounted on the ceiling at corner locations. The radiation pattern also provides a better isolation between the transmitting and receiving antennas for this application. The design approach ensures that broadband performance can be achieved while improving the gain of the antenna.

CHAPTER 4
PRELIMINARY RESULT OF BEAM-STEERING BROADBAND MICROSTRIP ANTENNA

4.1 Director and Reflector

The advantages of wideband antenna and the advantages of parasitic patch antenna are combined and validated by fabrication and measurement. In this chapter, the effects of modifying the broadband directional microstrip antenna on the antenna characteristics such as reflection coefficient, radiation pattern, gain, or beam steering capability are discussed. The modification can include varying the width and/or length of the partial ground plane, adding stub(s) on the partial ground plane, varying the width, length, and/or location of the added stub, or varying the number, shape, gap, or location of the directors. These modifications will significantly change the performance of the antenna, however, it is important to evaluate the effects of the modification on the antenna characteristics, since these effects may be exploited to improve the antenna performance. Specifically, the modification on the broadband directional microstrip antenna can give a beam steering capability to the broadband directional microstrip antenna.

In the previous chapter, the reflector in conventional Yagi patch antenna has been eliminated. In this section, roles of directors and ground plane have been investigated. In particular, the fact that the remaining partial ground plane can actually work as a reflector is illustrated. In addition, the directors' role is illustrated.

Simulations show that changing the shape or location of ground plane or director can tailor beam shape. For example, a ground plane with a stub moves the beam away from the added stub. In other words, beam is 'reflected' to the opposite direction from where the stub is added (Figure 4-1 B). As opposed to the ground plane, when directors

are placed on the side of original location, beam is formed in that direction of the directors. In other words, beam is steered towards the direction of the directors (Figure 4-1 C). Thus, it can be seen that the ground plane is working as a reflector and the parasitic patchs are working as directors.

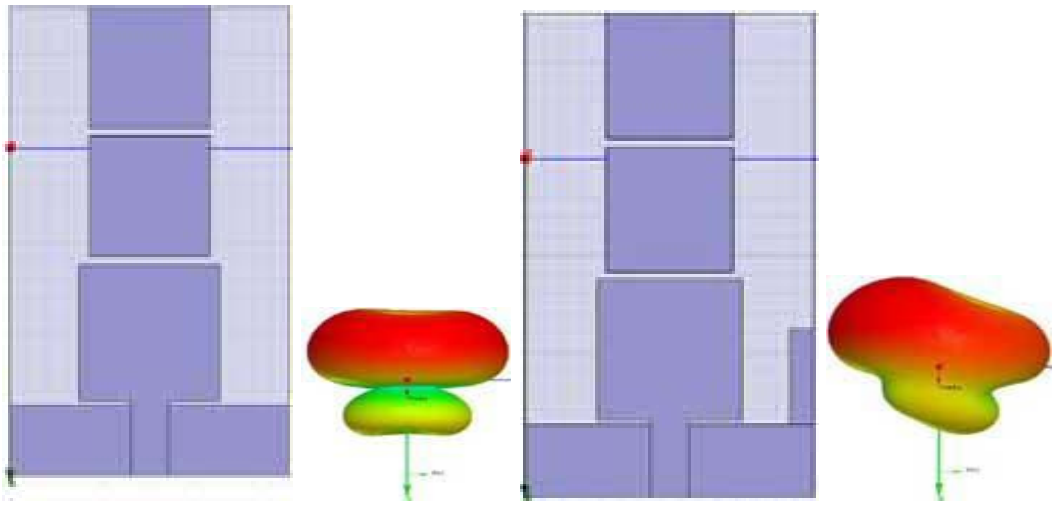

A B

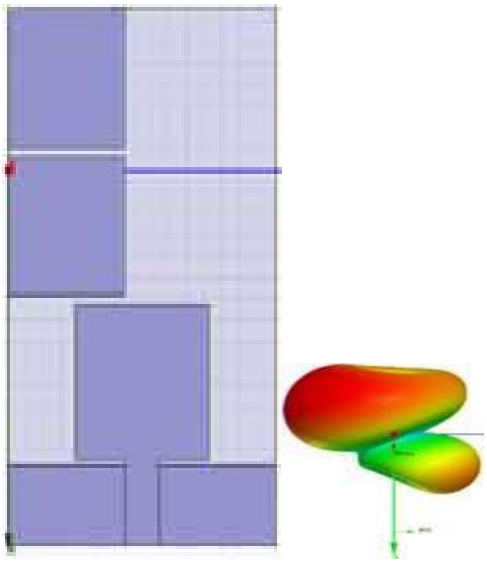

C

Figure 4-1. Modifications to the broadband directional microstrip antenna and their 3-D radiation patterns: (A) Original layout (B) Layout with a stub added to the ground plane (C) Layout with two directors shifted to the left from the original layout

4.2 Influence of Gap Value between Patches on Beam Pattern

In this section, influence of different gap values between patches on beam pattern is investigated. An antenna as shown in Figure 4-2 was set up for this simulation.

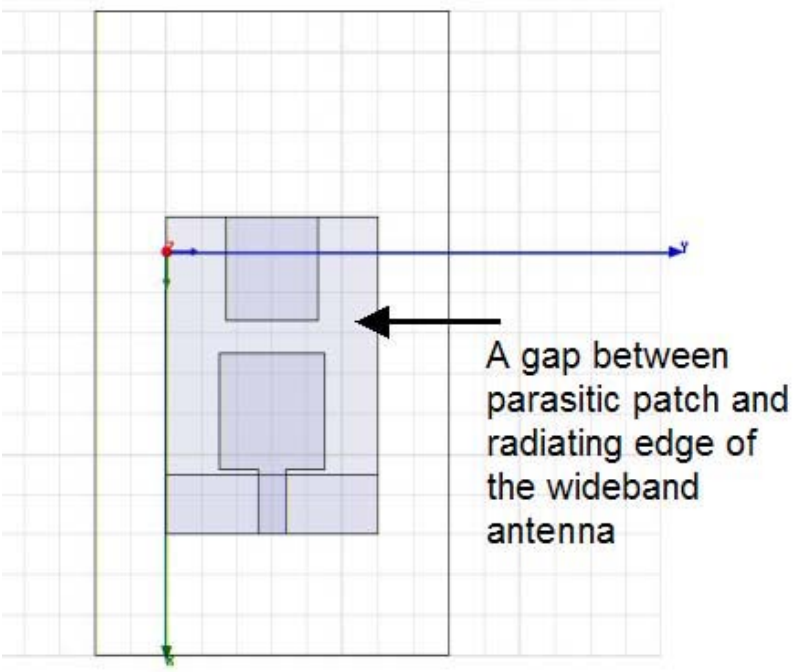

Figure 4-2. A gap between parasitic patch and radiating edge of the wideband antenna

As seen in Figure 4-2, only one parasitic patch is used for simplicity. Figure 4-3 shows the relationship between the gap value and the 3-D radiation pattern.

It is well known that a microstrip patch antenna without a parasitic patch radiates mainly in its broadside direction and radiates very little along the direction of the ground plane. This is the reason that a microstrip patch generally couples very little energy to its nearby patches, when the patches' separation becomes large. Consequently, in order for the microstrip patches to function similarly to the Yagi dipoles, the adjacent patches need to be placed very closely to each other so that a significant amount of coupling can be obtained through surface waves in the substrate [Huang2].

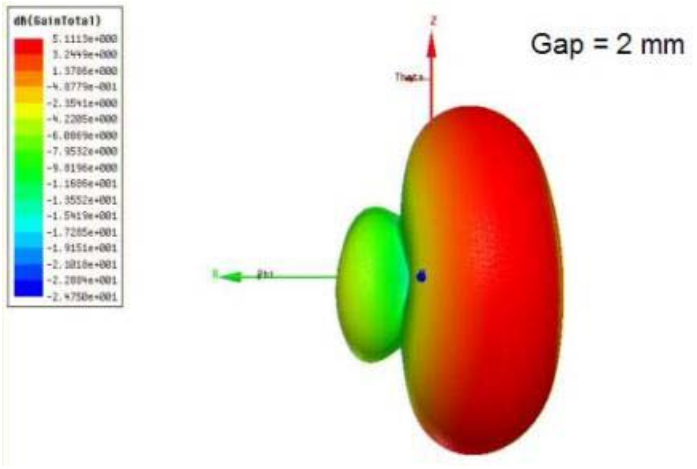

A

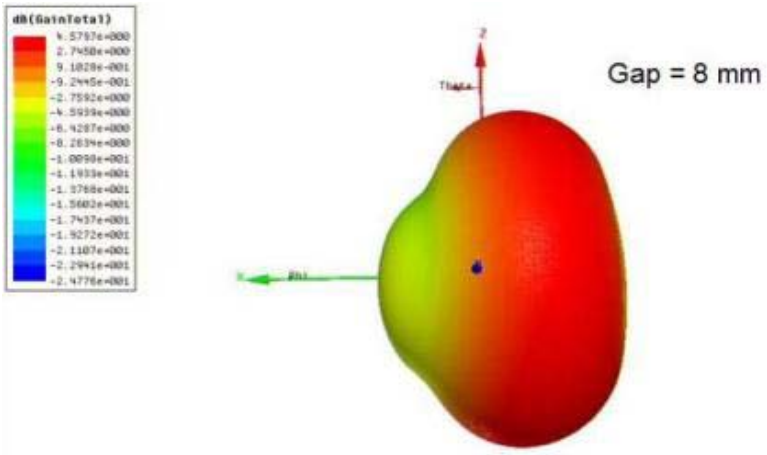

B

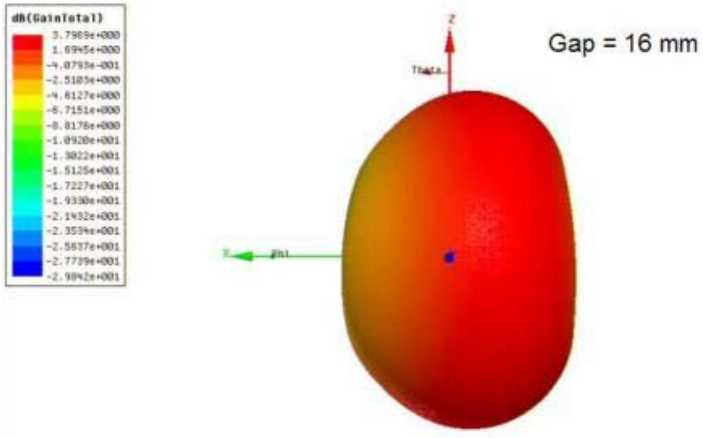

C

Figure 4-3. The relationship between gap value and the 3-D radiation pattern

It was also found experimentally that the gap distance between two patch edges should be equal to or less than the dielectric substrate thickness [Huang1]. From Figure 4-3, it can be seen that as the gap becomes smaller (within a certain limit), the gain becomes higher. It is due to the concentration of the beam towards the parasitic patch due to coupling effect. Table 4-1 summarizes the trend.

Table 4-1. Trend of Gain vs. gap between main and parasitic patch

Gap	Gain
2 mm	5.1 dB
8 mm	4.6 dB
16 mm	3.8 dB

4.3 Influence of Shape or Location of Parasitic Patch on Beam Pattern

Beam pattern gets affected as parasitic patch shape changes. Figure 4-4 shows the examples. As seen in Figure 4-4, it is shown that the beam shape can be complementary to the shape of parasitic patch. In other words, the beams are filling the space where the patch is not occupying. Thus, beam can be directed towards specific direction using this effect.

In addition, the coupling effect still exists between the trace layers even when parasitic patches are separated from the main antenna. In other words, beam shape can be tilted not only in the XY direction but also in Z direction as shown in Figure 4-5. Thus, by replacing only the parasitic patch part from one to another mechanically, different beam shape can be formed while using the same main patch part.

4.4 Influence of A Stub Added to Ground Plane on Beam Pattern

The simulation shown in Figure 4-1 showed that the ground plane is functioning as a reflector because beam is steered away from an added stub to the ground plane. In this section, the stub and its influence on beam pattern is further investigated in depth.

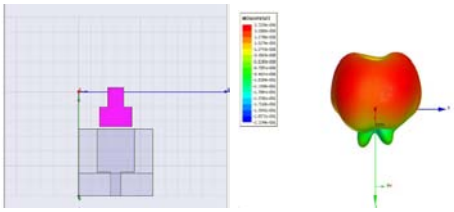

A

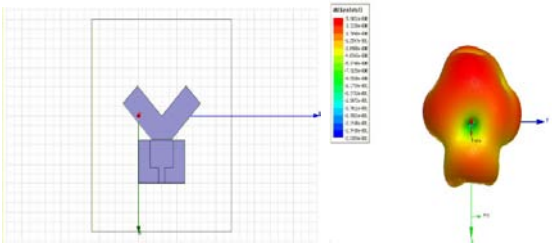

B

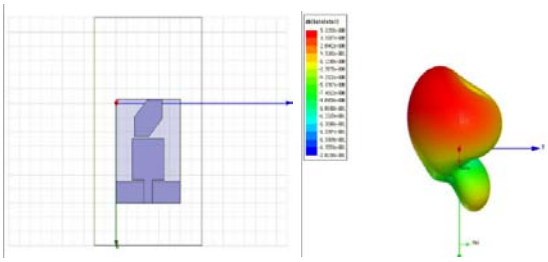

C

Figure 4-4. The relationship between parasitic patch shape and the 3-D radiation pattern

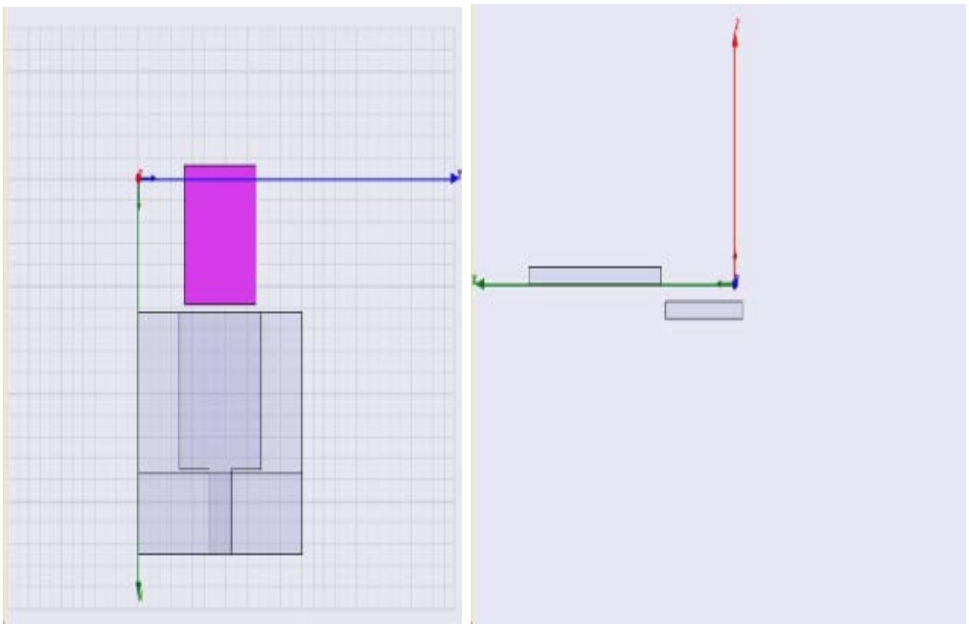

A B

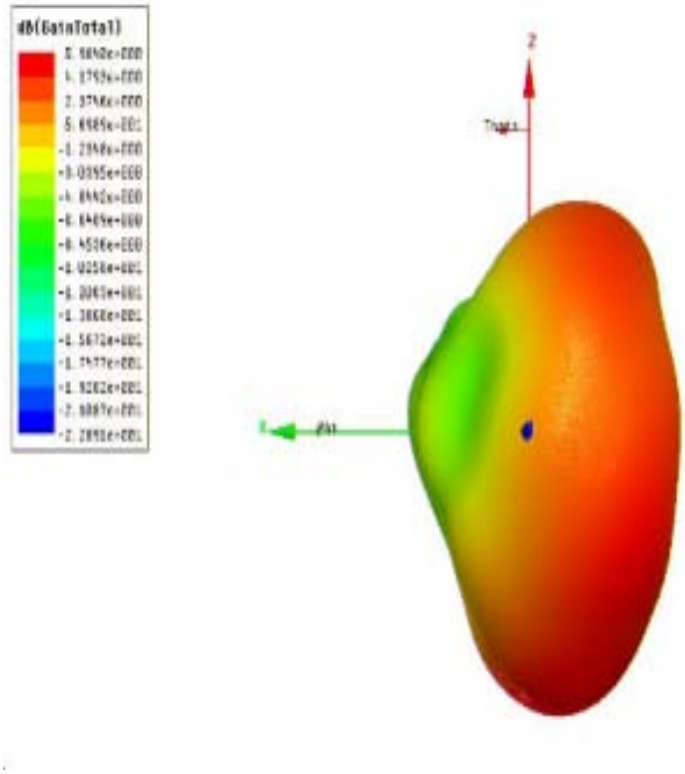

C

Figure 4-5. A parasitic patch placed in – Z direction separated from main patch (A); a view from +Y direction (B); and its 3-D radiation pattern (C)

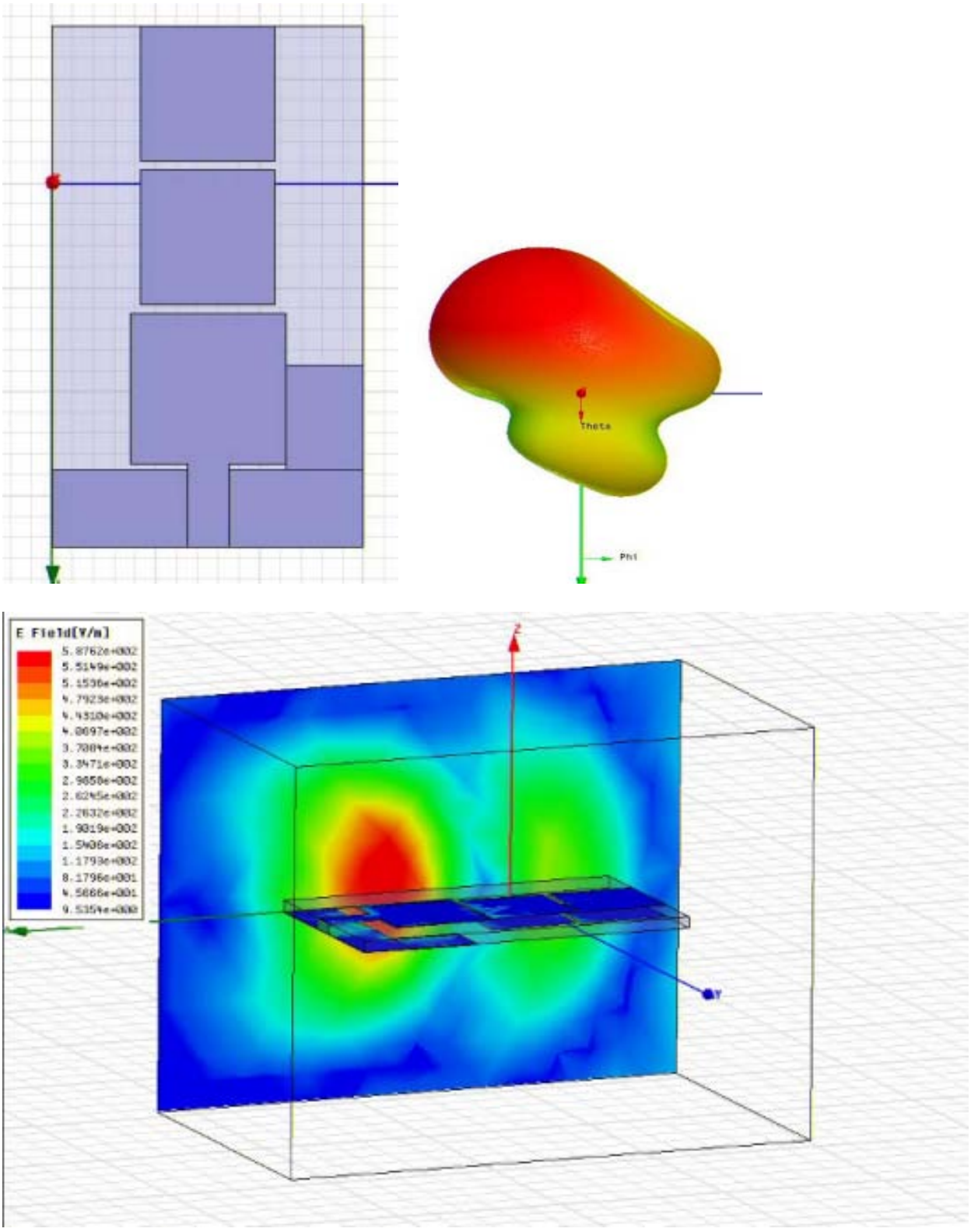

Figure 4-6. An example of an added stub and its 3-D radiation pattern and the magnitude of the E-field at 4.5 GHz

Specifically, the effect of variation of width or length of stub attached to the ground plane to beam pattern is investigated. As shown in Figure 4-6, a stub that has a length shorter than the main patch and a width that is fully occupying the space between the main patch and the substrate boundary is added to the ground plane. The stub has a width of 7.5 mm and length of 10 mm. Its 3-D radiation pattern shows a gain value of 5.65 dB and E-field magnitude that is concentrated in the main patch. To show the E-field magnitude, a plane is placed 25mm from the center of feed in –Y direction. Both of the 3-D radiation pattern and E-field magnitude are plotted at 4.5 GHz.

Figure 4-7 shows another example of an added stub. In this case, only the length of the stub is increased to 30 mm from the Figure 4-6. Through the modification of the stub length, the gain has increased to 5.93dB and the E-field magnitude is concentrated more to the parasitic patch.

Figure 4-8 shows yet another example of an added stub and its 3-D radiation pattern and the magnitude of the E-field at 4.5 GHz. In this case, only the stub width is reduced to 2.5mm from the Figure 4-6 and located at the substrate boundary. This time, the gain value is reduced to 5.4 dB.

Figure 4-9 shows yet another example of an added stub and its 3-D radiation pattern and the magnitude of the E-field at 4.5 GHz. In this case, the stub width and length are unchanged from Figure 4-8. Instead, the location of the stub is moved 2.5 mm in the Y-direction. This time, the gain value is 5.55 dB.

Through these simulations shown in Figure 4-6 ~ Figure 4-9, trends were found and the trends are summarized in Table 4-2. Based on the trends, beam pattern and gain can be modified and increased by modifying the stub location and dimension.

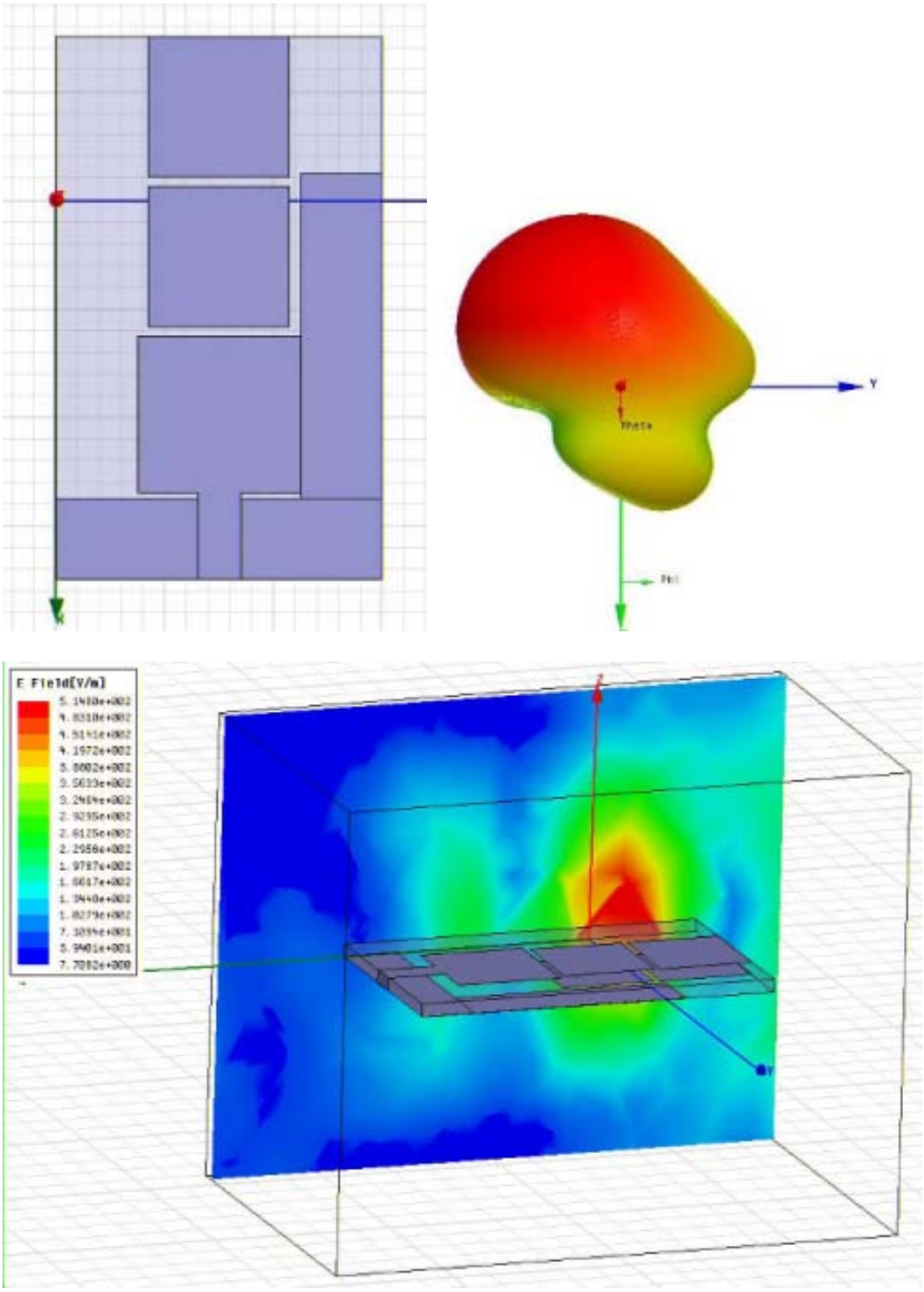

Figure 4-7. Another example of an added stub and its 3-D radiation pattern and the magnitude of the E-field at 4.5 GHz

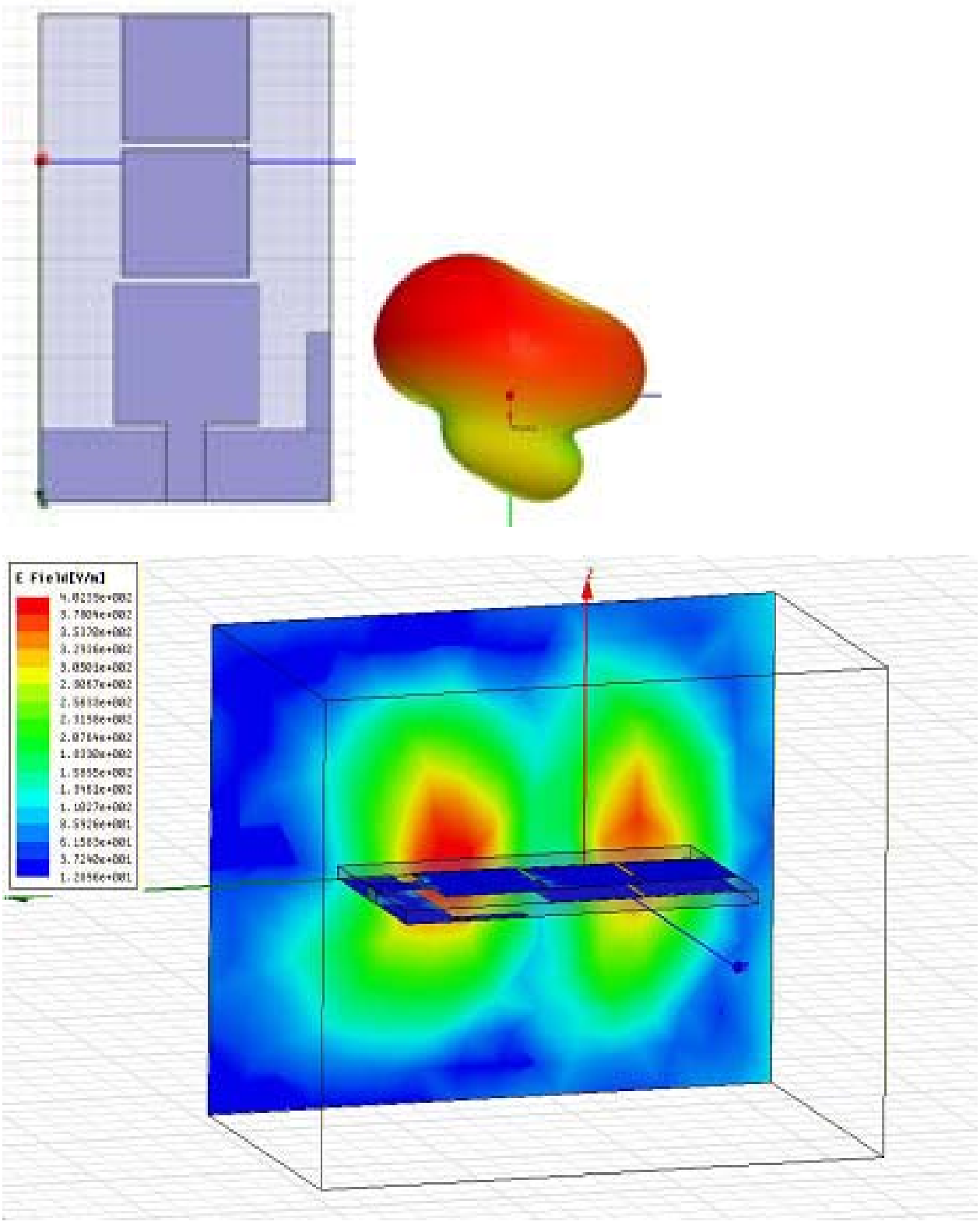

Figure 4-8. Yet another example of an added stub and its 3-D radiation pattern and the magnitude of the E-field at 4.5 GHz

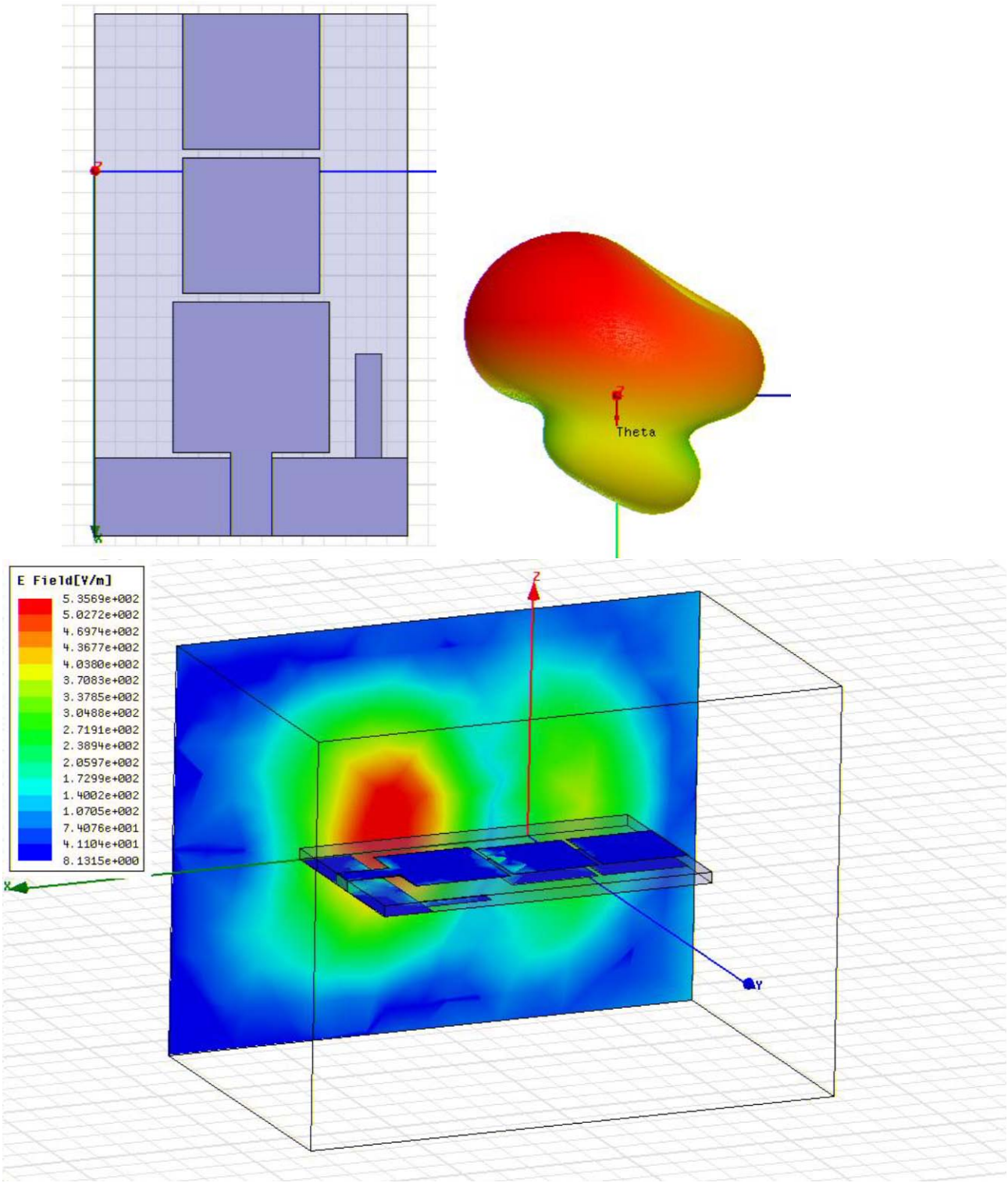

Figure 4-9. Yet another example of an added stub and its 3-D radiation pattern and the magnitude of the E-field at 4.5 GHz

Table 4-2. Trends of E-field distribution and gain as the stub changes

Stub	E-field distribution	Gain
Increase in length	More concentrated on parasitic patch side	Increases
Decrease in width	More concentrated on parasitic patch side	Decreases
Moved towards driven element	More concentrated on driven element	Increases

However, the broadband characteristics or the reflection coefficient has not been considered among the effects of stub because the beam pattern was the main concern of the investigation. Figure 4-10 shows a change in reflection coefficient when the stub was added. As shown in Figure 4-10, the stub compromises the reflection coefficient of the original antenna shown in Figure 3-3, in other words, the broadband is split into two bands.

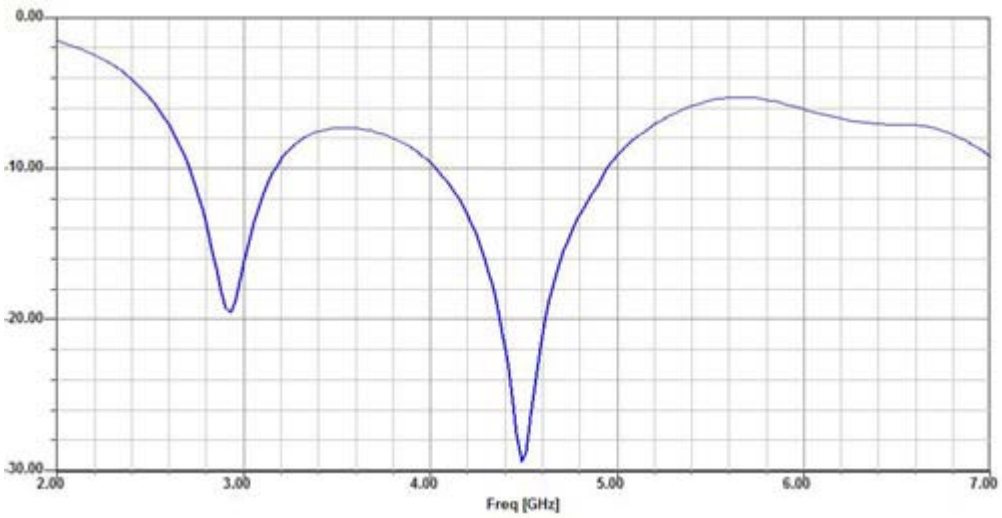

Figure 4-10. Reflection coefficient of the antenna shown in Figure 4-8

After all, it is shown that if the stub shape can be modified in real time, a beam steering can be realized. Especially, if electrical length of the stub can be modified, the beam can be steered electronically. A diode has been used to modify the antenna's electrical length.

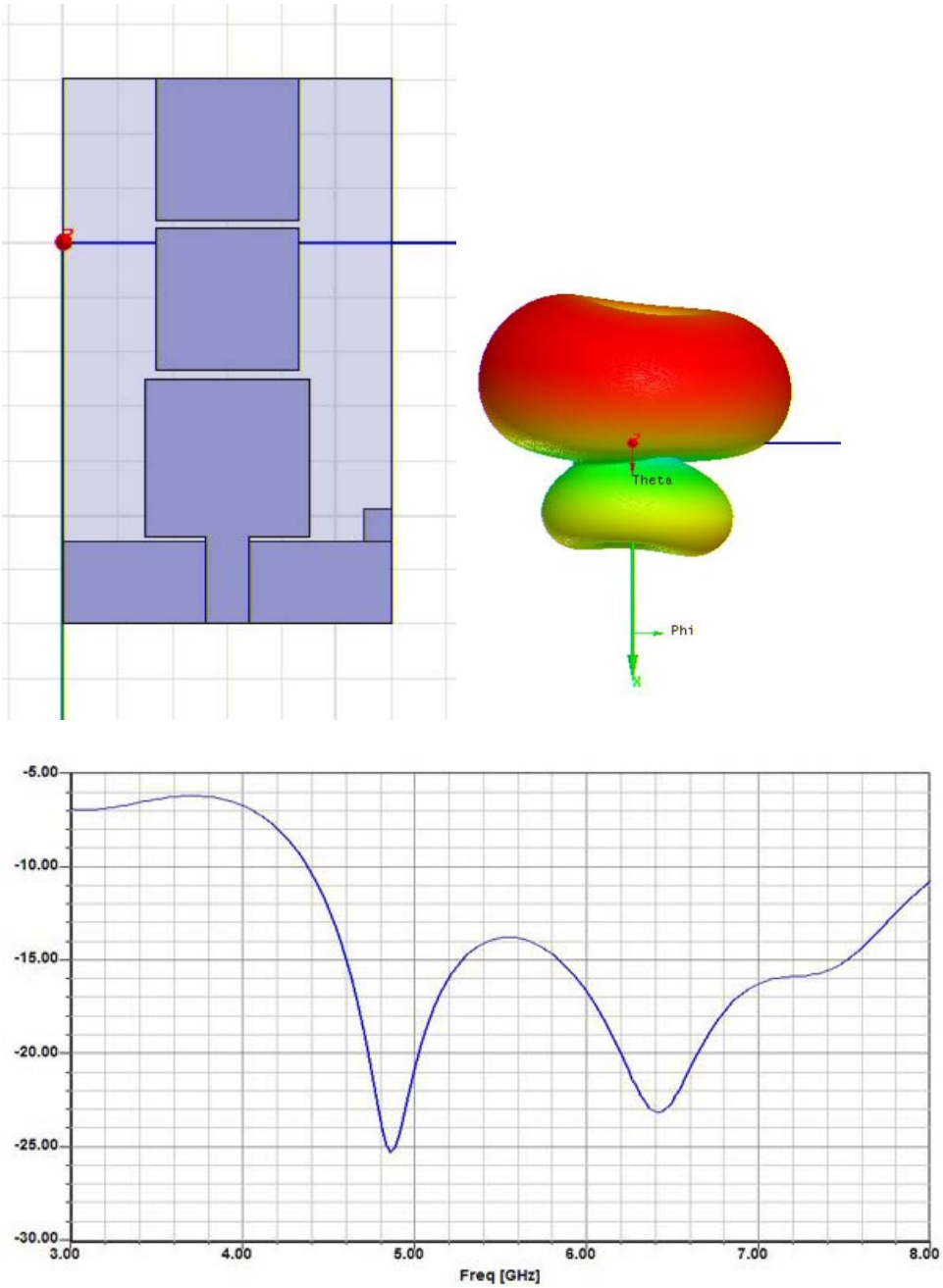

Figure 4-11. Reflection coefficient of an antenna with shortened stub

Figure 4-11 shows a layout of an antenna with a shortened stub compared to the stub shown in Figure 4-10. This stub has a size of 3 mm X 3mm. The short stub recovers the original broadband characteristic (4.3 – 7 GHz), however, as seen in the 3D radiation pattern of Figure 4-11, the beam steering became compromised i.e.,

weakly tilted beam. As shown in the Figure 4-10 and Figure 4-11, as the stub changes, not only the beam pattern changes, but also the reflection coefficient changes. Again, it can be seen that these antenna parameters are in a trade-off relationship. It requires numerous simulations to optimize the stub shape that affects the beam pattern while maintaining the broadband bandwidth. Figure 4-12 summarizes the relationship between stub, s11, and radiation pattern in a concise manner.

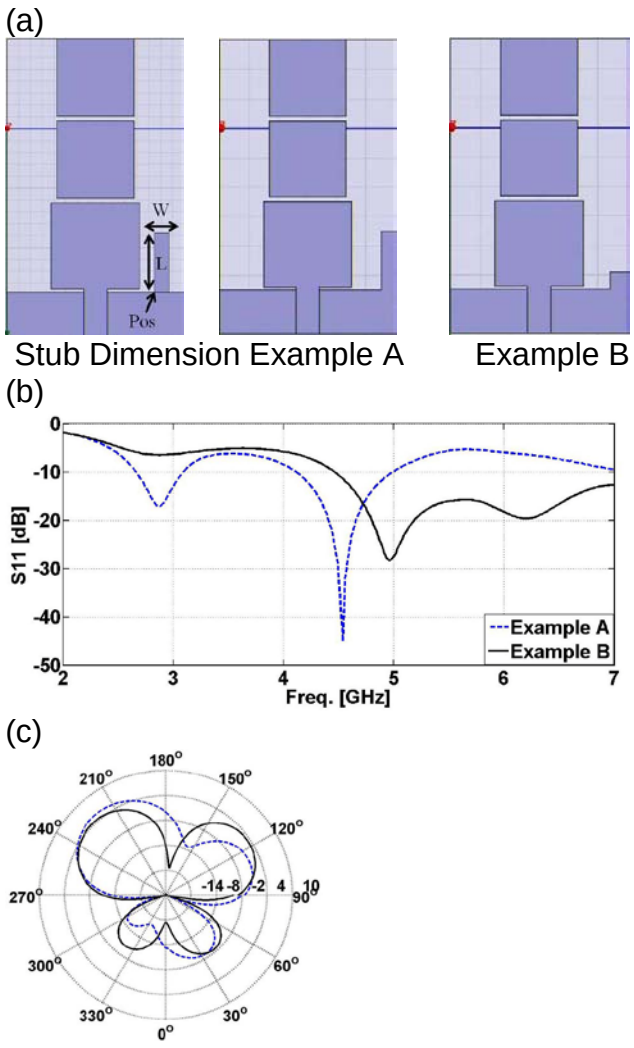

Figure 4-12. Broadband microstrip antenna with added stub; (a) Stub dimension, Example A: W=2.5 mm, L= 10 mm, Pos=12.5mm (from center), Example B: W=3 mm, L= 3 mm, Pos=12 mm; (b) Reflection coefficient; (c) Radiation pattern

4.5 Simulated Layout of Various Stubs, Its Beam Pattern, and Its S11

In 4.4, the layout that has only one stub on one side of the antenna has been simulated. In this section, simulation layouts that include stubs on both sides to perform horizontal beam steering in both directions are shown in detail. Also, in 4.4, the s11 was not considered, but for optimized layout, the s11 needs to be considered every time a modification is made. Thus, the following simulations include layout, its radiation patterns, and its reflection coefficient.

Description of the design 1: Stub shape is modified to investigate the influence of stub shape on the beam pattern. The stub is formed by uniting two rectangles of trace layers with finite conductivity. The dimensions of the two rectangles are 2.5 mm X 3.5 mm and 2.5 mm X 7 mm. The beam pattern shown is sampled at 3.5 GHz and has a gain value of 4dB. The shape change does not significantly change the beam pattern from the optimized layout.

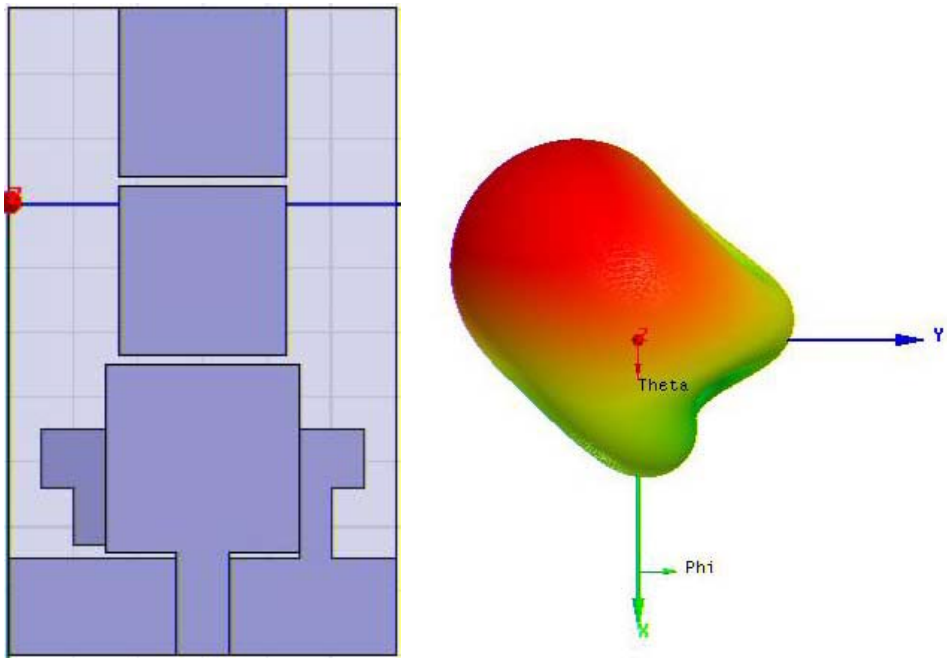

Figure 4-13. Design 1: Stub shape variation

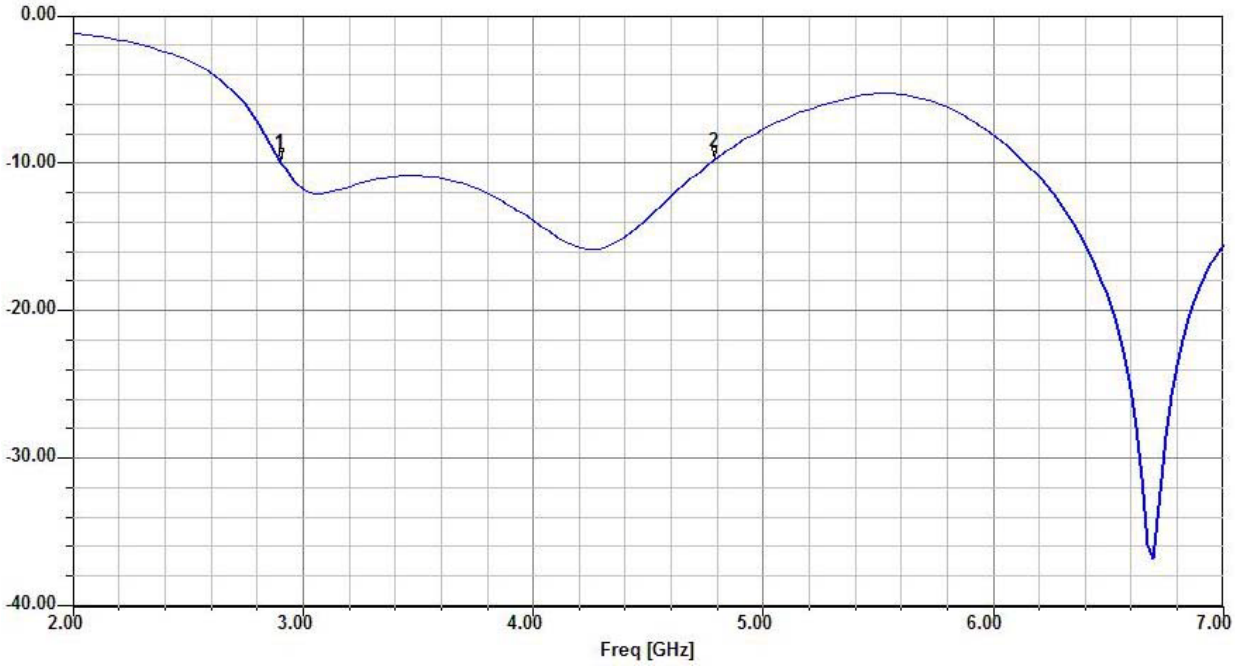

Figure 4-13. Continued

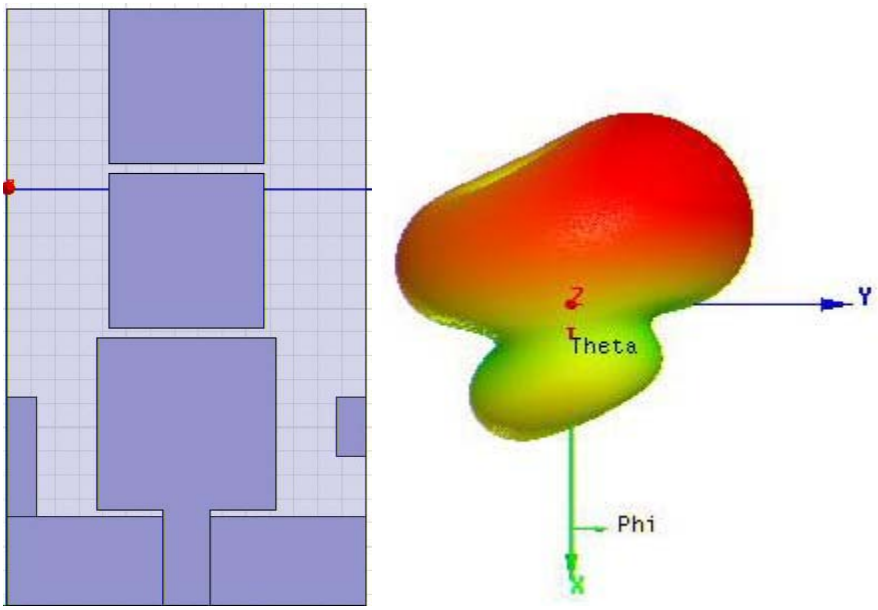

Figure 4-14. Design 2: Stub location and gap

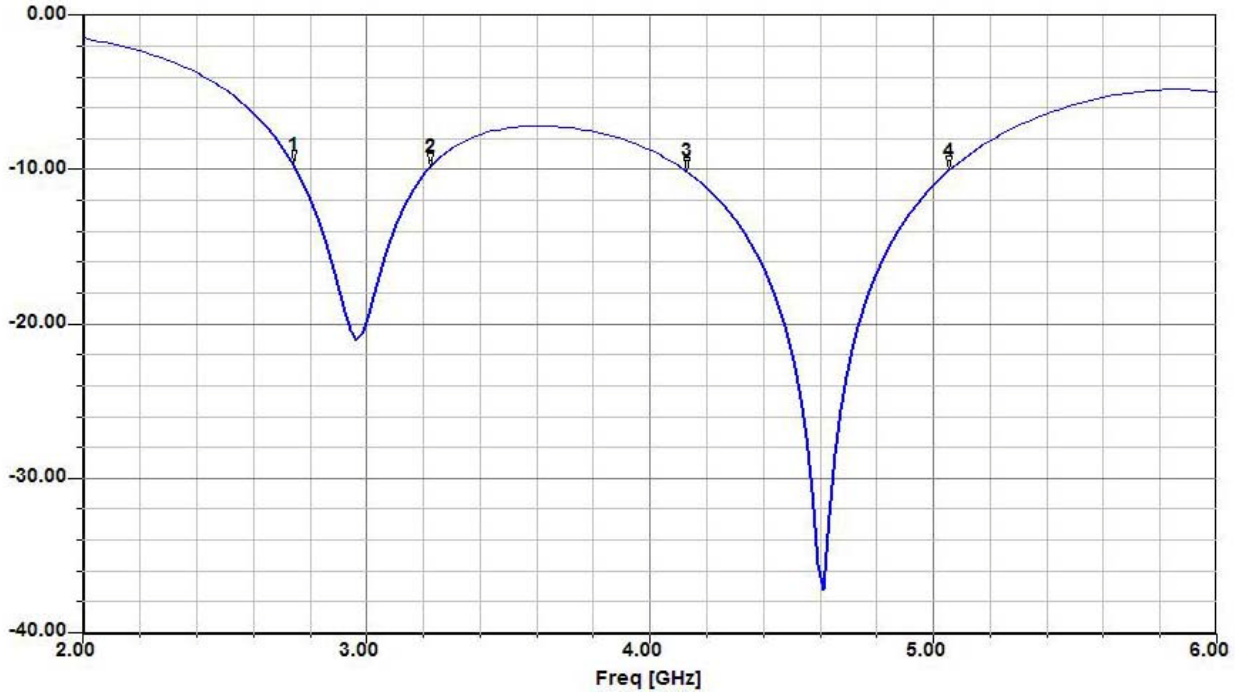

Figure 4-14. Continued

Description of the design 2: The stub dimension is 2.5 mm X 10 mm as in the optimized layout, but for the OFF status stub, the gap between the stub and partial ground plane is 5mm, not 1 mm as in the optimized layout. A strong beam steering is observed with a gain value of 5.6 dB. However, the s11 is negatively affected as shown.

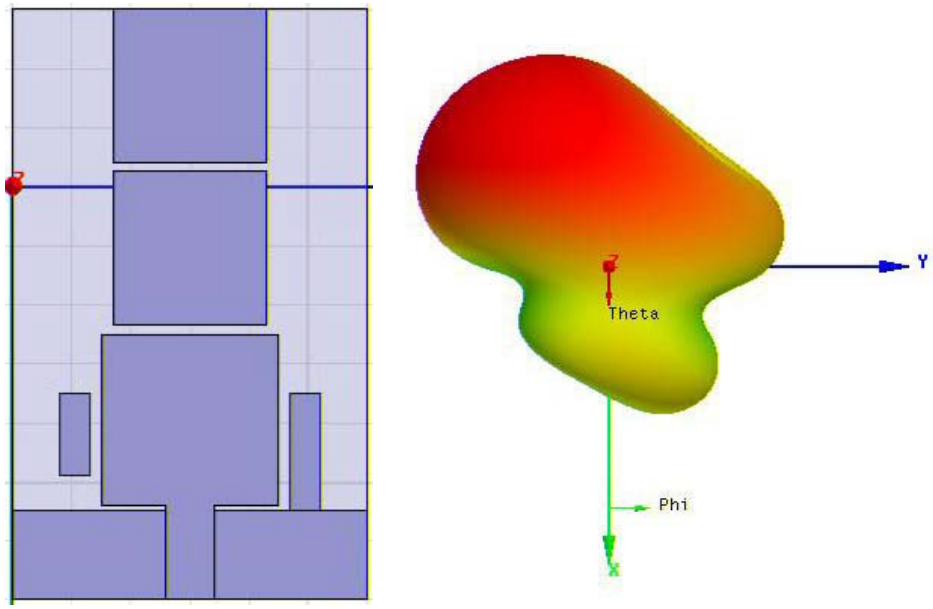

Figure 4-15. Design 3: Stub location and gap

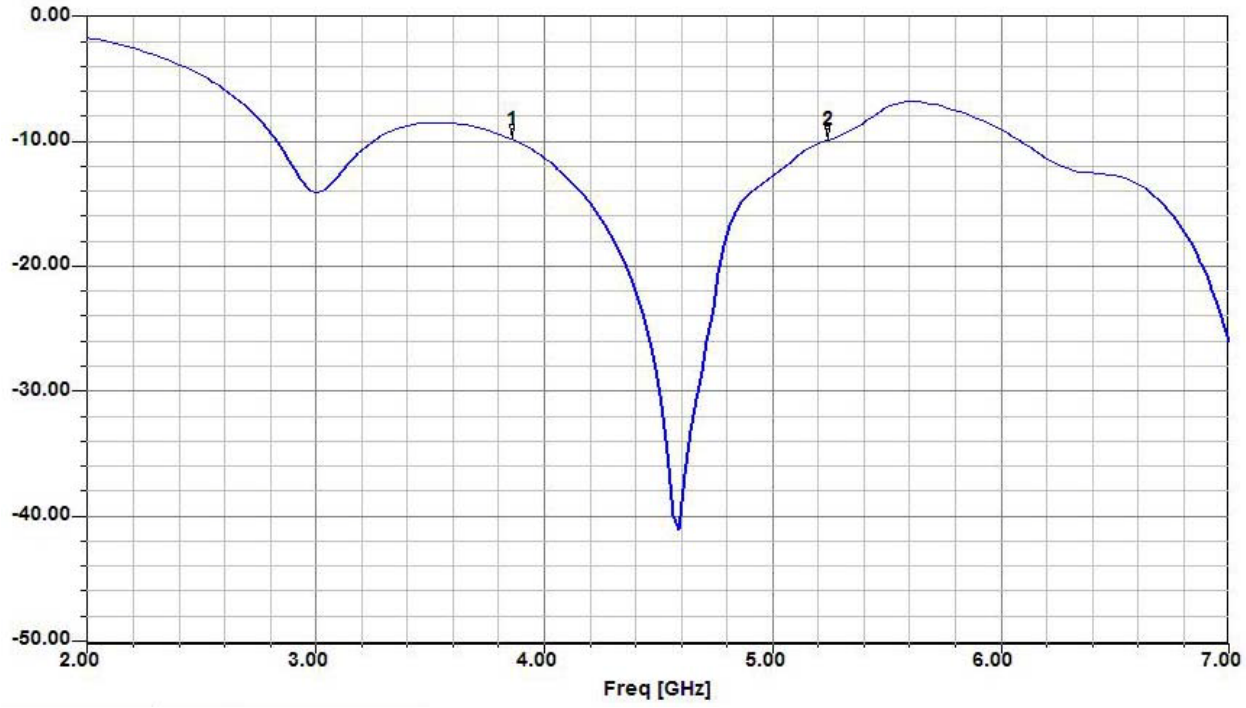

Figure 4-15. Continued

Description of the design 3: The stub dimension is 2.5 mm X 10 mm. For the OFF status stub, the gap between the stub and partial ground plane is 3mm. The location of the stub is 4 mm away from the side. A strong beam steering of 5.7 dB is observed at a sampled frequency of 4.5 GHz. However, the s11 is negatively affected as shown.

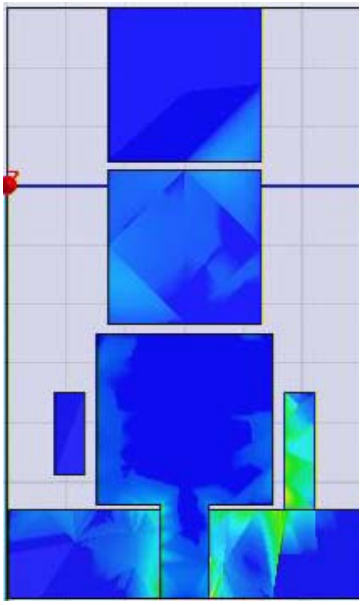

Figure 4-16. Surface current density of Design 3

Figure 4-16 shows an additional simulation result or a surface current density of the design 3. In this figure, it is clearly shown that the ON status stub has higher surface current density than the OFF status stub, thus, it results in beam steering.

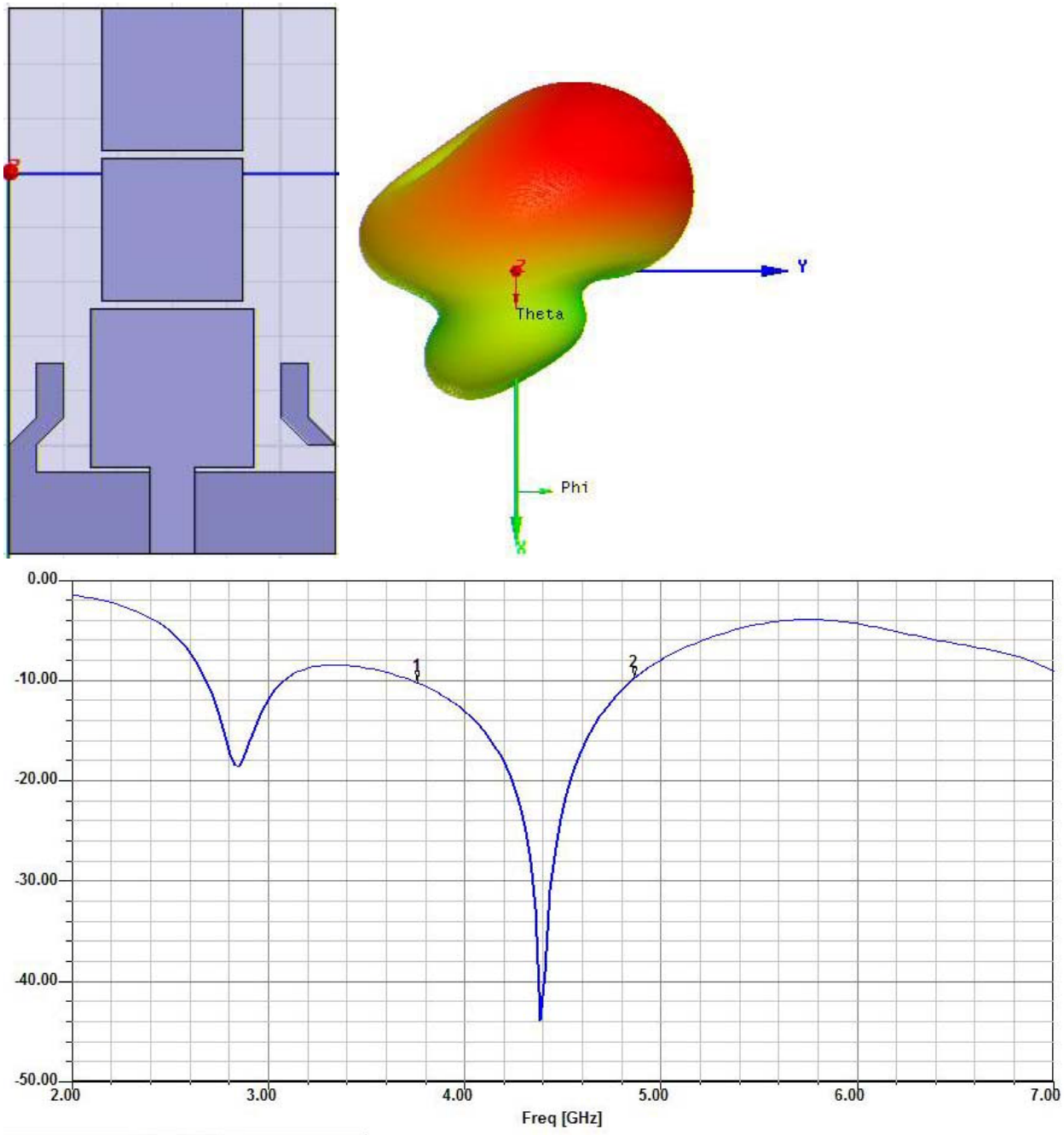

Figure 4-17. Design 4: Stub shape variation

Description of the design 4: It's another stub shape variation. The stub is mitered. The mitered angle is 45˚ and width of the stub is 2.5 mm. The part of the stub after mitered is 5mm long and 2.5 mm away from the main patch. The OFF status stub is 2.5 mm away from the partial ground plane. A strong beam steering is observed at 4.5 GHz with a gain value of 5.66 dB. However, the s11 is negatively affected as shown.

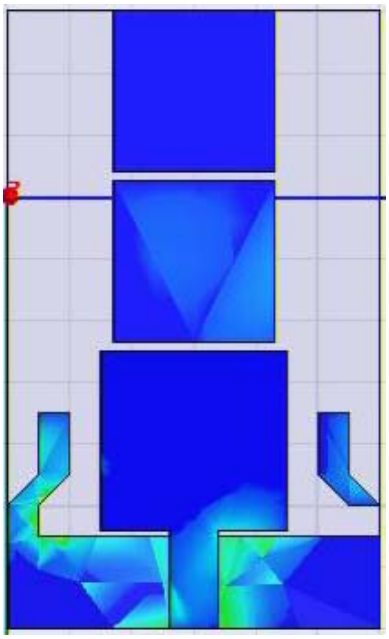

Figure 4-18. Surface current density of Design 4

Figure 4-18 shows an additional simulation result or a surface current density of the design 4. In this figure, it is clearly shown that the ON status stub has higher surface current density than the OFF status stub. However, there is still weak current on the OFF status stub due to coupling between the OFF status stub and the main patch and the partial ground plane.

Description of the design 5: It is a slight change from design 4. In detail, the stub is mitered at two points and the distance between the main patch and the mitered stub is 1 mm. The other dimensions of the stub remain same as design 4. Still a strong beam

steering is observed at 4.5 GHz with a gain value of 5.62 dB. However, the s11 is negatively affected as shown.

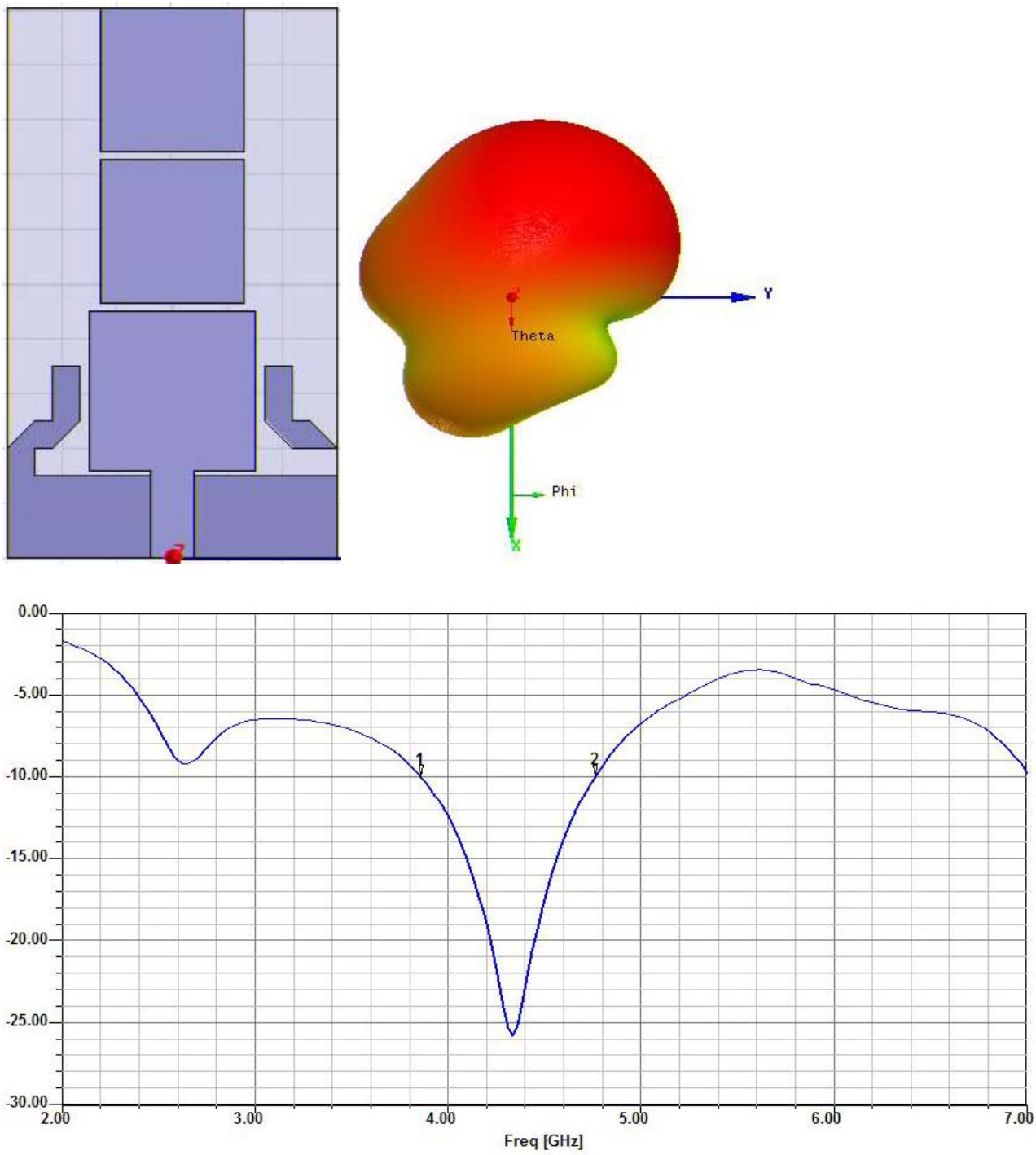

Figure 4-19. Design 5: Stub shape variation

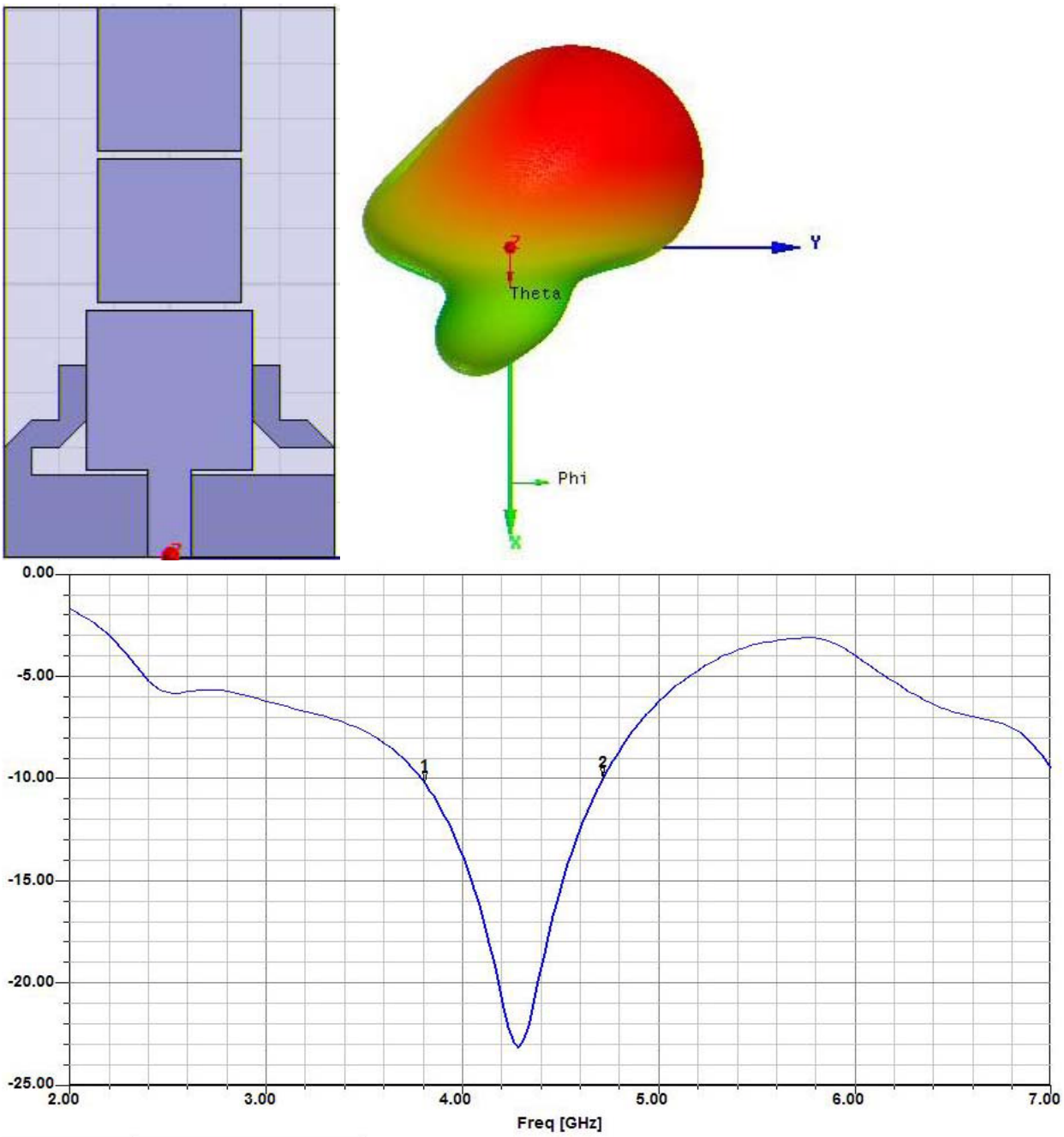

Figure 4-20. Design 6: Stub shape variation

Description of the design 6: It's another stub shape variation. In particular, it's yet another slight change from design 4, i.e., the distance between the main patch and the mitered stub is now 0 mm. The other dimensions of the stub remain same as design 4. Still a beam steering is observed at 4 GHz with a gain value of 5.1 dB. However, the s11 is negatively affected as shown.

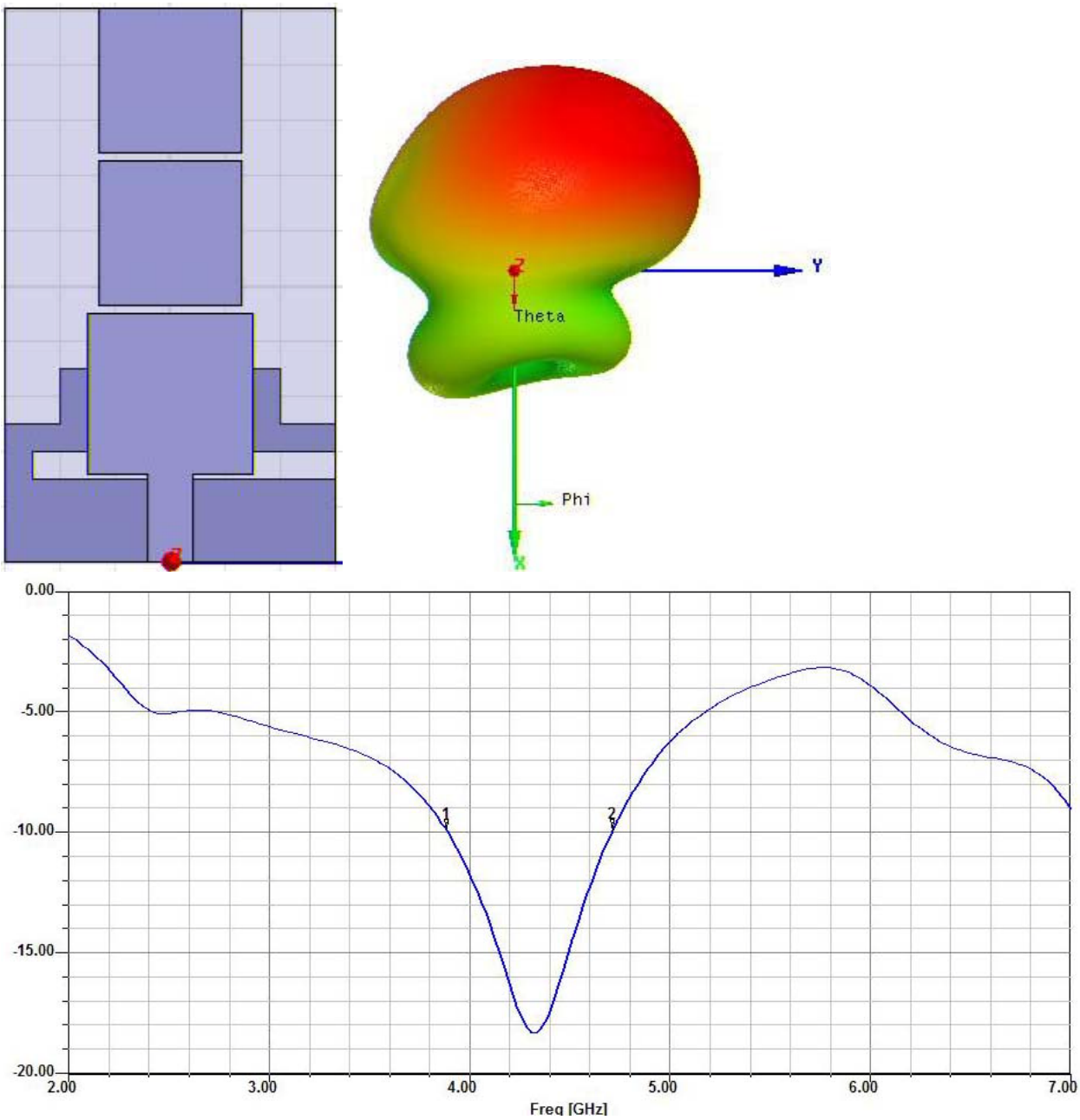

Figure 4-21. Design 7: Stub shape variation

Description of the design 7: Here, the stub is bent but not mitered. The width of the stub is 2.5 mm and the tip of the stub is 10 mm away from partial ground plane and the bent part of stub is 2.5 mm away from partial ground plane and the gap between the stub and the main patch is 0 mm. A beam steering is observed at a sampled 4.5 GHz with a gain value of 5.3 dB. However, the s11 is negatively affected as shown.

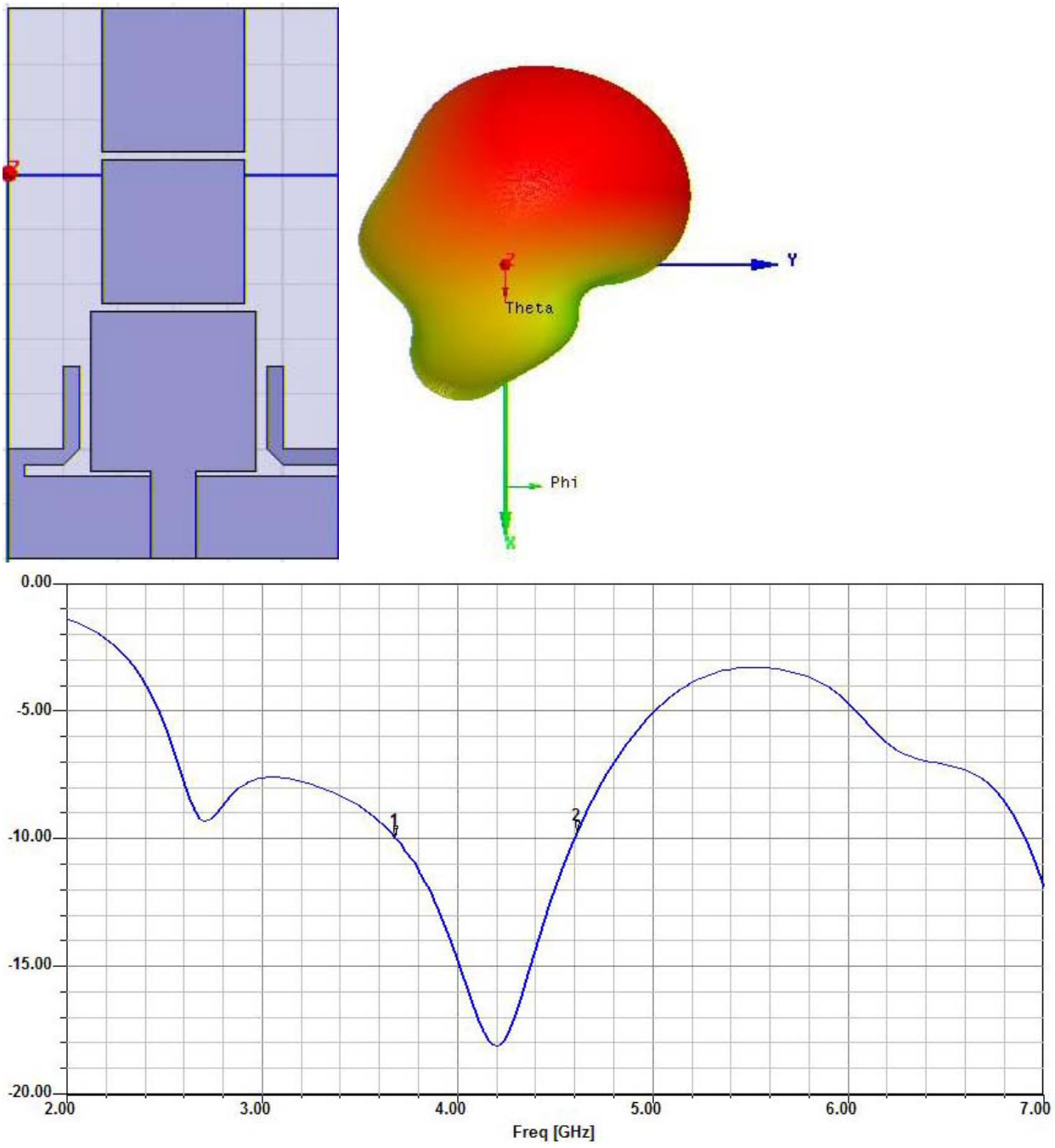

Figure 4-22. Design 8: Stub shape variation

Description of the design 8: The stub width is reduced to 1.5 mm and mitered. The distance between the main patch and the stub is 1mm. The OFF status stub is 1mm away from the partial ground plane. A beam steering is observed at a sampled

frequency of 4.5 GHz with a gain value of 5.13 dB. However, the s11 is negatively affected as shown.

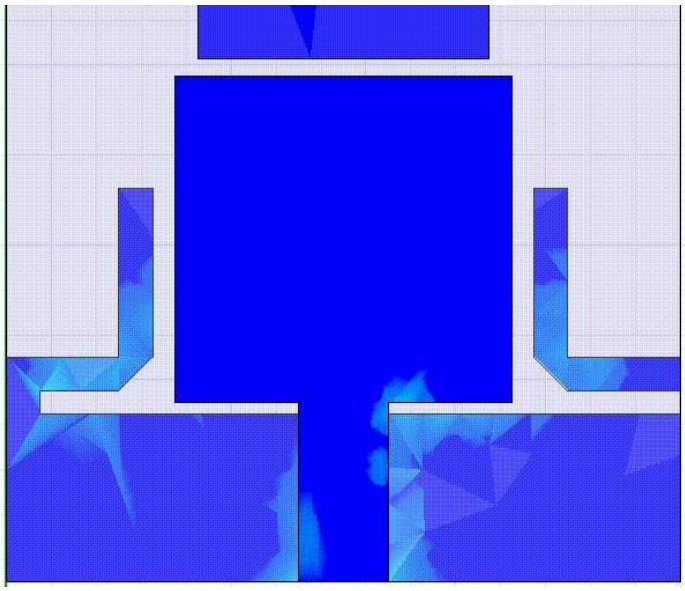

Figure 4-23. Design 8: Stub shape variation

Figure 4-23 shows a zoomed in view of the surface current of the design 8. Even if there is current in the OFF status stub, a beam steering occurs because it's less than the current on ON status stub.

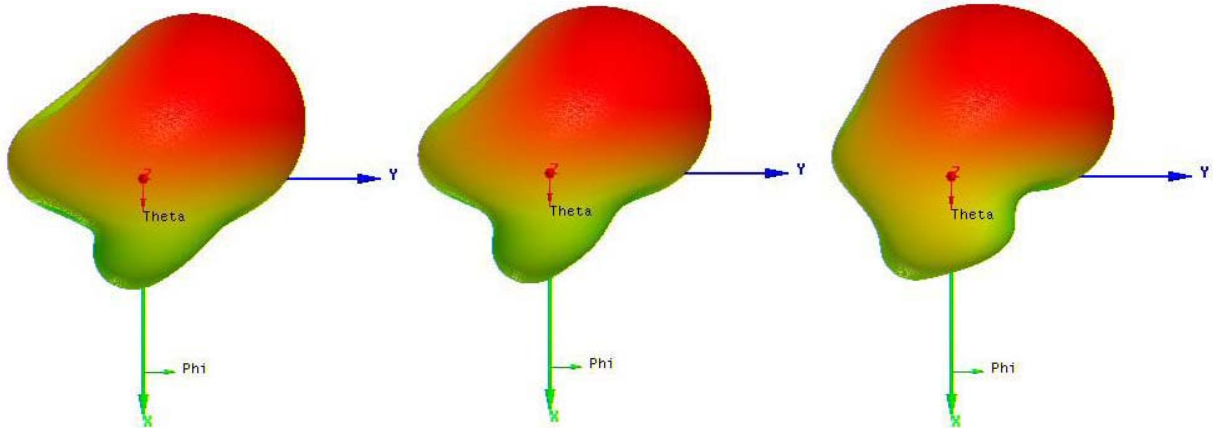

Figure 4-24. Beam patterns of design 8 at different frequencies

Figure 4-24 shows beam patterns of design 8 at different frequencies. In particular, from left to right, 4.5dB at 3.8GHz, 4.8dB at 4GHz, and 4.9dB at 4.3GHz. It can be seen that the gain increases as the s11 decreases.

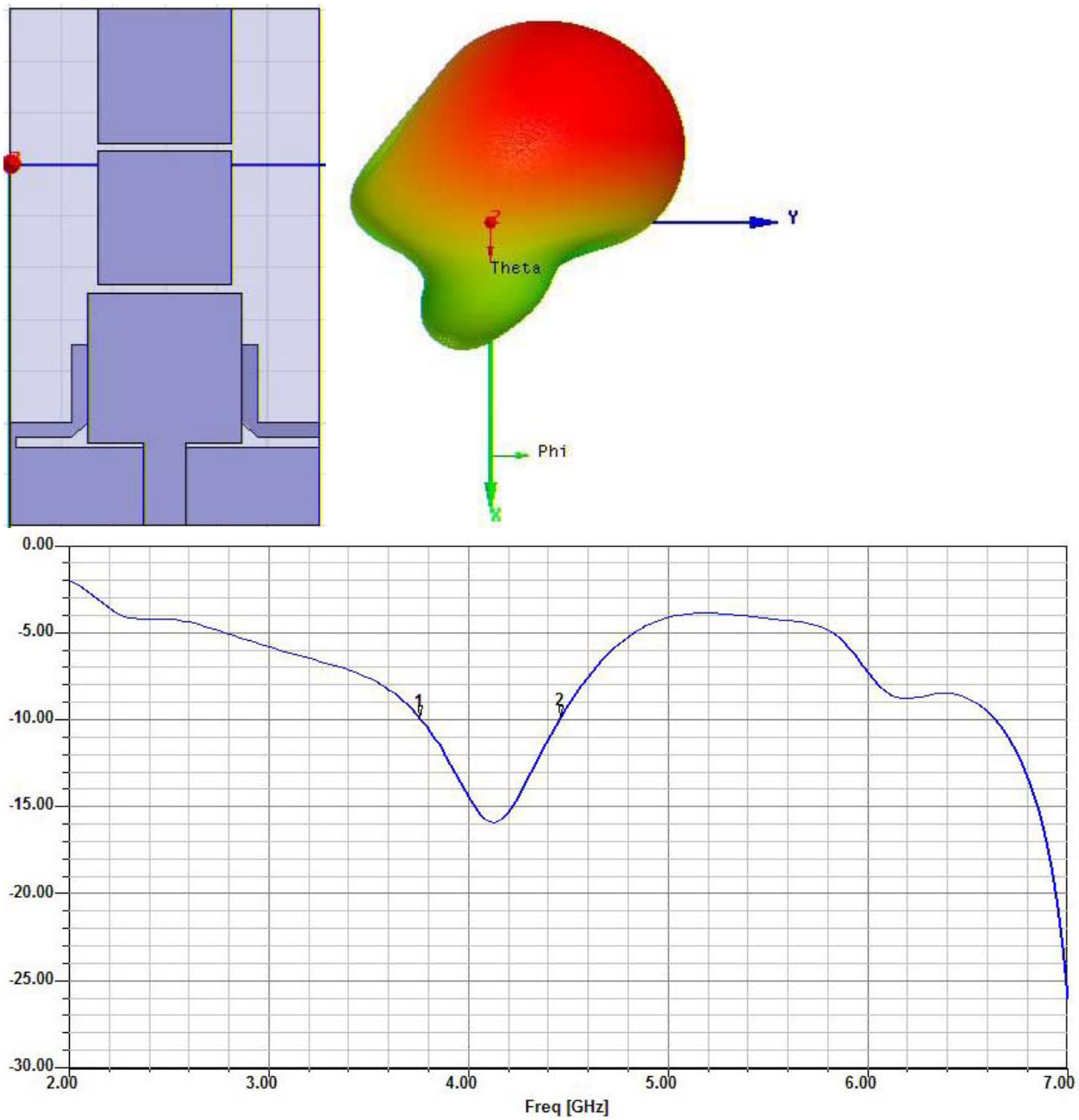

Figure 4-25. Design 9: Stub shape variation

Description of the design 9: The difference between the design 8 and design 9 is that in design 9, the connection between the stub and the partial ground plane has reduced width. In design 8, the ON state connection dimension was 1 mm X 1 mm. In design 9, it is 1 mm X 0.5 mm. Even with the narrowed connection to the ON status

stub, beam steering is observed. A gain value of 4.85 dB is shown at a sampled frequency of 4 GHz.

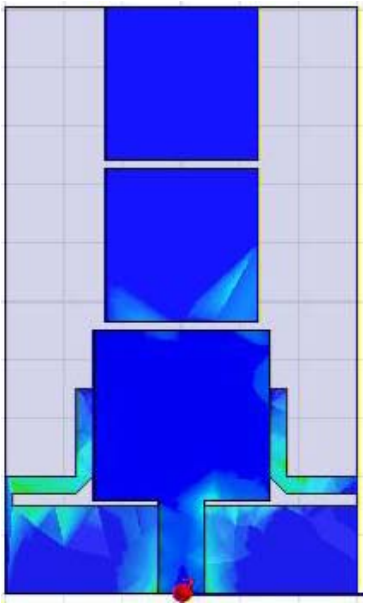

Figure 4-26. Surface current density of Design 9

Figure 4-26 shows the surface current of the design 9. Even if the ON status connection is reduced, a higher current is flowing through that connection than the OFF stub, where current exists through coupling. Thus, beam steering occurs.

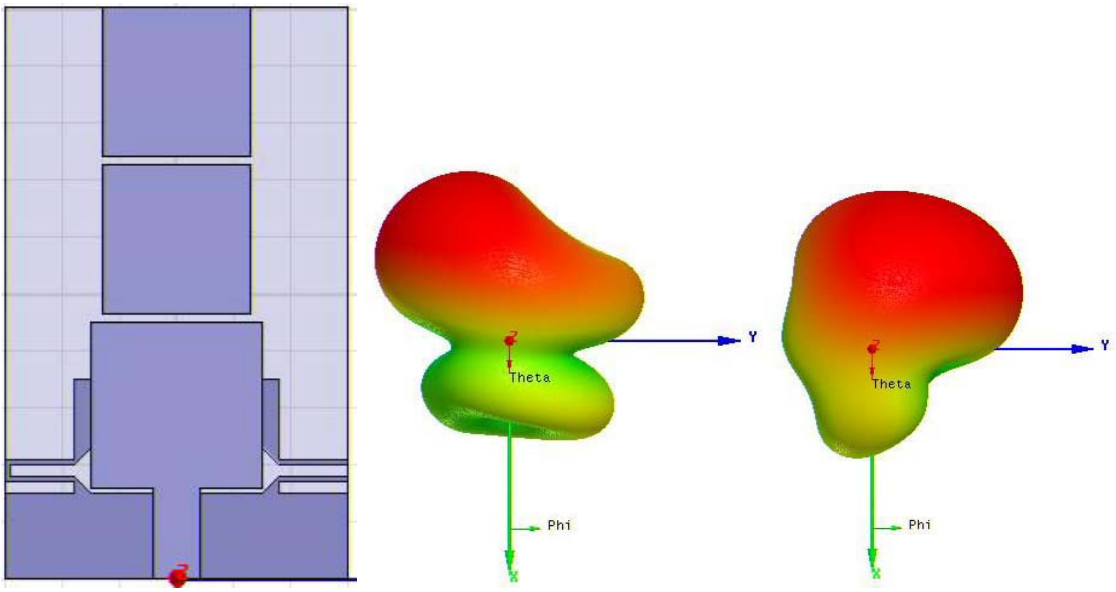

Figure 4-27. Design 10: Stub shape variation

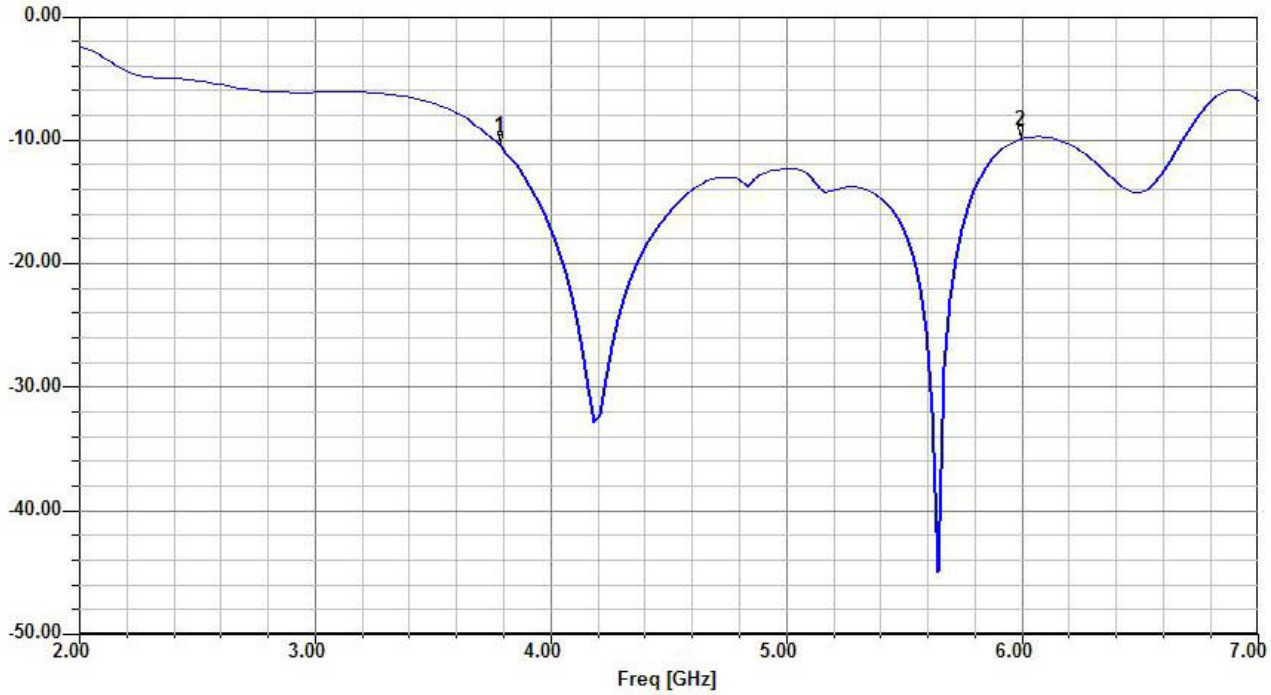

Figure 4-27. Continued

Description of the design 10: The stub is modified and bent at four points. This layout was tried to position the ON/OFF switching to the side. It was to see if this approach can minimize the current flowing to the OFF status stub. Very interesting results are shown. In detail, when the stubs are modified greatly, i.e., bent at four points, the beam steering become inconsistent, i.e., the beam is steered towards the connected ON status stub at a certain frequency and the beam is steered towards the OFF status stub at other frequency. A very strong beam steering is observed at 5 GHz with a gain value of 6.23 dB(left), while a weak beam steering is observed at 4GHz with a gain value of 4dB(right). Also, the broadband (3.8GHz ~6.7GHz) is observed as shown.

Figure 4-28 shows the surface current of the design 10 at 4.5 GHz. Substantial amount of current is flowing to the OFF status stub through coupling and it is the possible reason for the inconsistent beam steering at different frequencies.

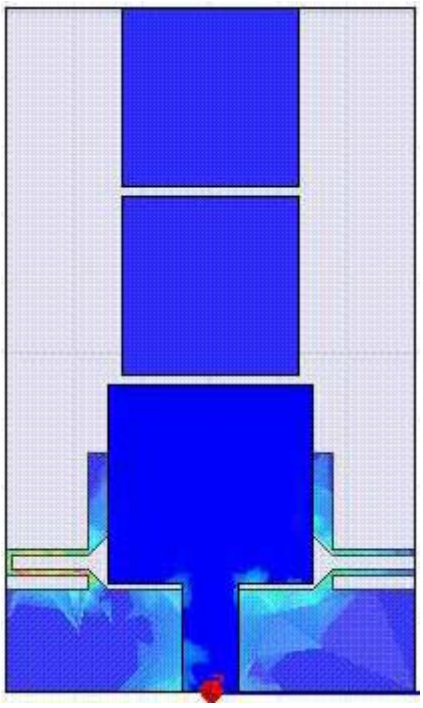

Figure 4-28. Surface current density of Design 10

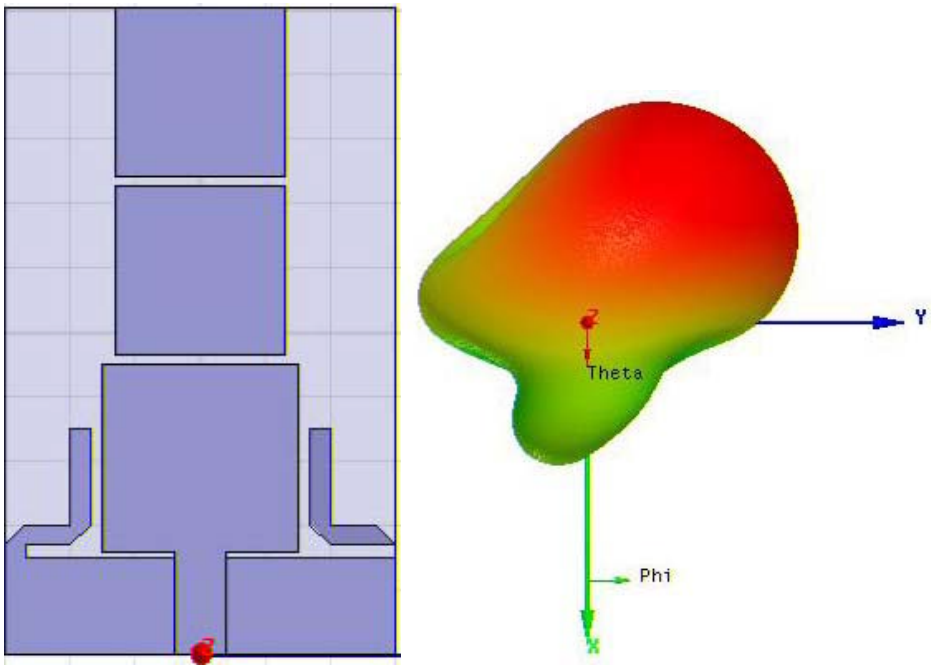

Figure 4-29. Design 11: Stub shape variation

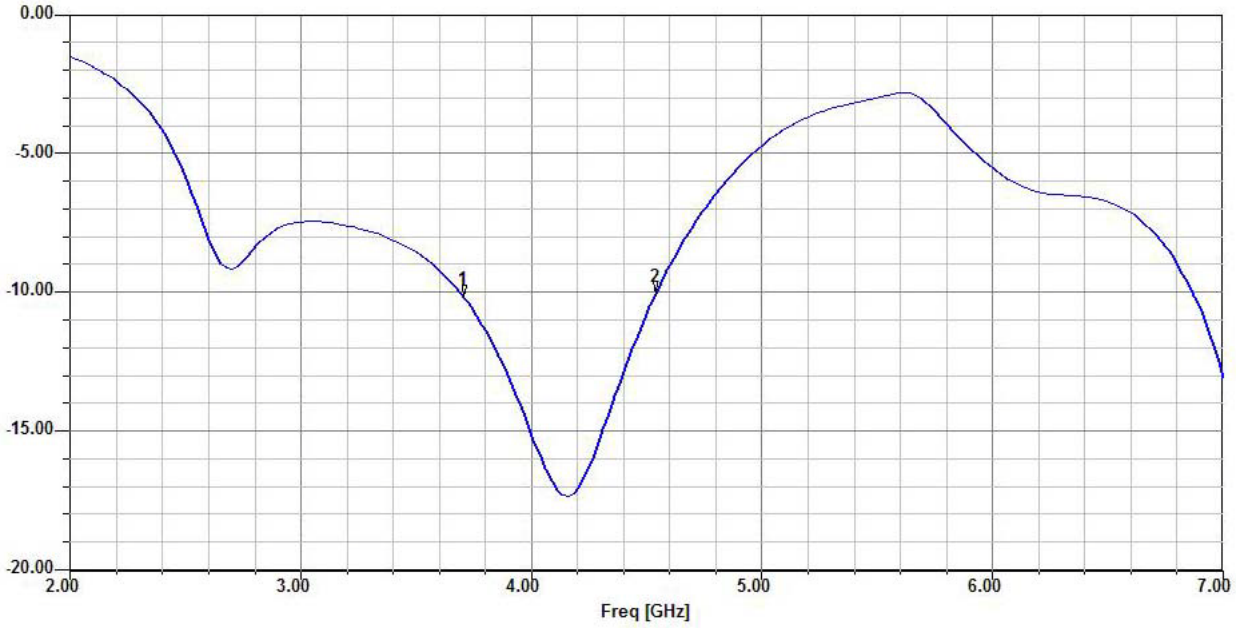

Figure 4-29. Continued

Description of the design 11: The stub width is 1.5 mm and mitered at two points to position the switching location at sides of the antenna. A beam steering is observed at a sampled frequency of 4.5 GHz with a gain value of 4.9 dB. However, the s11 became narrow.

4.6 Simulated Layout of Various Parasitic Patches, Its Beam Pattern, and Its S11

Stub that is connected to the partial ground plane can steer beam horizontally as shown in 4.5. In addition, parasitic patches can be also used to steer beam horizontally. The advantage of the beam steering using the parasitic patch, instead of stub, is that the parasitic patch does not affect the s11 significantly as stubs do. The disadvantage of beam steering using parasitic patch is that the beam steering is relatively weaker than the beam steering using stubs and the switching might be difficult to implement in fabrication.

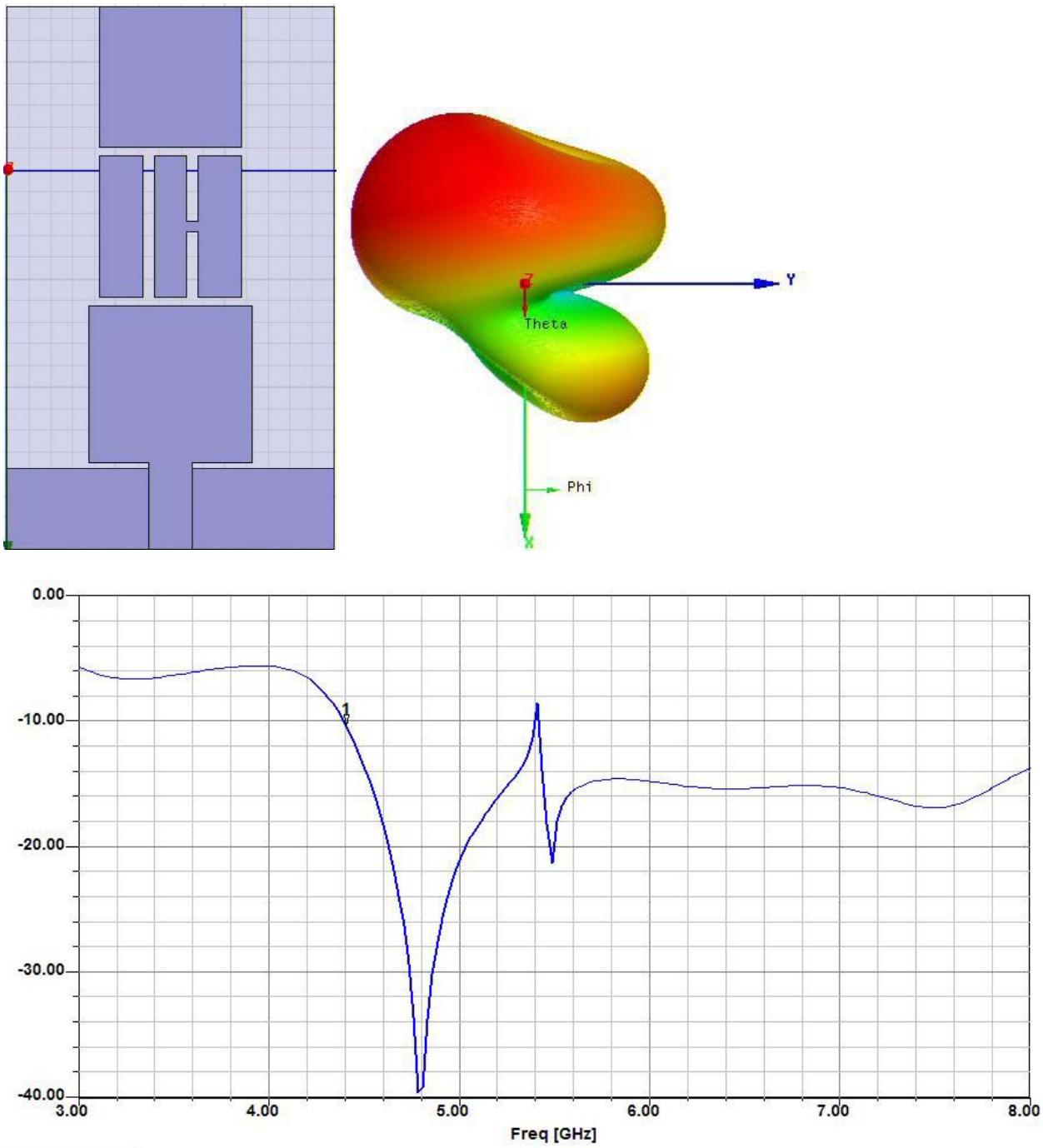

Figure 4-30. Design 12: Parasitic patch variation

Description of the design 12: The parasitic patch is modified to show beam steering. The ON status side of the parasitic patch is connected to the middle piece of the parasitic patch. The connection is 1 mm X 1 mm. The middle piece is 3 mm X 13 mm. The horizontal beam steering shown is sampled at 4.5 GHz and show 4.9 dB of

gain. S11 remains almost unchanged from the broadband directional microstrip antenna. Description of the design 13: The parasitic patch is modified to show horizontal beam steering. The ON status side of the parasitic patch is connected to the middle

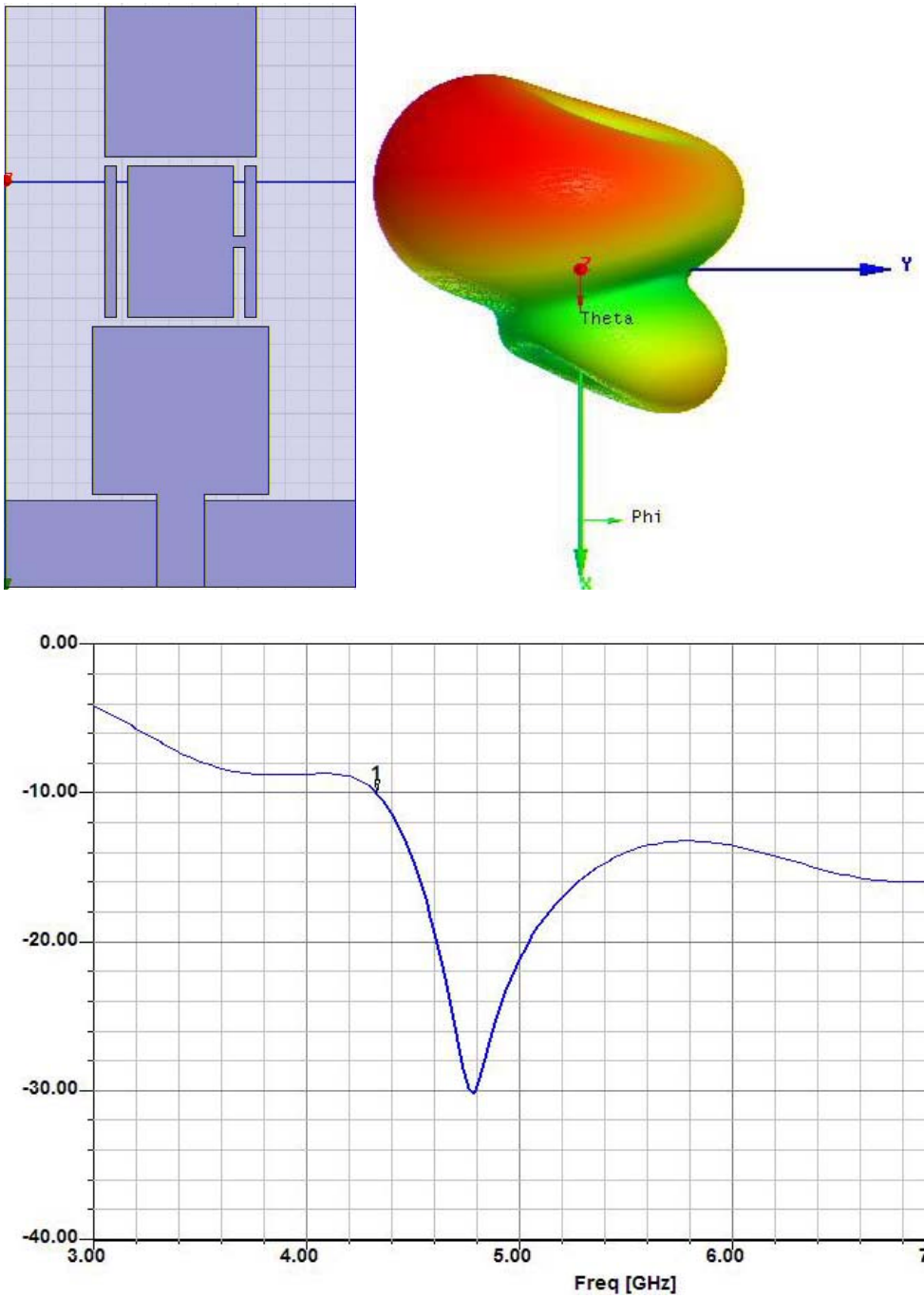

Figure 4-31. Design 13: Parasitic patch variation

piece of the parasitic patch. The connection is 1 mm X 1 mm. The middle piece is 9 mm X 13 mm. The beam steering shown is sampled at 5 GHz and show 4.8 dB of gain. S11 remains almost unchanged from the broadband directional microstrip antenna.

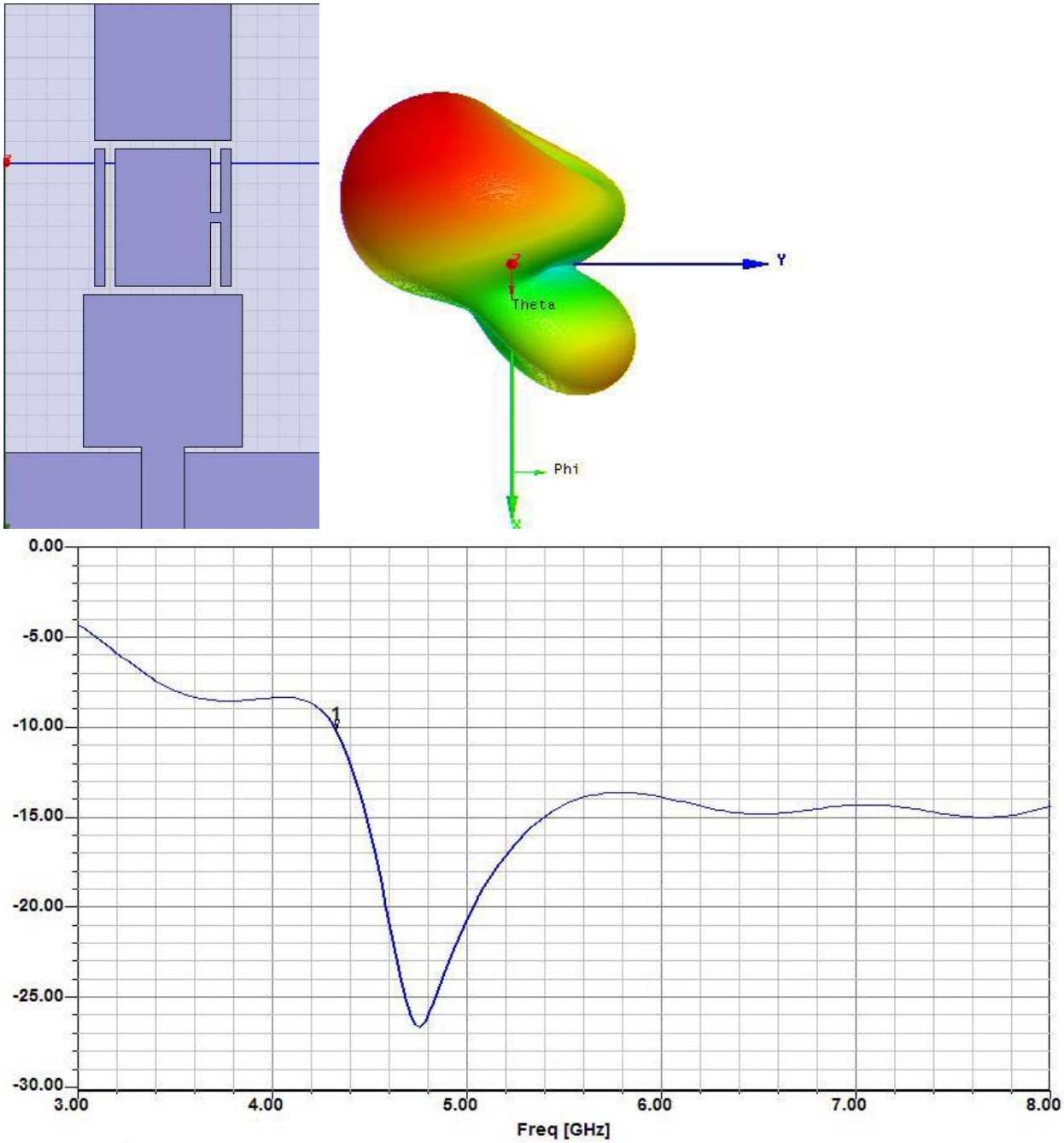

Figure 4-32. Design 14: Parasitic patch variation

Description of the design 14: The parasitic patch is modified to show horizontal beam steering. The layout is same as design 13 except there is no bottom parasitic patch. Compared to design 13, which has both top and bottom parasitic patches, the design 14 shows gain value of 4.6dB at 5GHz. Thus, it can be determined that the bottom parasitic patch's contribution to the gain is 0.2 dB. S11 remains almost unchanged from the broadband directional microstrip antenna.

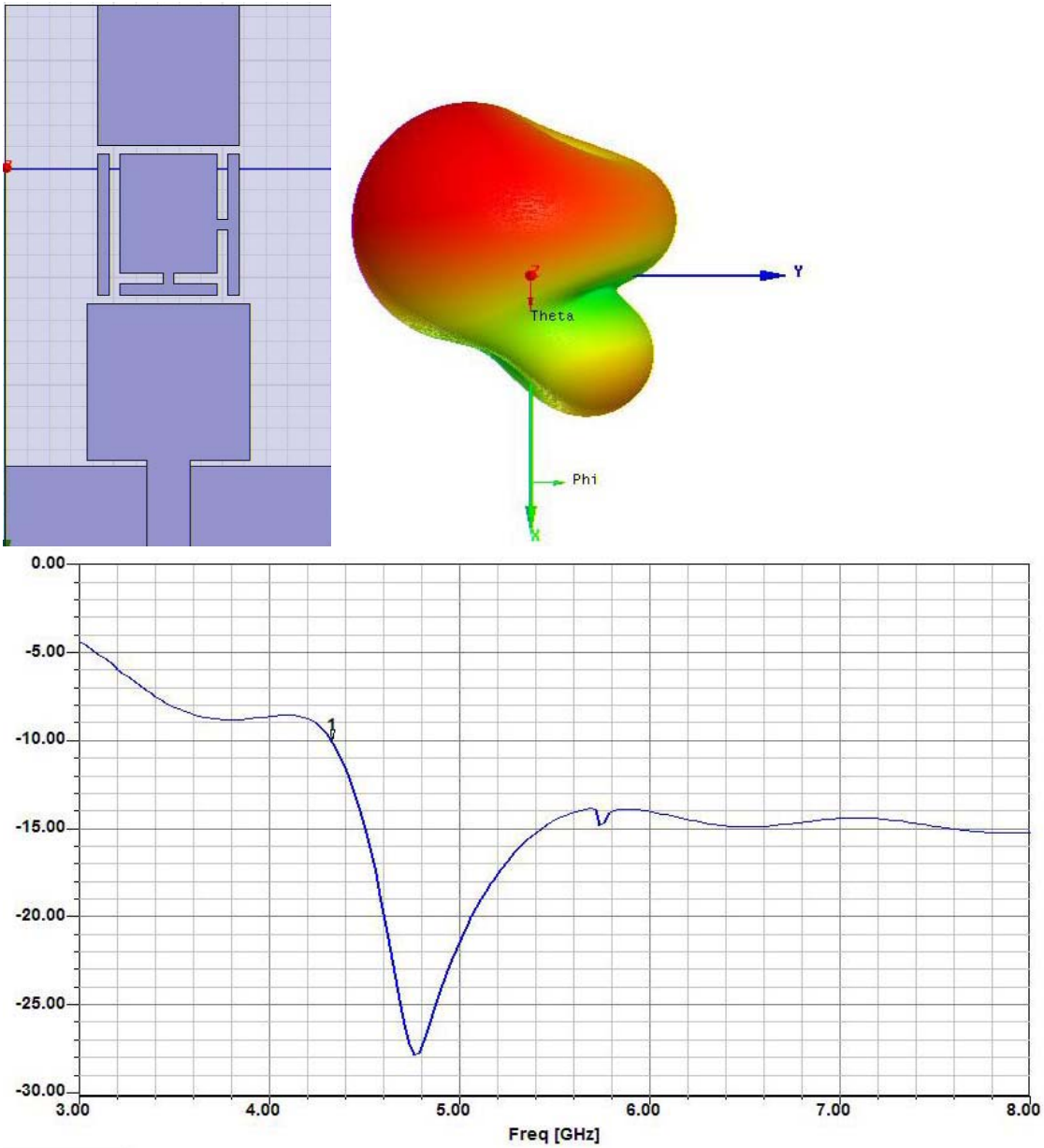

Figure 4-33. Design 15: Parasitic patch variation

Description of the design 15: The parasitic patch is modified to show horizontal beam steering. The layout has two switching positions, which are shown as two of the 1 mm X 1mm squares. This layout was simulated to see if this can increase gain further. However, the gain was only 4.6 dB at a sample frequency of 4.5 GHz. S11 remains almost unchanged from the broadband directional microstrip antenna.

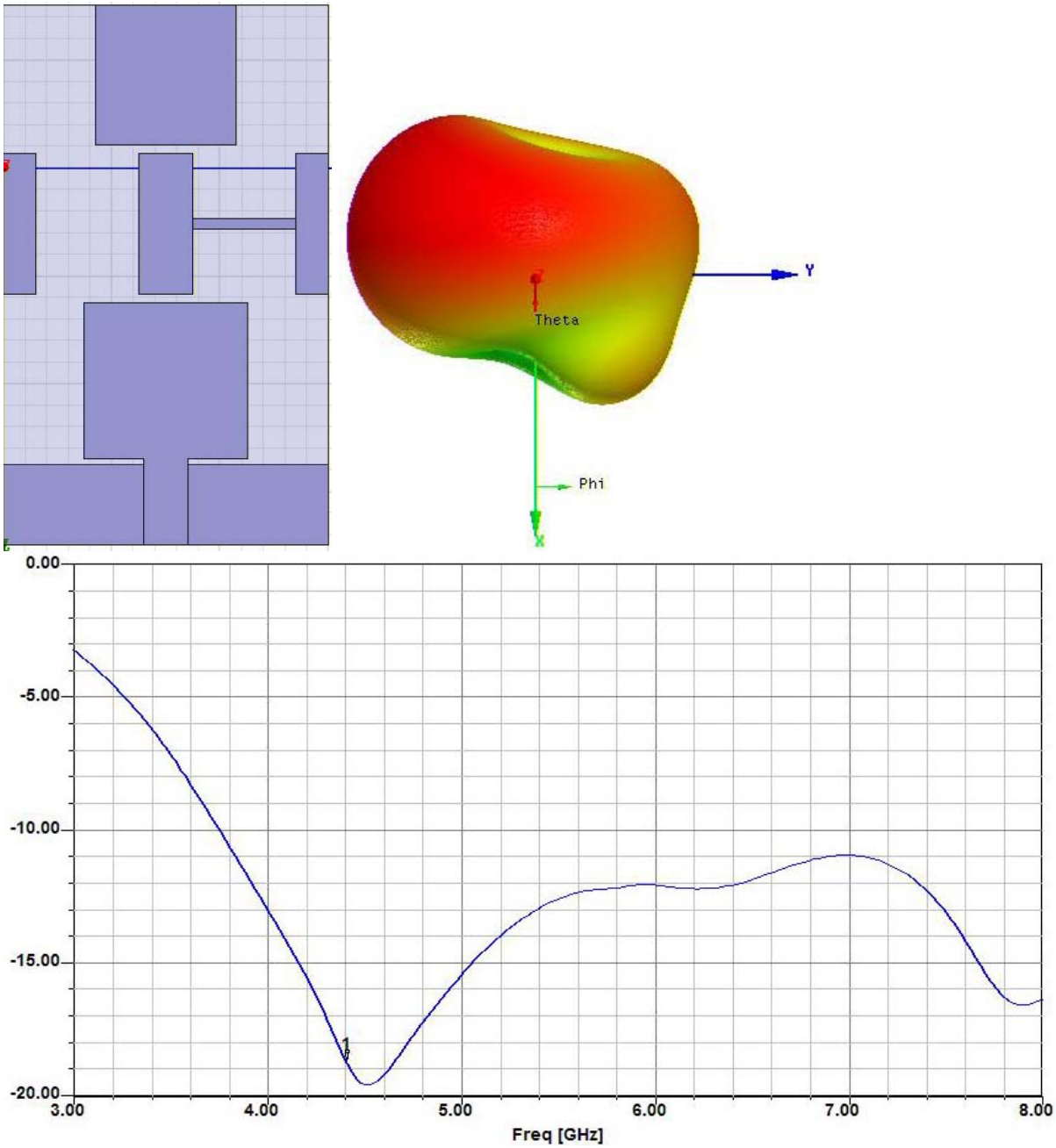

Figure 4-34. Design 16: Parasitic patch variation

Description of the design 16: The parasitic patch is modified to show beam steering. The layout has two pieces of patches on both sides of middle piece of patch. The two pieces of patches on each side are 3 mm X 13 mm and the middle piece is 5mm X 13mm. The connection to the middle patch is 9.5mm X 1mm. A weak beam steering is observed. The gain was 4 dB at a sample frequency of 4.5 GHz. S11 remains almost unchanged from the broadband directional microstrip antenna.

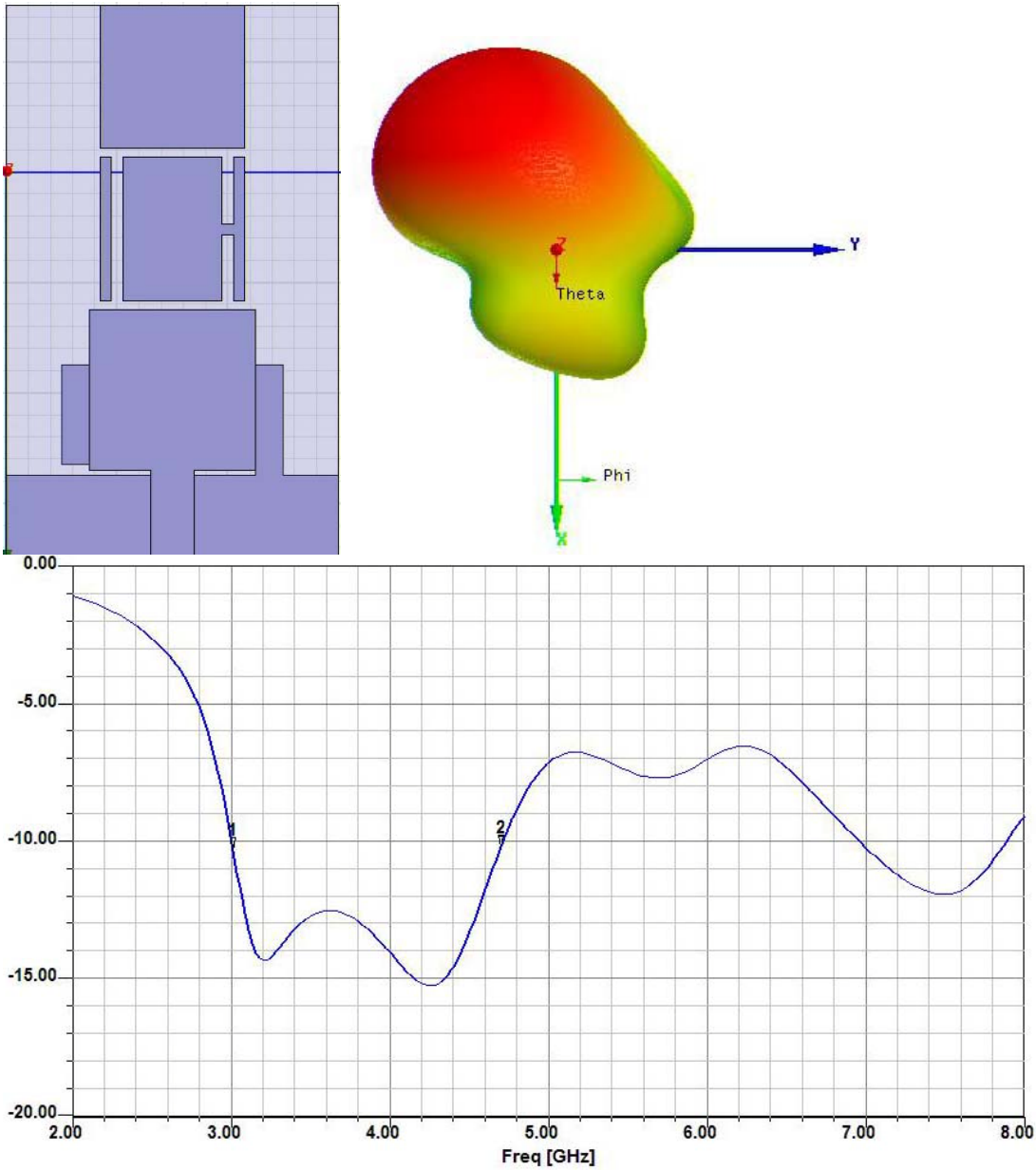

Figure 4-35. Design 17: Combination of Parasitic patch and stub

Description of the design 17: Finally, the parasitic patch modification and stub is combined to see if it results in higher gain and stronger beam steering. However, the gain sampled at 4GHz is only 5.2 dB. S11 is shifted to lower frequency due to the added stub and the parasitic patch does not affect the lowered s11.

4.7 Intermediate Fabrication and Measurement Results: Regular Diode and RF Diode

In addition to the intermediate simulation results, detail of the intermediate fabrication and measurement results is described. Specifically, in HFSS, switching is not simulated in detail because OFF status stub is simulated as a disconnected trace layer and ON status stub is simulated as a connected trace layer. Even if the parasitic capacitance is taken into account by setting the trace layer property of the gap, there is still unknown factors in real implementation. In particular, wires, soldering, battery and resistors that are located close to the antenna are difficult to be considered in simulation. Also, switching devices such as diode cannot be simulated in HFSS. Thus, the actual performance is heavily dependent on the switching device. The key to the beam steering in actual measurement is to find a switching device that has the least amount of OFF current at OFF status.

The optimized layout that was found out through simulations was fabricated using the typical lithography and etching process on FR4. The layout used was OFF-OFF state because the switching devices will be connecting the gap between the stub and the partial ground plane.

A very inexpensive diode was tested first as the switching device. Specifically, Jameco 1N914 (C = 4pF, Rs = less than 100 Ω) was chosen for it’s availability. Figure 4-36 shows the picture of antenna with the diodes on both side.

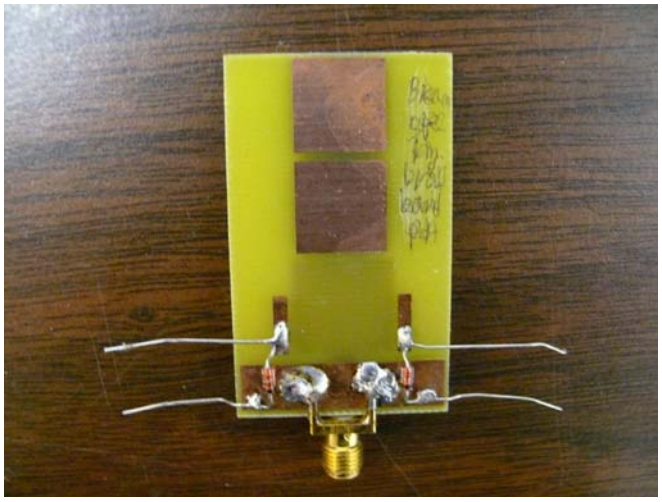

Figure 4-36. Antenna with diodes

Figure 4-37 shows the antenna with diodes and circuit for switching the diodes. On the left, two 1.5 V mercury batteries are used on each side of antenna and LED was also used for an easy indication of the ON side. Resistors are used to prevent diode damage. On the right, the two batteries are replaced with one 3V mercury battery for its easy connection. The value of resistor was calculated based on the data sheet of diode as shown in Figure 4-38. In other words, the resistor was chosen to flow a forward current of 300mA.

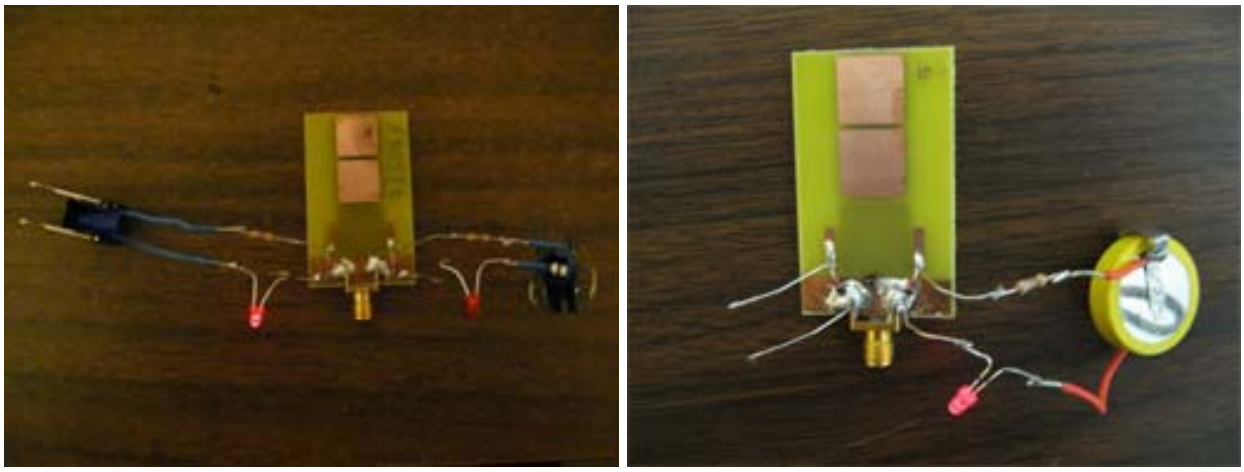

Figure 4-37. Antenna with circuit

The measured s11 is shown in Figure 4-39.The s11 is ON/OFF status of the antenna. However, it is quite different from the simulated s11 of ON/OFF status shown

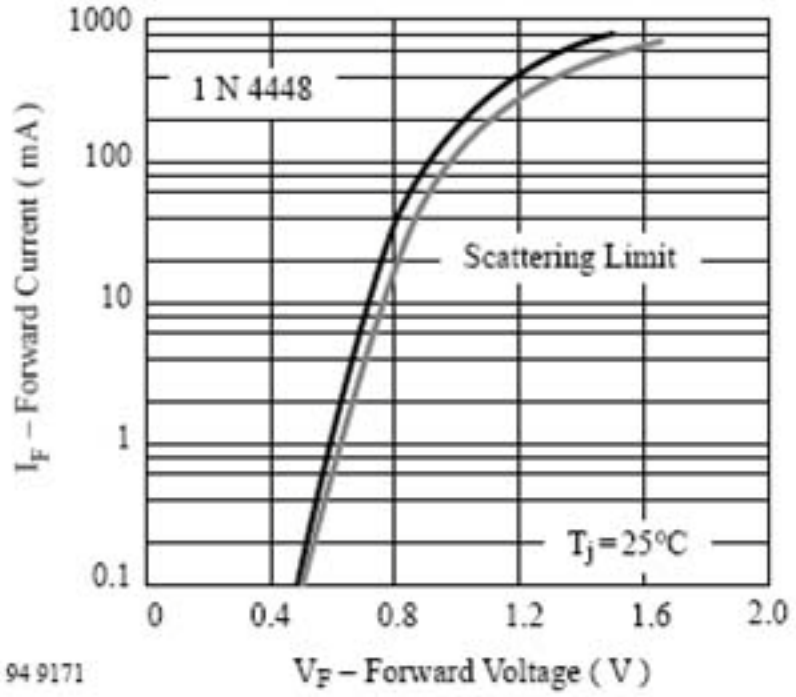

Figure 4-38. Forward current characteristic of 1N914

in Figure 5-2. Please note the noise is from the cable that connects the antenna and the network analyzer. To troubleshoot, instead of actual switching devices, a wire was soldered between the partial ground plane and the stub to represent ON status, as shown in Figure 4-40. Its s11 was measured and shown in Figure 4-41. It shows very similar s11 as in simulation of ON/OFF status shown in Figure 5-2. Thus, the problem is narrowed down to the switching device performance. In order to switch properly, the switching device should show a good OFF status at high frequency. Thus, the switching device needs to have a lowest possible parasitic capacitance value.

Just out of curiosity, LED was tested as a switching device as shown in Figure 4-42 and the measured ON/OFF s11 showed 2.6~3.2 GHz, which is quite different from the simulated ON/OFF s11.

A search for a diode that is suitable for RF application has begun and it appeared the AVAGO 5082-3039 RF diode is a suitable candidate. It has a capacitance value of

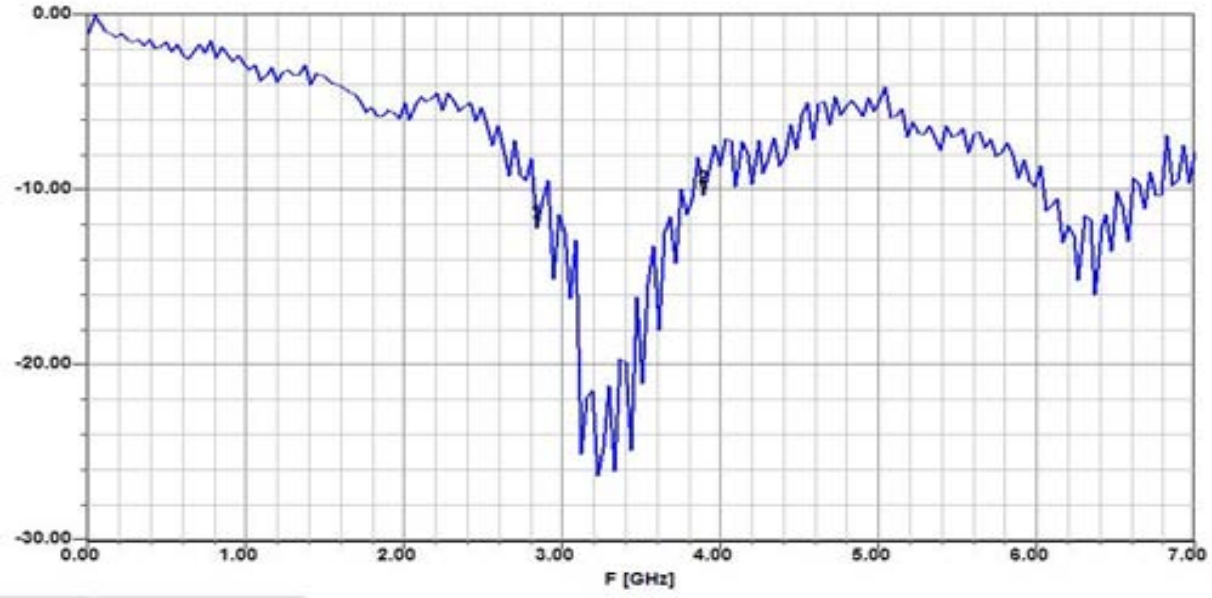

Figure 4-39. S11 of the antenna shown in Figure 4-36

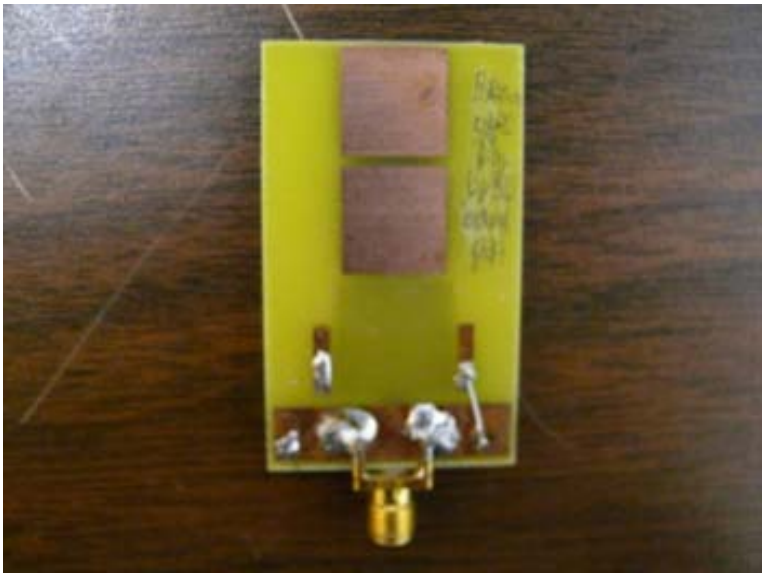
Figure 4-40. Antenna with fixed ON/OFF status using wire

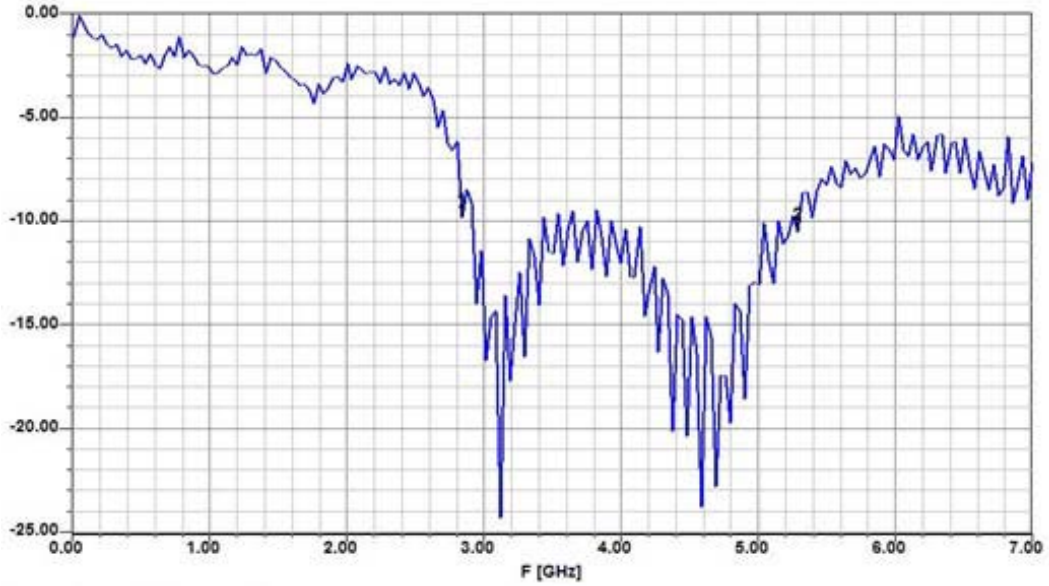

Figure 4-41. S11 of the antenna shown in Figure 4-40

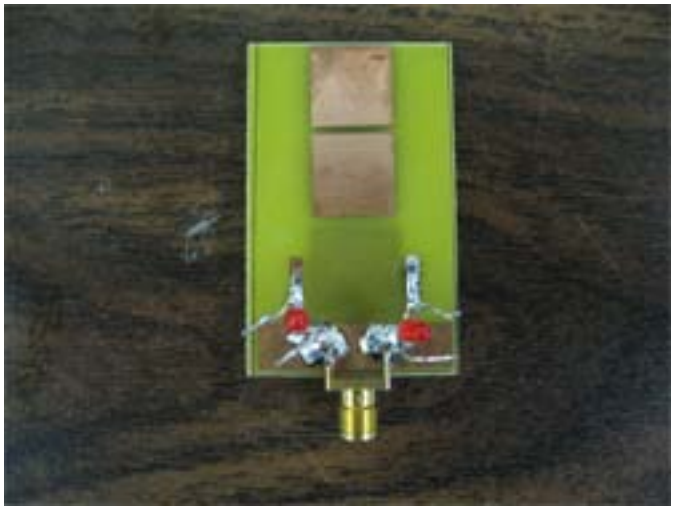
Figure 4-42. LED as switching device for the antenna

0.25 pF, i.e., sixteen times smaller the 1N914 and a series resistance value of 1.25 Ω, about eighty times smaller than the 1N914. The forward current characteristic of this diode is shown in Figure 4-43. It was used to calculate the necessary resistor value of the circuit to prevent the diode from being damaged. Figure 4-44 was used to see the capacitance value of the diode when the reverse voltage was applied.

Figure 4-45 shows the antenna with the RF diode. From this point, also a variable resistor was used because of its easy adjustment of current value. Increasing the

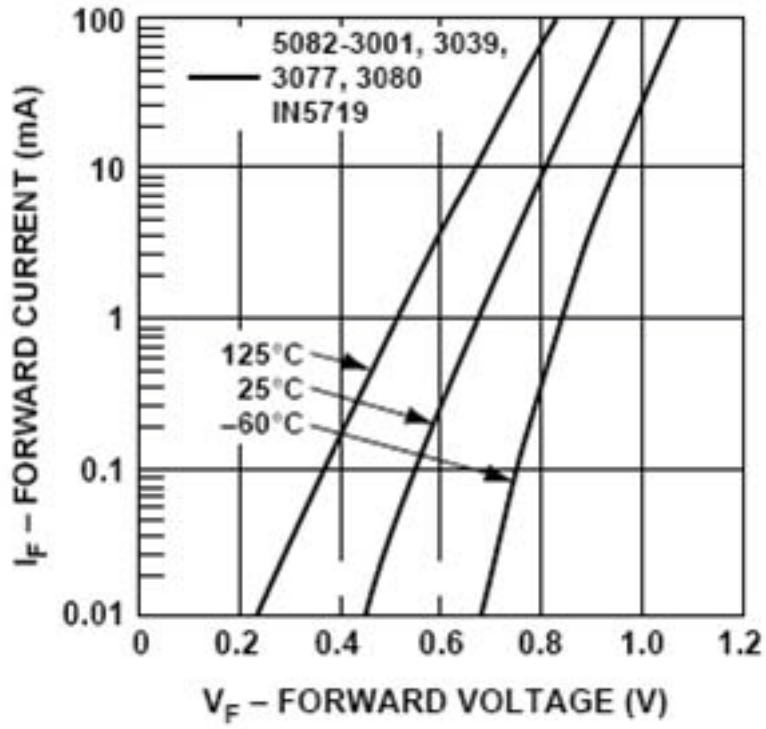

Figure 4-43. Forward current characteristic of AVAGO 5082-3039 RF diode

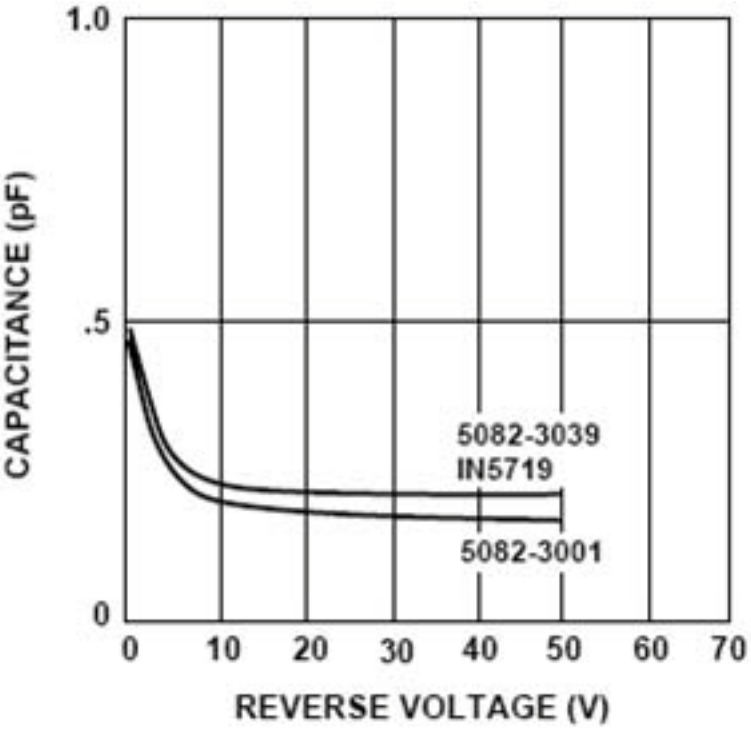

Figure 4-44. Capacitance vs. reverse voltage of AVAGO 5082-3039 RF diode

current value that is higher than the forward current did not affect the s11. Figure 4-46 shows the measured s11 of antenna with RF diode, an ON/OFF status. It shows a bit of similarity with simulated s11 but the 3~4.2 GHz is above -10 dB. Thus, it needs to be improved. It is because even with the relatively low capacitance value, the diode is not completely OFF at high frequency.

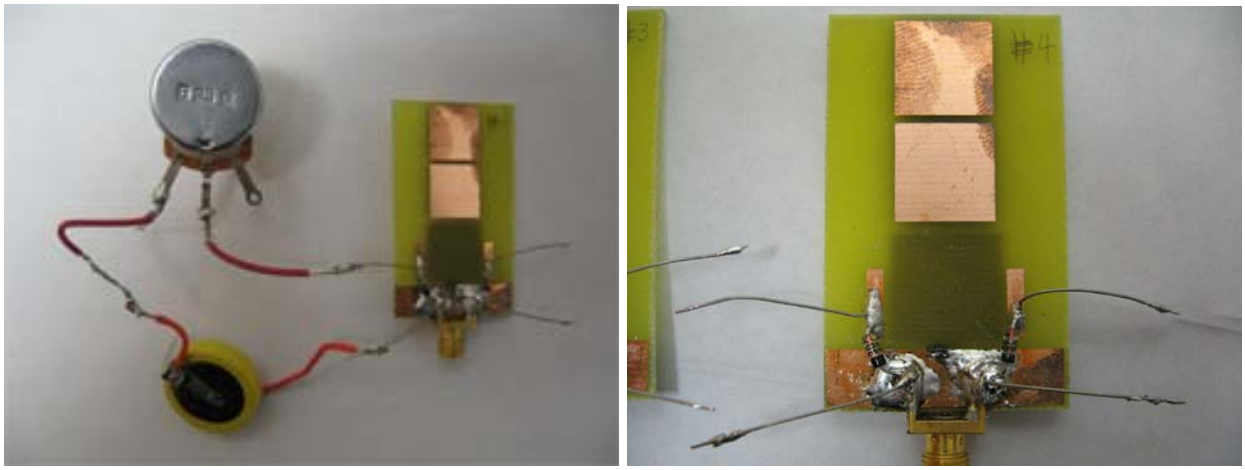

Figure 4-45. Antenna with RF diode and variable resistor

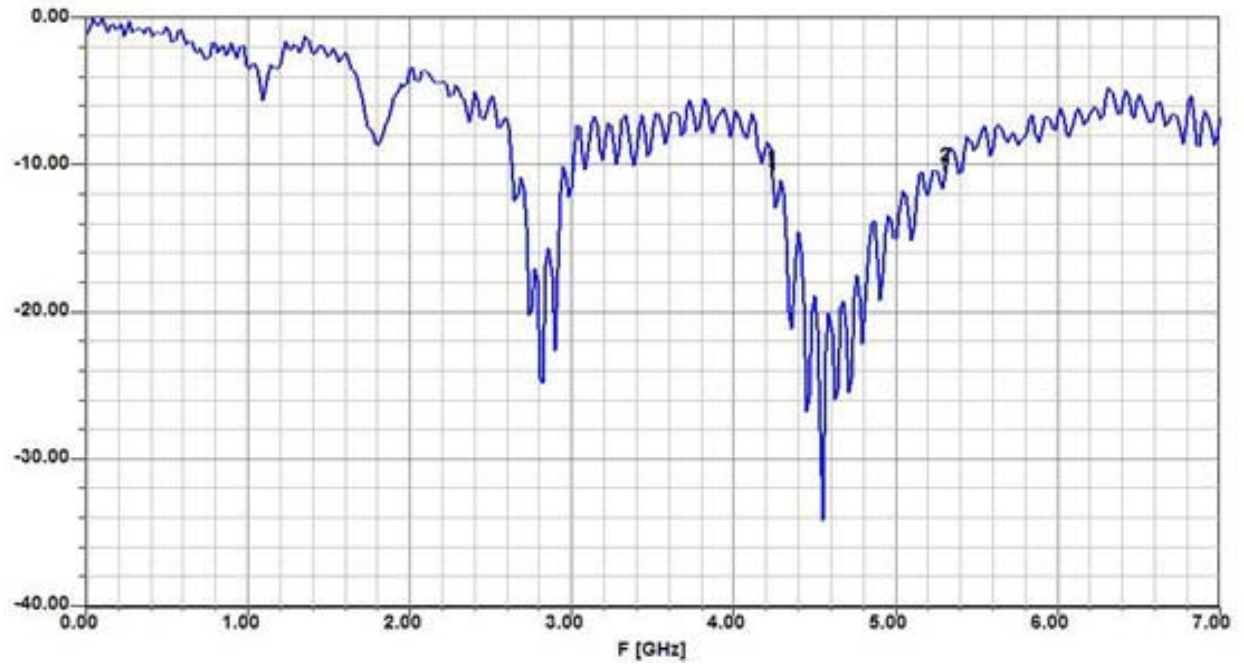

Figure 4-46. Measured s11 of antenna with RF diode, ON/OFF status

From numerous measurements, the following facts are found. First, soldering affects11 substantially. Different soldering locations were tried to see if the s11 can be improved. This repeated heat from soldering could have damaged diode performance. Second, even if this diode is RF diode, it is a non-surface mount type diode, thus, the connection between the stub and the partial ground plane is more like 3 dimensional, rather than 2 dimensional. Third, the soldering amount can be different from left side stub and right side stub. This results in a non symmetrical s11. In other words, the ON/OFF and OFF/ON s11 are different from each other. Thus, the soldering amount needs to be minimized for symmetrical s11 for each status. Fourth, the diode polarity is critical. The cathode should be connected to the partial ground plane and the anode to the stub. Otherwise, the s11 deviates from the simulated value substantially. Last, the current needs to be checked each time of measurement. It is because the battery can be heated easily and that can cause the voltage drop and subsequent current drop, which means the current flowing to the ON status diode can be below the minimum forward current. It was found out that the mercury battery overheats quickly. Thus, it was replaced with two of the AA size battery.

4.8 Rough Radiation Pattern Measurement Method

Even though the s11 shown in Figure 4-46 still needs to be improved, the radiation pattern needs to be measured concurrently with s11, because the beam steering is the most important characteristic of this antenna. Once the s11 was measured, the rough radiation pattern was measured at randomly sampled frequencies where the s11is below -10dB.

The description of the rough radiation pattern method is as follows. The rough radiation pattern measurement method can give you a quick look at the radiation pattern roughly. Figure 4-47 shows the diagram of rough radiation pattern measurement method. It is easy to set up and can give a quick beam pattern by rotating the antenna under test (AUT) in a plane of interest, i.e., either azimuthal plane (the horizontal plane) for azimuth (horizontal) antenna gain pattern or vertical plane for elevation antenna gain pattern. It does not give the accurate gain value but can give you gain value at each position that is relative to each other.

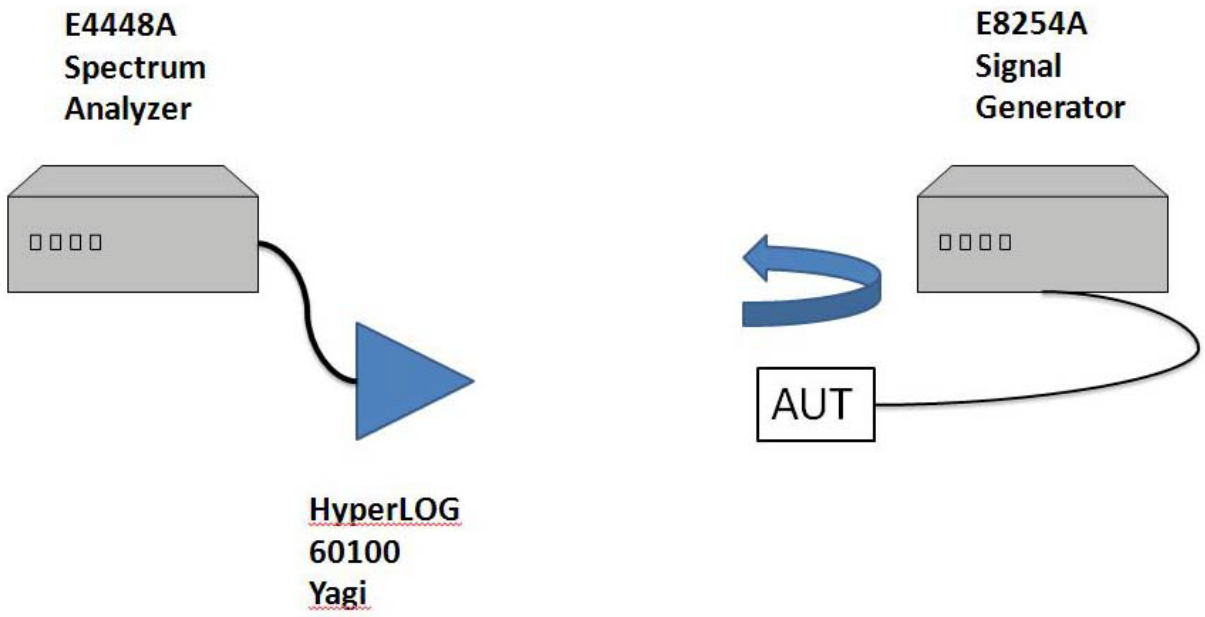

Figure 4-47. Rough radiation pattern measurement method diagram

Figure 4-48. HP E8254A Signal Generator

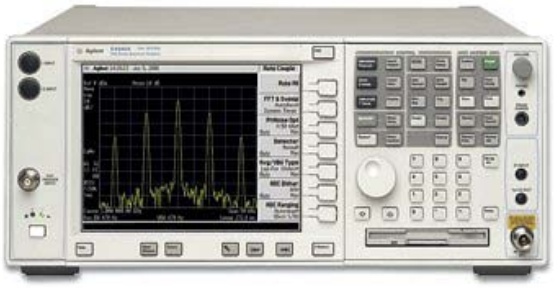

Figure 4-49. HP E4448A Spectrum Analyzer

Figure 4-50. HyperLOG 60100 Yagi antenna

Figure 4-51. Gain of the Yagi antenna

As shown in Figure 4-47, the AUT is connected to the signal generator and the standard gain antenna is connected to the spectrum analyzer. The Yagi antenna which is equivalent to standard gain antenna(SGA) in anechoic chamber shows a relatively constant gain of 5dB from 680MHz-10GHz as shown in Figure 4-51, thus, it is suitable as a SGA. Figure 4-52 shows the actual picture of the measurement set up.

Figure 4-52. Rough radiation pattern measurement method picture

The distance between the SGA and AUT needs to have a minimum far-field distance and it can be calculated using the following Friis equation 4-1.

$$\frac{Pr}{Pt} = GtGr\left(\frac{\lambda}{4\pi R}\right)^2$$

(4-1)

Pr: Power received by the receiving antenna

Pt: Power input to the transmitting antenna

Gt: Gain of the transmitting antenna

Gr: Gain of the receiving antenna

R: Distance between antennas

Also, when λ is smaller than the largest dimension of antenna (D), the following equation can be used. The calculated minimum distance is about 60 cm.

$$R = \frac{(2D)^2}{\lambda} \quad (4\text{-}2)$$

R: Minimum far-field distance (in meters)

D = Largest dimension of antenna (in meters)

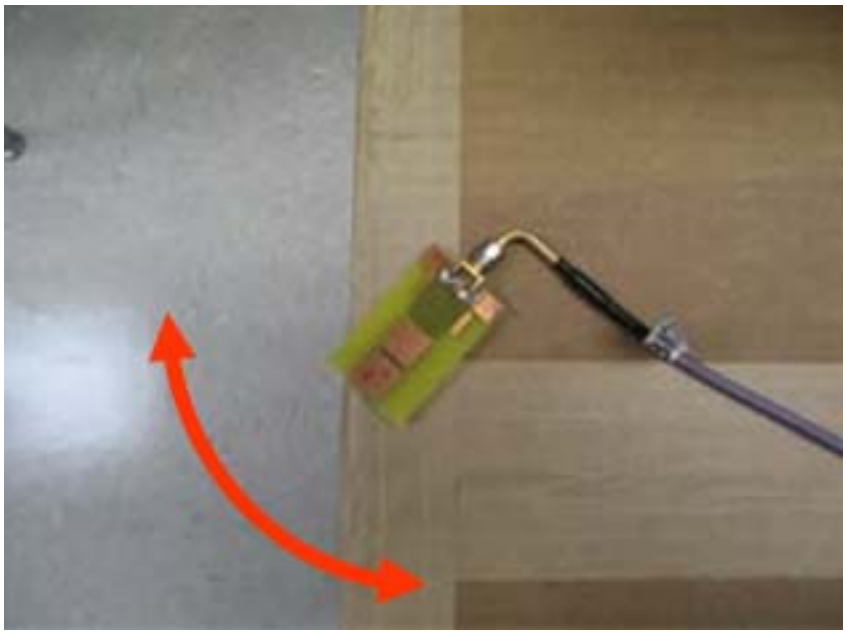

Figure 4-53. Rough radiation pattern measurement method: Antenna rotation

As shown in Figure 4-53, the antenna is horizontally rotated for detecting relative change in gain value. At first, the antenna was rotated at a certain state, i.e., ON/OFF or OFF/ON. However, this method caused too much variation in gain value because the circuits have to rotate along with antenna and it is physically not easy to rotate the antenna at one spot. Thus, later, the antenna was fixed at a position and the switching was performed to see a difference in gain value between switching. It is much easier to see the difference in gain by this method.

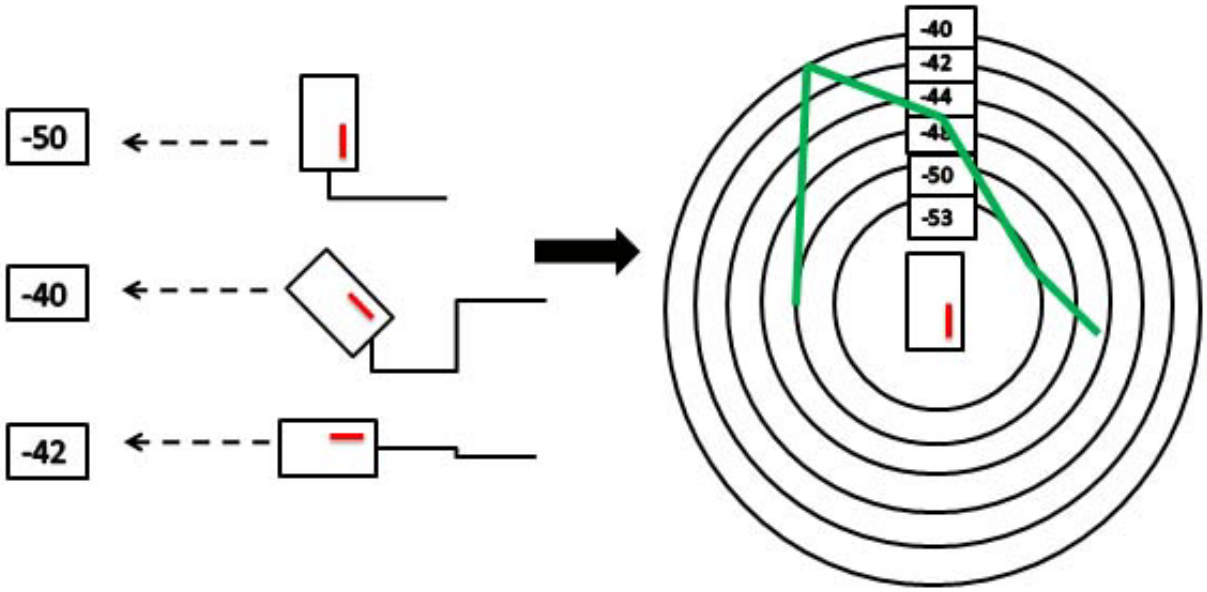

Figure 4-54. Rough radiation pattern sketch

Figure 4-54 shows the rough radiation pattern diagram. On the left, the values are the values of gain shown on the spectrum analyzer at the corresponding antenna position. The short bar inside the rectangle denotes the ON state diode and the beam is steered away from the bar as expected.

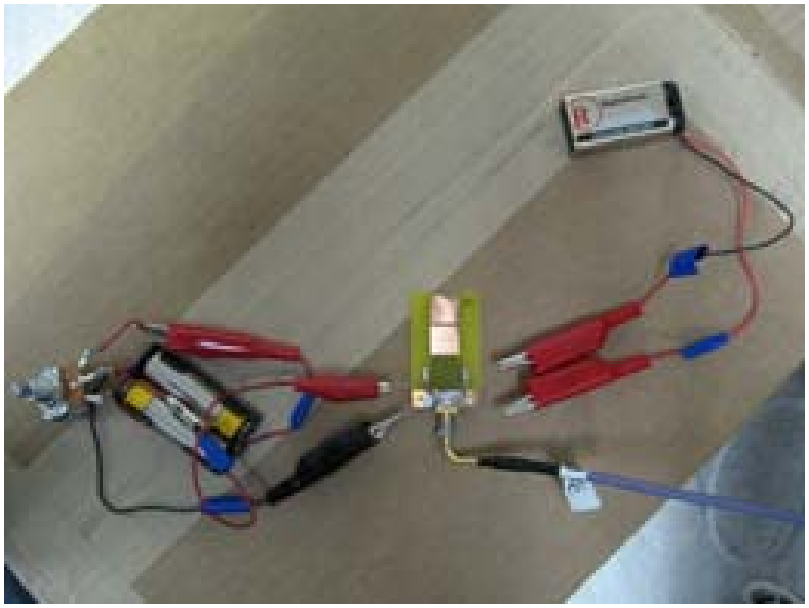

Figure 4-55. Antenna with circuit for rough radiation pattern measurement

As shown in Figure 4-55, Multi-meter is always needed to check the appropriate amount of current. The forward current value was kept at about 120mA. Varing the forward current amount using variable resistor did not affect much on rough radiation pattern as it didn't in s11 measurement. Also, as shown in the figure, alligator clips are used for easy switching and replacement of circuit. In addition, as shown in Figure 4-55, reverse voltage is applied to the OFF status diode to maximize its off status. According to Figure 4-44, -9 V would reduce the OFF status diode's capacitance value from 0.5 pF to 0.2pF. This can contribute to the OFF status.

4.9 Intermediate Fabrication and Measurement Results: Alternate Approaches

While working on the configuration of diode connecting the stub and partial ground plane, alternative approach to beam steering were investigated concurrently because the diode showed a different s11 from simulation even if it showed a beam steering from rough radiation pattern.

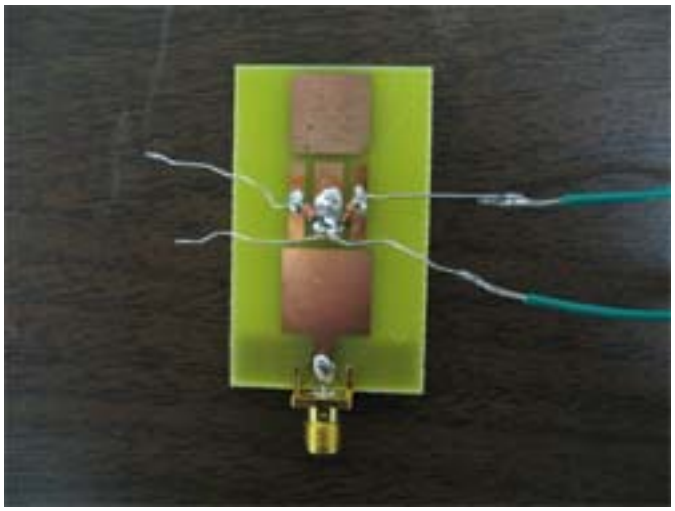

Figure 4-56. Beam steering using parasitic patch

As described previously, the horizontal beam steering was shown in simulation using the parasitic patch modification. The advantage of this approach is that unlike stub, the parasitic modification does not change s11. However, this frequency range is

unchanged from the broadband directional microstrip antenna (4.3GHz ~7GHz) thus, the FR-4 loss is bigger than the beam steering using stub which lowers the frequency range. Thus, it is not preferred. Other alternative method would be steering beam in just one direction by switching only one diode connected to only one side of stub because diode on each side can cause two not fully OFF status (or “pseudo” ON) and the difference in current between pseudo ON on one side and ON on the other side can be smaller than the difference in current between a complete OFF on one side and ON or pseudo ON on the other side. Also, increasing gap from 1 mm might be an option.

Another alternative approach is using mechanical switches. As opposed to diode, mechanical switch can be opened up and can be modified to serve the purpose. One of the mechanical switches that were considered was microelectromechanical systems (MEMS). Figure 4-57 shows an example of switch using MEMS. However, after further consideration, MEMS approach was discarded because first, it is for more small application (~ µm).Second, it's used in application where a high speed switching is required. Last, the cost will be increased. In other words, MEMS is too 'fancy' for this application. Other easily available small mechanical switches were tested as shown in Figure 4-58.

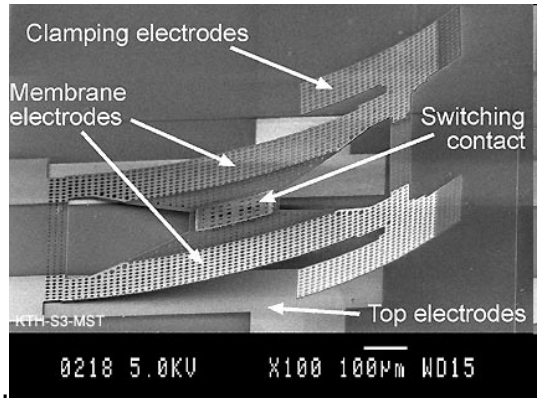

Figure 4-57. MEMS switching example

Figure 4-58. Mechanical switch: Slide switch (Radioshack 275-0004)

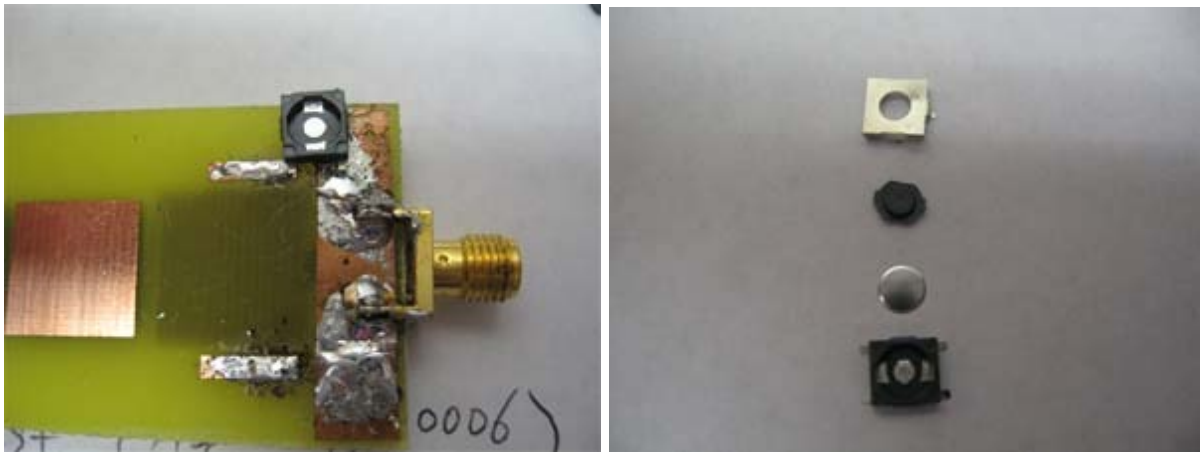

Figure 4-59. Mechanical switch:Tact switch (Radioshack 275-0006)

Neither of the switches worked very well. The slide switch works when only one side is used but when both sides are connected, results were not good. The tact switch didn't work at all because it was ON even if it’s not pressed.

Handmade slide switch shown in Figure 4-60 worked quite well. Two metal pieces can slide towards the stub direction alternately. A motor can be used to provide this kind of motion. Another mechanical switch that was tested is relay. Commercially available relays such as Radioshack 275-232, 275-005, 275-240 were tested and 275-005 was

chosen for its physical dimension. As shown in Figure 4-61 and Figure 4-62, the relay was opened and metal arm was attached to the moving parts of the relay. As shown in Figure 4-63, the s11 shows very good agreement with HFSS simulation. Proximity of the metal piece of the off status relay doesn't affect the s11. Also, the rough radiation pattern showed good agreement with simulation.

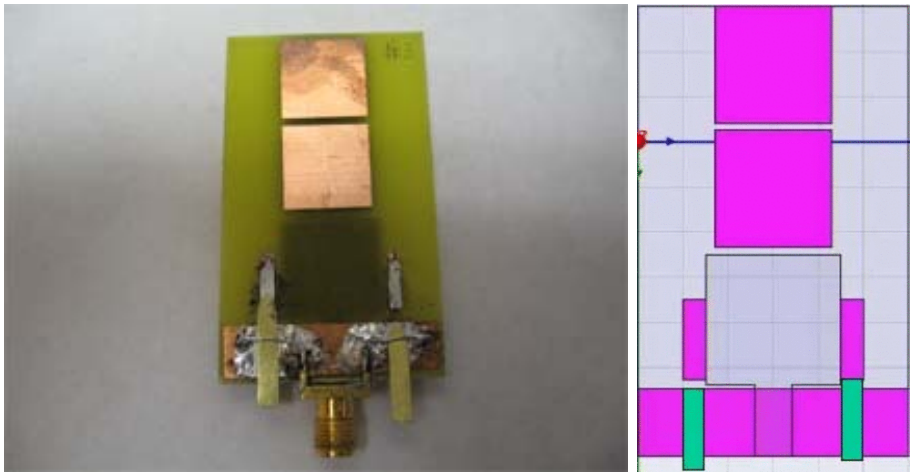

Figure 4-60. Antenna with handmade slide switch

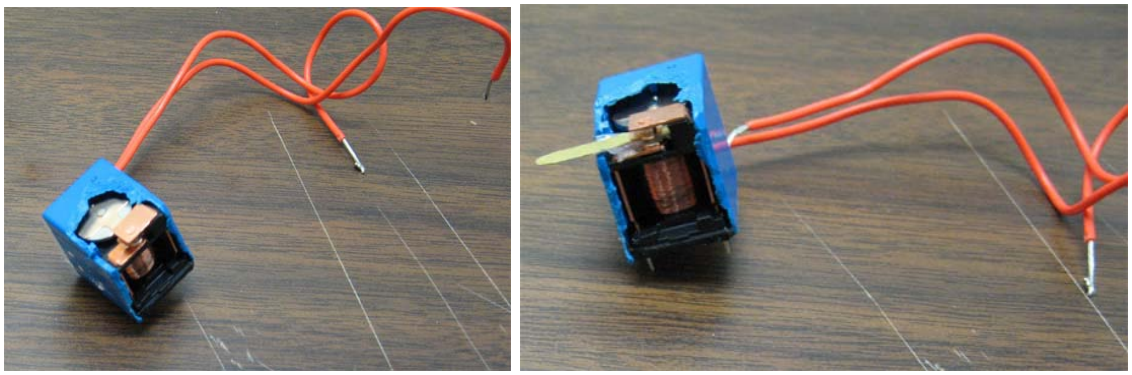

Figure 4-61. Relay (Radioshack 275-005)

In particular, the change of peak value shown on spectrum analyzer closely matches the simulation at each of the frequencies i.e., relative gain difference between the beam directions. Also, the magnetic field did not affect the antenna performance in either s11 or rough radiation pattern. However, the biggest disadvantage of using relay as a switch in antenna application is that relay requires too high voltage (9V) and

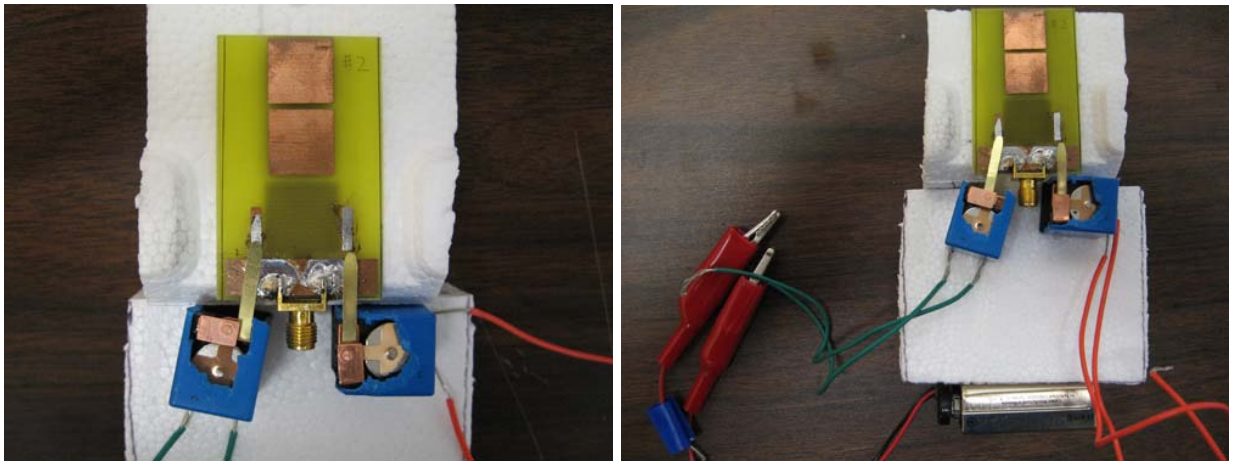

Figure 4-62. Antenna with relay in a platform

Figure 4-63. S11 comparison of simulation and antenna/relay measurement

current. Thus, it's not realistic in actual application.

Another approach is using RF switch. Minicircuit CSWA2-63DR+ was tested. It is a single pole, double throw (SPDT) type switch. It was chosen mainly because of its high isolation (36dB~50dB between2 ~6GHz) and its dimension (L= 4 mm X W=4 mm X H=1.25mm). Figure 4-64 shows its schematics and the switch. Figure 4-65 shows the pad configuration. Figure 4-66 shows the isolation between RF1 pin and RF2pin.Figure 4-67 shows how the switch pins would fit between the stub and the partial ground plane.

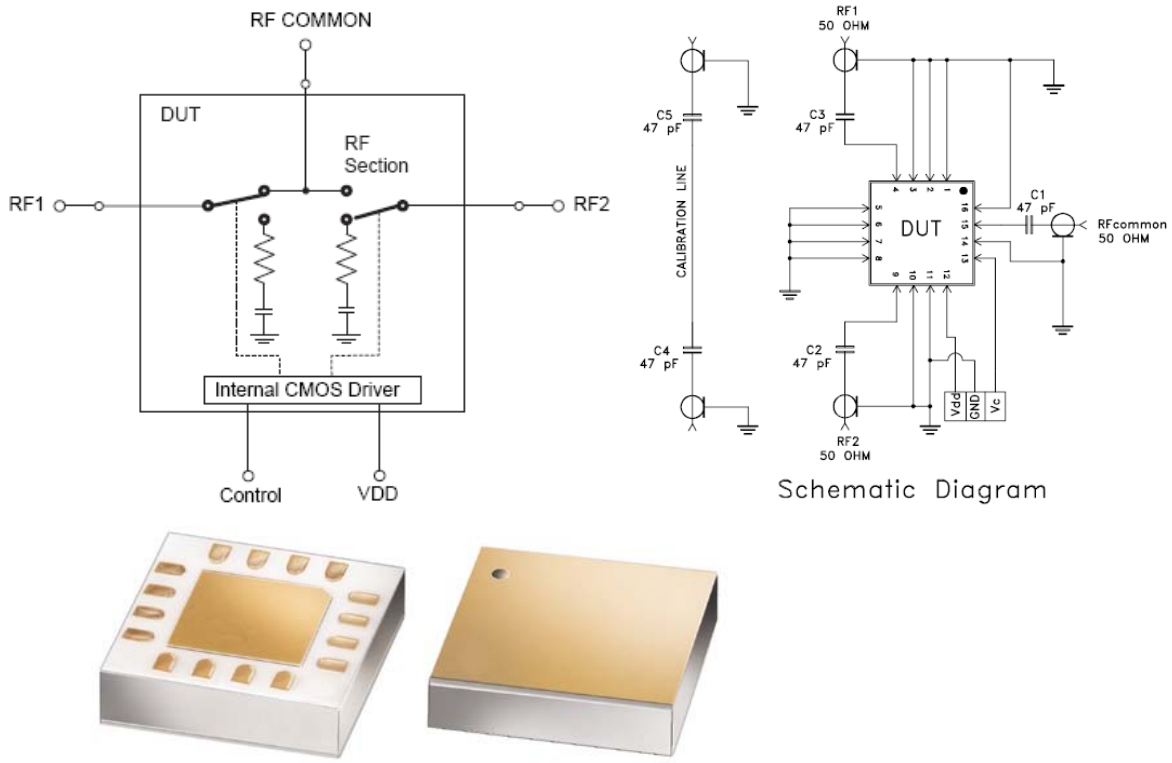

Figure 4-64. Schematics and switch

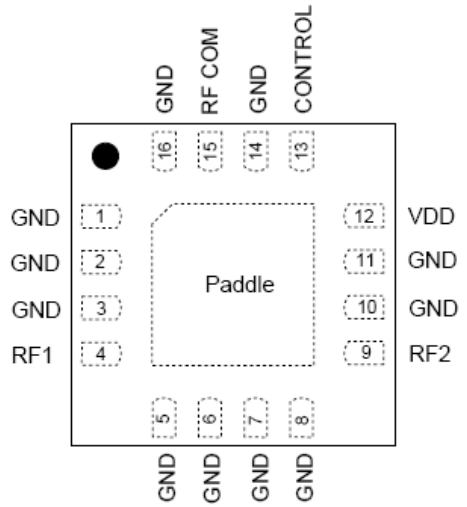

Figure 4-65. Pad configuration

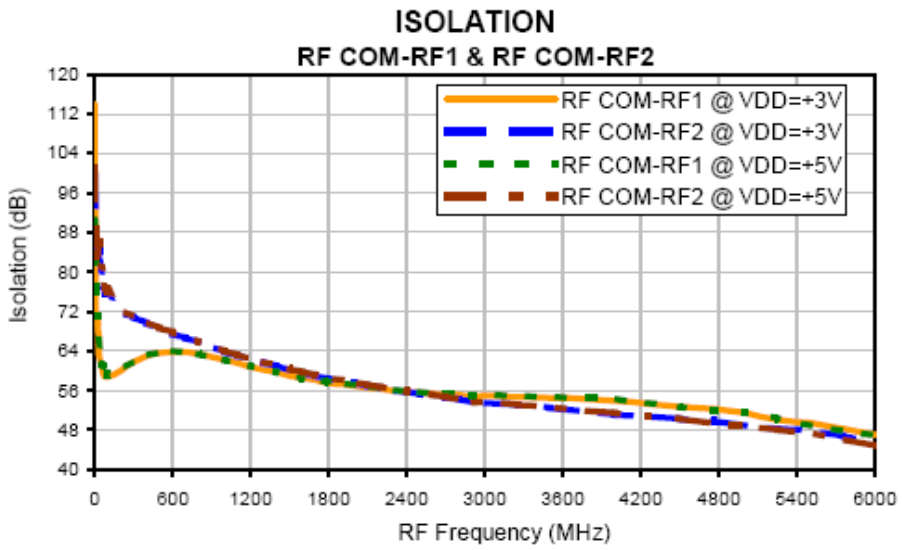

Figure 4-66. Isolation between RF1 pin and RF2 pin

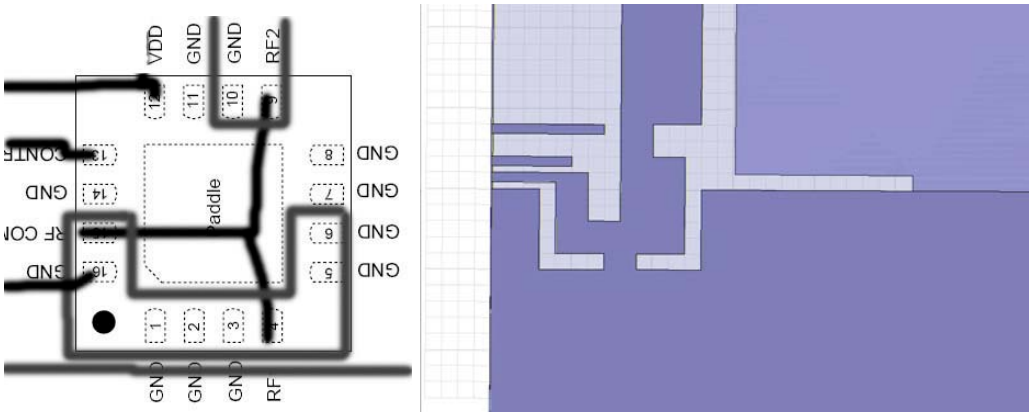

Figure 4-67. Pin connection between the stub and the partial ground plane

Figure 4-68 shows the initial wiring of the RF switch. However, it was determined patterning trace layer is an appropriate method. Also, from this point, epoxy was used instead of lead for soldering.Figure 4-69 shows the simulation of the antenna with one of the stub connected in RF switch configuration. In particular, it shows the surface current density. Figure 4-70 shows its s11 and Figure 4-71 shows its radiation pattern sampled at 4.5GHz with gain value of 5.5dB. Figure 4-72 shows the antenna with pattern for RF switch and the antenna with RF switch installed.

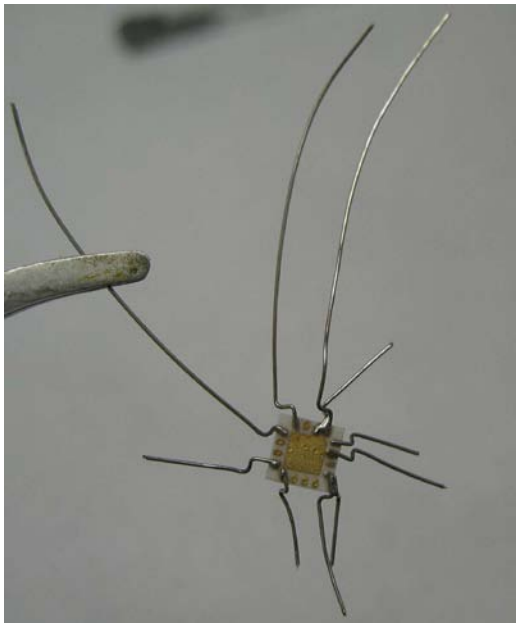

Figure 4-68. Wiring of RF switch

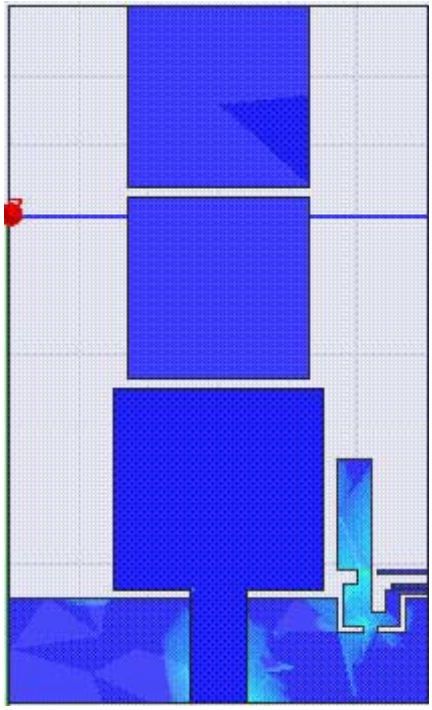

Figure 4-69. Antenna with one of the stub connected in RF switch configuration

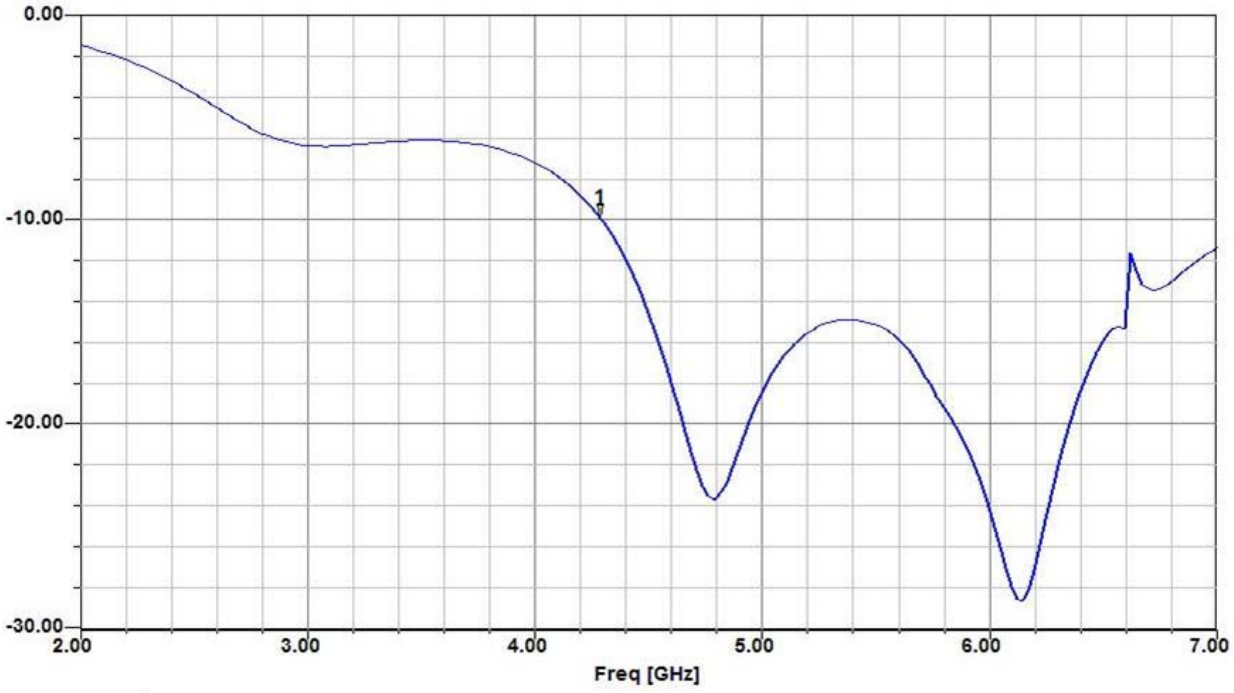

Figure 4-70. S11 of antenna shown in Figure 4-69

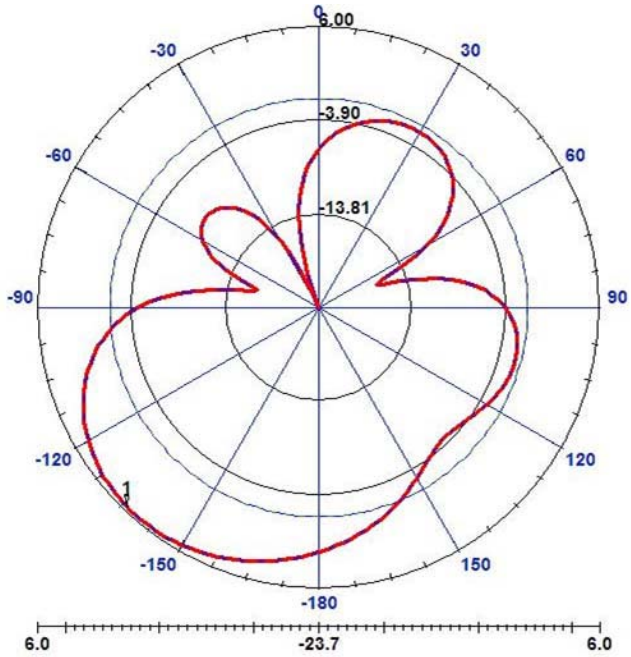

Figure 4-71. Radiation pattern of antenna shown in Figure 4-69

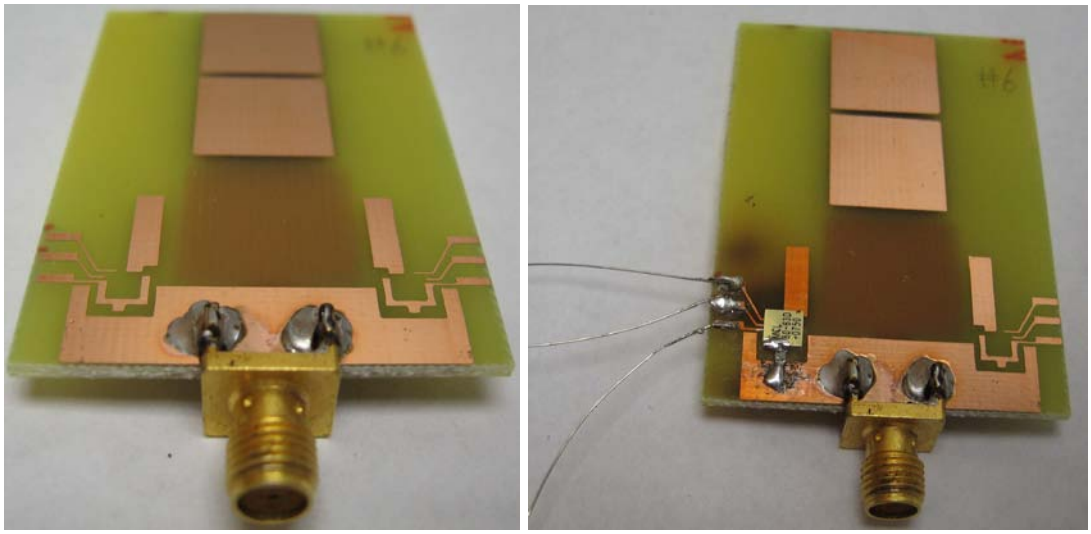

Figure 4-72. Antenna with pattern for RF switch and the antenna with RF switch

Figure 4-73 shows the microscopic view of the RF switch on the antenna. In the picture, 47pF capacitor is shown as it was required in the schematic shown in Figure 4-64.

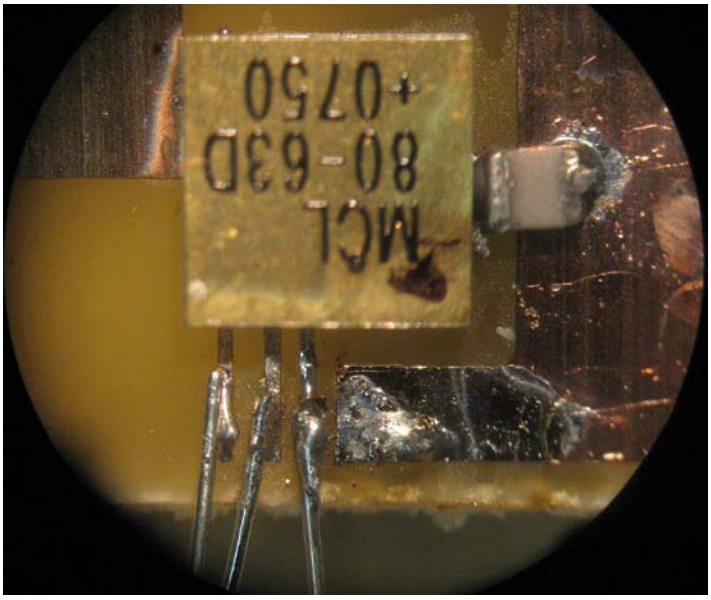

Figure 4-73. Microscopic view of the RF switch on the antenna

The s11 and rough radiation pattern of the antenna with RF switch were measured repeatedly. However, the measurement of the s11 and rough radiation pattern showed quite different result from the simulation. Thus, it was determined that the RF switch is

not suitable for this application. However, from the RF switch approach, useful techniques were acquired. First, trace layer pattern is used instead of wires to connect the device to antenna and to circuit. Second, epoxy soldering is used rather than the lead soldering. Last, surface mount type RF diode is sought after, instead of using non-surface mount type RF diode.

Surface mount type RF diode was searched and it was determined that BAP64-02 is suitable for this application because of its small capacitance and series resistance value(C=0.5pF and Rd=1.4 Ω) and small size (case 1.25mm X 0.85mm). Figure 4-74 shows the data of the BAP64-02.

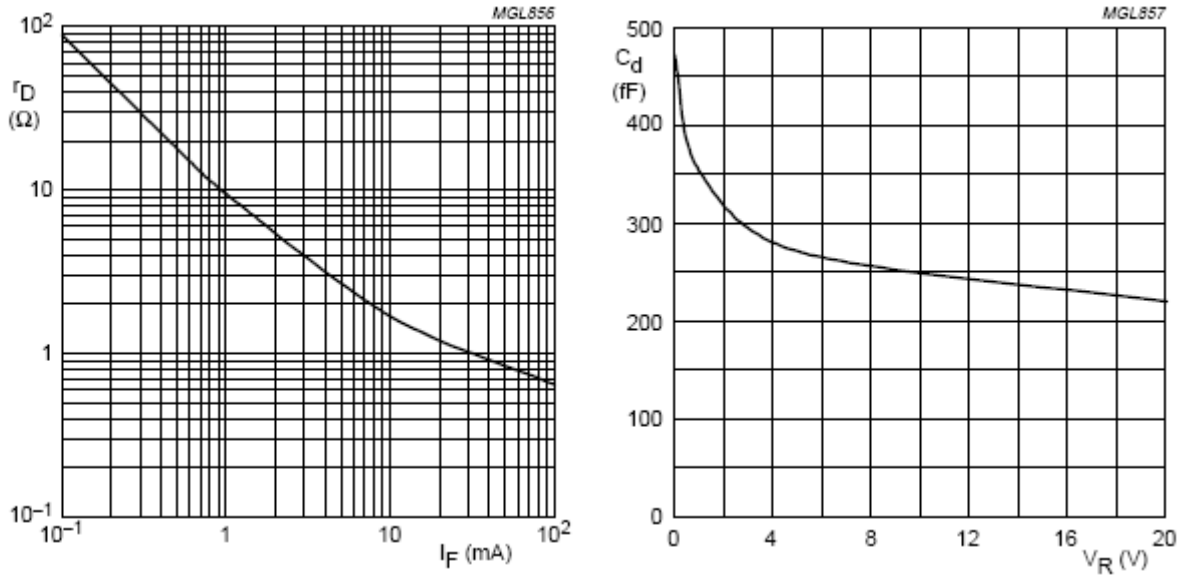

Figure 4-74. Forward resistance as a function of forward current and diode capacitance as a function of reverse voltage

When the surface mount type RF diode is used with patterned trace layer, along with the applied reverse voltage to the OFF status diode, measurement data that resembles the simulation data are obtained. The detail is shown in 5.4. Thus, it turned out the previous wires affected s11 substantially.

4.10 Summary

Effects of modifying the broadband directional microstrip antenna on the antenna characteristics such as reflection coefficient, radiation pattern, gain, or beam steering capability are investigated. The modification can include varying the width and/or length of the partial ground plane, adding stub(s) on the partial ground plane, varying the width, length, and/or location of the added stub, or varying the number, shape, gap, or location of the directors. It is important to evaluate the effects of the modification on the antenna characteristics, since these effects may be exploited to improve the antenna performance. Also, whenever the antenna modification is performed to improve one particular antenna parameter, it is required to check if that modification affects other antenna characteristics negatively.

Stub shape can affect s11 substantially and most of time negatively affects the broadband characteristics. Beam pattern does not change substantially even though the stub shape is changed substantially. Most of the OFF/ON combination of the both stubs show beam steering, that is, the beam is steered away from the ON status stub. Even the ON stub connection is reduced, the current flowing through that connection is still stronger than the current flowing to OFF status stub through coupling. When the stub is modified greatly, the beam steering pattern can be inconsistent. In addition to horizontal beam steering using stubs, parasitic patches can be also used to steer beam horizontally. The advantage of the beam steering using the parasitic patch, instead of stub is that the parasitic patch does not affect the s11 significantly as stubs do. The disadvantage of beam steering using parasitic patch is that the beam steering is relatively weaker than the beam steering using stubs and the switching might be difficult to implement.

In addition to the simulation, different approaches were made for switching the antenna in fabrication and measurement. Non-RF diode, non-surface mount type RF diode were tested on the fabricated antenna. Rough radiation pattern measurement was performed for a quick radiation pattern measurement after each s11 measurement before actual radiation pattern measurement in anechoic chamber. Mechanical switches such as relay were tested and the result was satisfactory but it is not suitable for this application. RF switch was tested but it didn't yield satisfactory results. Finally, when the surface mount type RF diode is used with patterned trace layer along with the applied reverse voltage to the OFF status diode, measurement data that resembles the simulation data are obtained.

CHAPTER 5
A BEAM STEERING BROADBAND SINGLE MICROSTRIP ANTENNA USING DIODES

5.1 Horizontal Beam Steering

Figure 5-1 (A) shows the proposed antenna. By switching the two diodes, electronic beam steering can be realized horizontally. Figure 5-1 (B) shows a state where one of the stubs is electronically connected to the partial ground plane. Figure 5-2 and Figure 5-3 show simulation results of the Figure 5-1 (B).

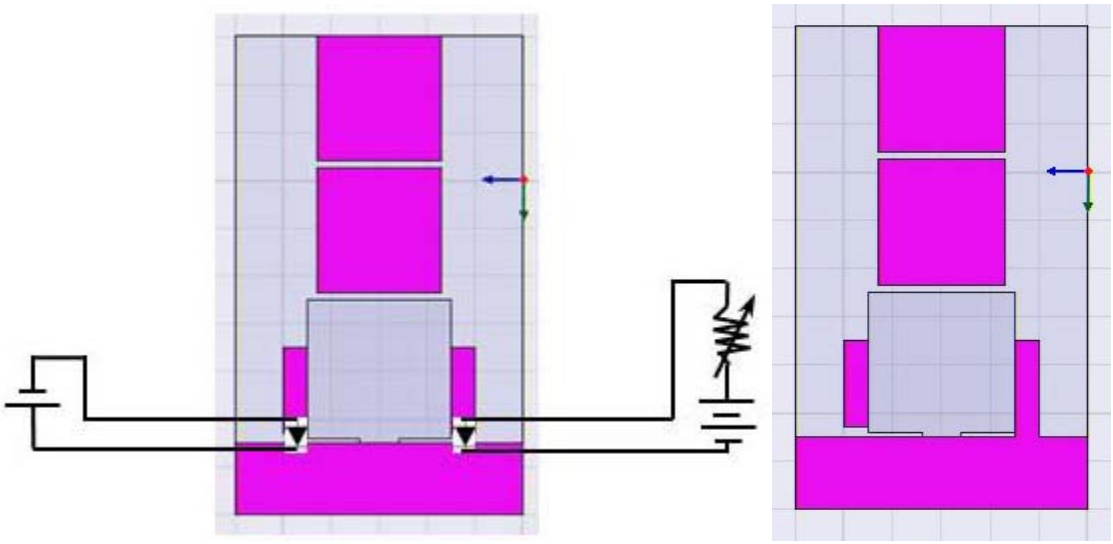

A B

Figure 5-1. A layout of the electronic beam steering broadband single microstrip antenna – (A) proposed antenna (B) simulating one of the diodes of the proposed antenna being turned on

As shown in Figure 5-2, this antenna operates from 3.08 GHz to 5.44 GHz. The broadband directional microstrip antenna showed broadband characteristics from 4.3 GHz (Figure 3-3). The additional stubs have lowered the operating frequency about 1.2 GHz from the original layout, which can be beneficial for vital sign detection.

Lower operating frequency can be beneficial for at least the following reasons. First, a larger penetration depth is possible and one good application will be a see-thru-

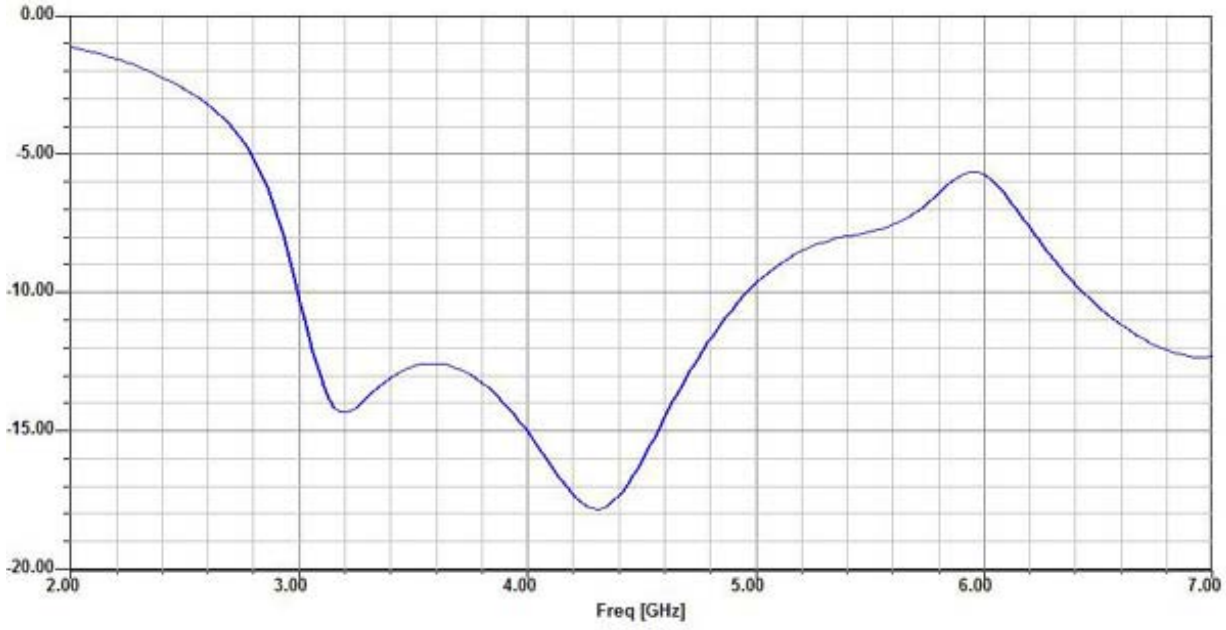

Figure 5-2. Reflection coefficient of the antenna shown in Figure 5-1(B)

wall radar application. Second, better vital sign detection is possible when the subject has large physiological movement. Last, at lower frequency, FR-4 loss tangent is smaller.

Also, as shown in Figure 5-3, the intended beam steering is shown over the operating band (sampled at 3.5, 4, 4.5, and 5 GHz). The radiation patterns are horizontal radiation patterns on XY plane to show that the added stub can steer the beam horizontally. It can be seen that the tilted angles are almost 30 degree from the XZ plane and are consistent in all of the frequencies. By the combination of turning the diodes on and off as shown in Figure 5-1, the beam can be steered horizontally 30 degree in both +Y and –Y direction.

Broadband beam steering is desired because of its use for radar application and tracking moving objects. In addition to the hallway application shown in Figure 3-10, a possible application will be search-and-rescue for victims, border patrols, entrance

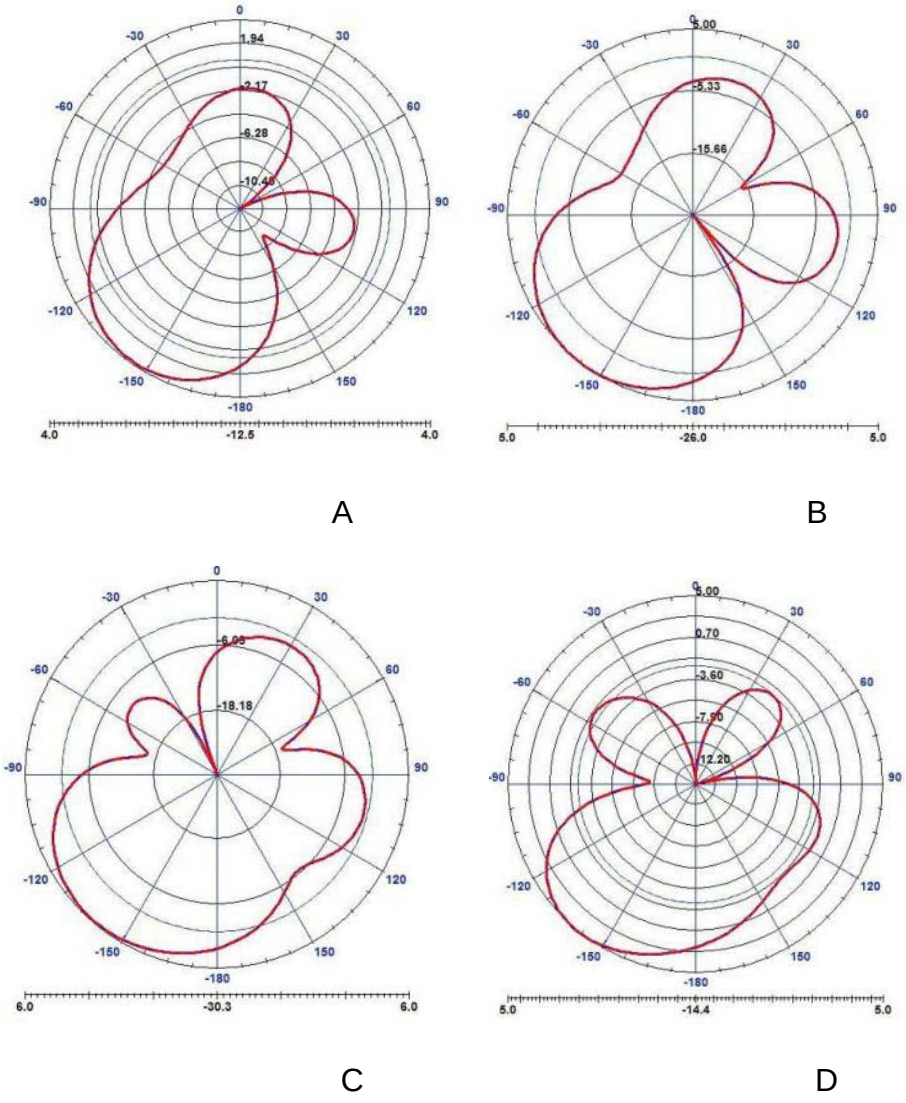

Figure 5-3. Radiation patterns of the antenna shown in Figure 5-1(B); (A) At 3.5 GHz, 3.75dB (B) At 4 GHz, 4.96dB (C) At 4.5 GHz, 5.54dB (D) At 5 GHz, 5dB

security, and so on. In this chapter, this design and simulation are validation by fabricating the antenna layout of Figure 5-1, measuring its reflection coefficient and radiation patterns.

5.2 Vertical Beam Steering

In addition to the horizontal electronic beam steering, vertical mechanical beam steering is possible once the substrate including the parasitic patch part is separated form the main patch. However, this requires a mechanical movement of the parasitic

patch parts, thus, it is not preferred method. In this section, a vertical electronic beam steering is simulated. This vertical beam steering can be useful as well as the horizontal beam steering because of its use for radar application.

Figure 5-4 shows the layout of the antenna for vertical beam steering. It shows still the same number of directors or two parasitic patches but the size of one of the parasitic patches, which is adjacent to the main patch is reduced to create a vertical beam steering effect. Figure 5-5 shows a layout of the antenna shown in Figure 5-4 with a diode connecting the two parasitic patches. The distance for the diode to connect is 4mm. By turning on and off the diode, the coupling between the patches can change, which in turn, cause the surface current on the parasitic patches to change, which leads to change of vertical beam pattern. Figure 5-6 shows a layout of the antenna where the diode of the Figure 5-5 is turned on.

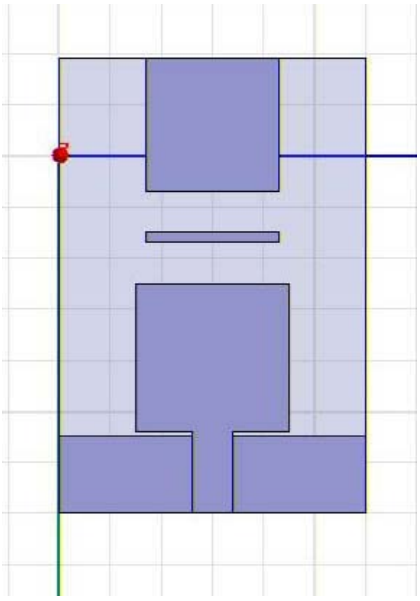

Figure 5-4. A layout of the vertical electronic beam steering broadband single microstrip antenna

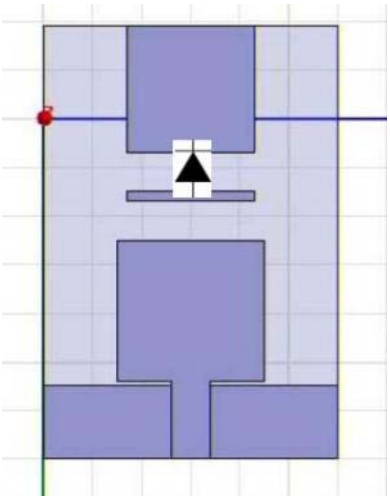

Figure 5-5. A layout of the vertical electronic beam steering broadband single microstrip antenna with a diode

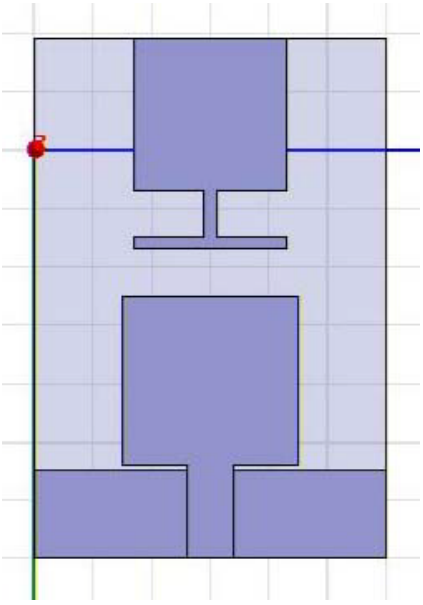

Figure 5-6. A layout for simulating the vertical electronic beam steering broadband single microstrip antenna with a turned on diode

Figure 5-7 shows the comparison of the surface currents between the antennas depending on the on/off states of the diode. Shown at the bottom of the Figure 5-7 are radiation patterns corresponding to each of the top layout. This time, the radiation patterns on XZ plane or vertical radiation patterns are shown to show the vertical beam

steering. The simulation shows that the beam is tilted vertically when there is surface current on the parasitic patch that is located further away from the main patch (Figure 5-7A). When there is no or weak surface current on the parasitic patch that is located further away from the main patch, beam stays in the broadside direction (Figure 5-7 B).

Although it's not shown here, when surface current animation function is used to see different phases of the surface currents on the parasitic patches, Figure 5-7 (B) shows weak currents on the parasitic patch. However the currents are very weak compared to the currents on patches of Figure 5-7 (A) and its influence on beam pattern is negligible. The radiation patterns show the tilted beam has a gain that is 1 dB higher than the non-tilted beam. The tilted angle is about 25 degree.

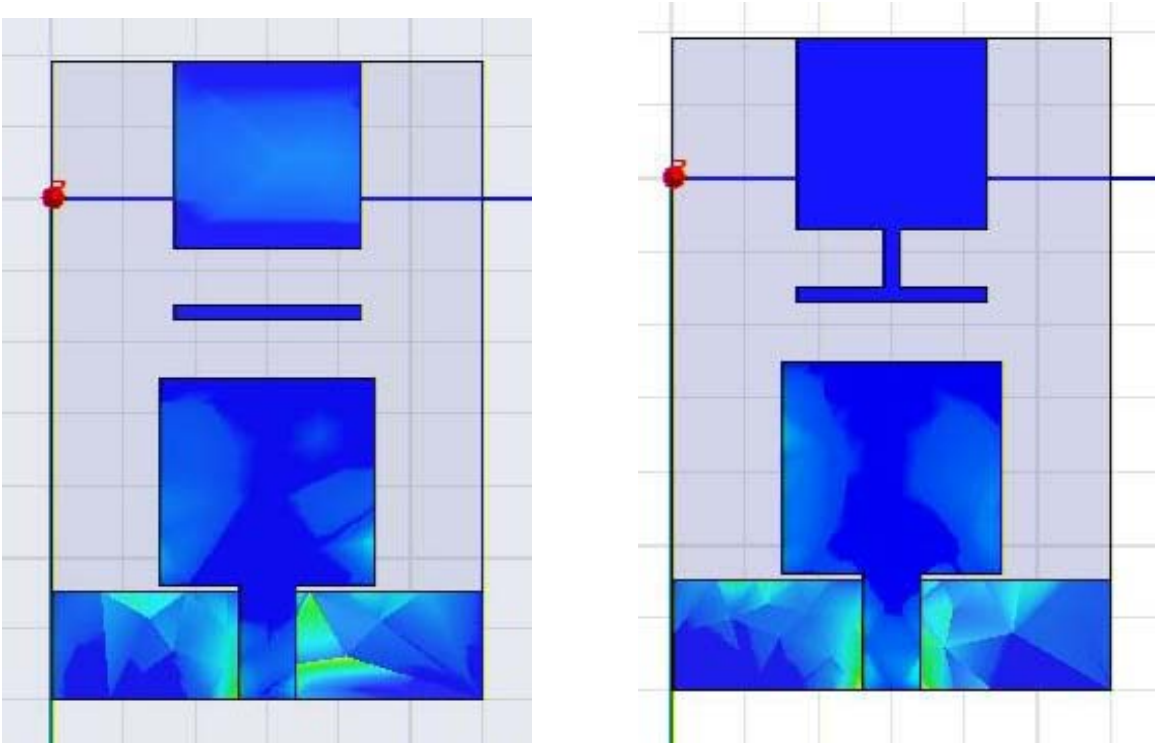

A B

Figure 5-7. A comparison of the surface currents and radiation patterns of the antennas of (A) Figure 5-4 (At 5 GHz, 5 dB) and (B) Figure 5-6 (At 5 GHz, 4 dB)

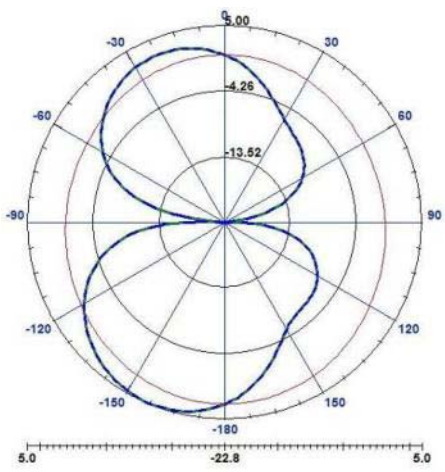

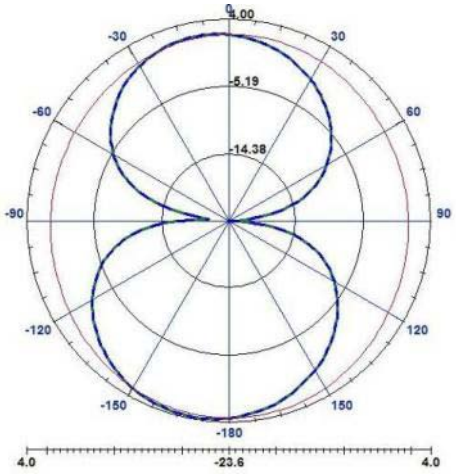

A B

Figure 5-7 Continued

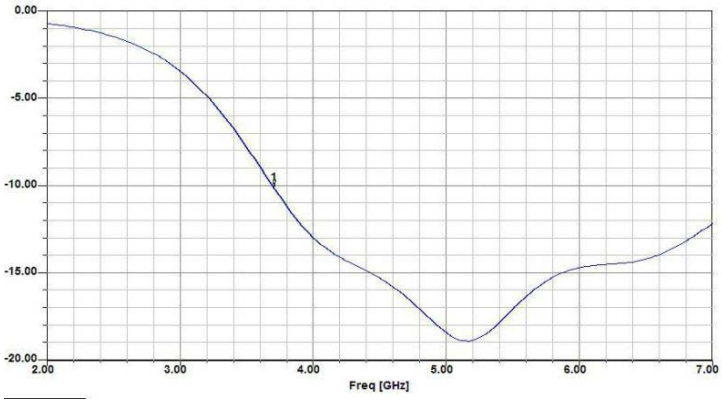

A

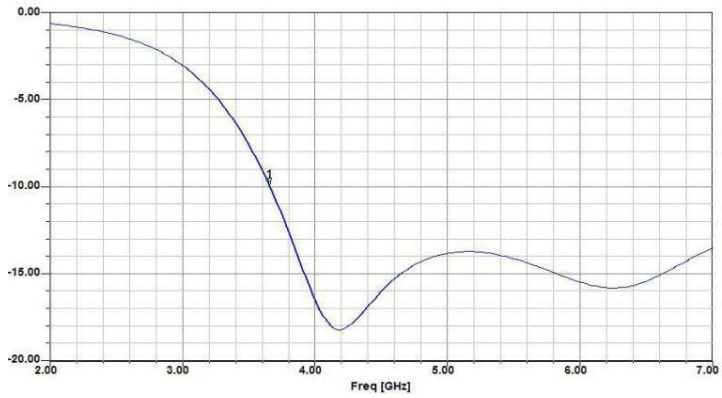

B

Figure 5-8. Reflection coefficients of the layouts of (A) Figure 5-4 and (B) Figure 5-6

In addition to the beam patterns, reflection coefficients are shown in Figure 5-8. The reflection coefficients show that the modification of the directors also reduces the lower end of the bandwidth to 3.7GHz from the original 4.3 GHz. as it happened in the modification of the partial back plane for horizontal beam steering. The radiation patterns showed the tilted beam has a 1 dB stronger gain than the non-tilted beam because the vertical steering is based on weakening the coupling between main patch and parasitic patches. Thus, when the beam is not tilted, the gain of the beam will not be as strong as the gain of the tilted beam. As opposed to the vertical beam steering, it should be noted that in the horizontal beam steering, same value of gain was exhibited due to its symmetry.

5.3 Fabricated Proposed Antenna

After performing simulations in Ansoft HFSS, the proposed antenna shown in the Figure 5-1 (A) was fabricated. The FR4 lamination with a dielectric constant of 4.4 was used as the substrate. Simple pattern application via photolithography and subsequent copper etching with ferric chloride were performed. Figure 5-9 shows the fabricated proposed antenna. Please note that the dimensions of the broadband antenna are same as the broadband directional microstrip antenna except the additional stubs on the partial ground plane [Park]. The stub is located 7.5 mm from the center and is adjacent to the side of the top driven element. The dimension of the stub is 2.5mm X 10mm for ON state and 2.5mm X 9 mm for OFF state or 1 mm gap between the stub and partial ground plane. The diode is BAP64-02 surface mount RF PIN diode. A DC bias-voltage is applied to control ON and OFF status of the diode. The PIN diode exhibits a resistance of 1.4 Ω and capacitance of 0.5 pF with the applied forward bias. For the ON status diode, a 3V DC was applied with a variable resistor (0~25 Ω). The

current to the diode was kept at 110mA. For the OFF status diode, 1.5V DC reverse bias was applied.In addition to the proposed antenna, a reference antenna having the identical layout of the simulation was fabricated for comparison. Figure 5-10 shows the picture of the reference antenna.

5.4 Input Reflection Coefficient (S11)

The input reflection coefficients of the reference antenna and the proposed antenna were simulated using HFSS and measured using an Agilent E8361A 10 MHz to

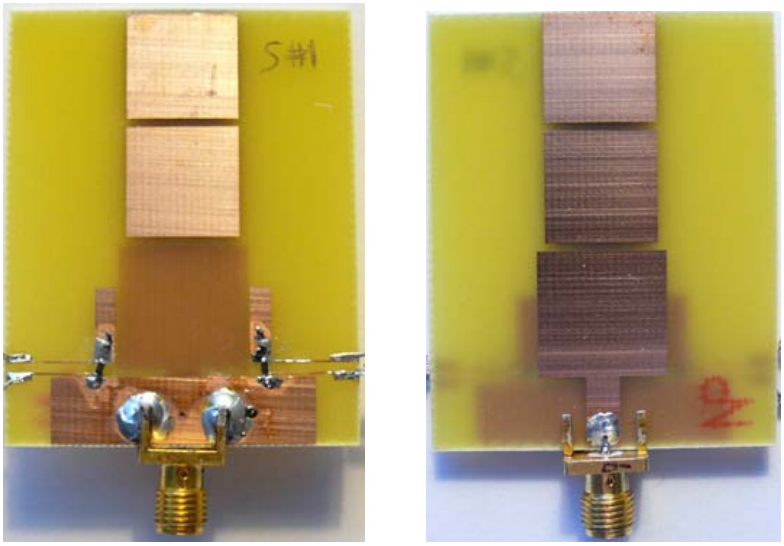

A B

Figure 5-9. Proposed antenna; (A) bottom layer; (B) top layer

67 GHz PNA series network analyzer as shown in Figure 5-11. When the pair of diodes are either ON and OFF or OFF and ON, the antenna operates from 2.8 ~ 4.8 GHz, where beam steering occurs by the peak gain appearing in the opposite direction of the ON state diode (Figure 5-14). When both diodes are OFF, the antenna operates from 3.7~4.4 GHz and no beam steering occurs. Simulated S11 shows good agreement with the measured s11 of the proposed antenna.

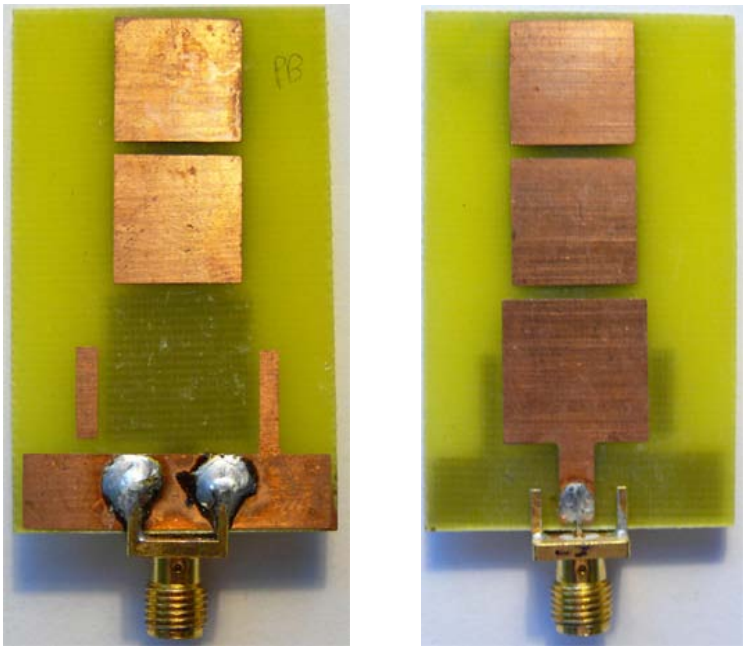

A B

Figure 5-10. Reference antenna; (A) bottom layer; (B) top layer

Compared to the previous antenna without stub [Park], the broadband frequency range has been lowered from 4.3~7GHz to 2.8–4.8 GHz by the added stubs. Lower operating frequency can be beneficial for the reasons stated previously.

5.5 Far-Field Radiation Patterns

The radiation patterns were measured in an anechoic chamber at the Antenna, RF and Microwave Integrated (ARMI) Systems Laboratory at University of Central Florida. For this broadband antenna, it would be ideal to measure the radiation patterns at frequencies with small interval between them, but instead, the radiation patterns were measured at 3, 3.5, 4, 4.5 GHz due to practical reasons. At each of the frequencies, E-plane that is horizontal to the substrate was measured and co-polarization and cross-polarization of the E-planes were measured. Figure 5-12 shows inside of the anechoic chamber.

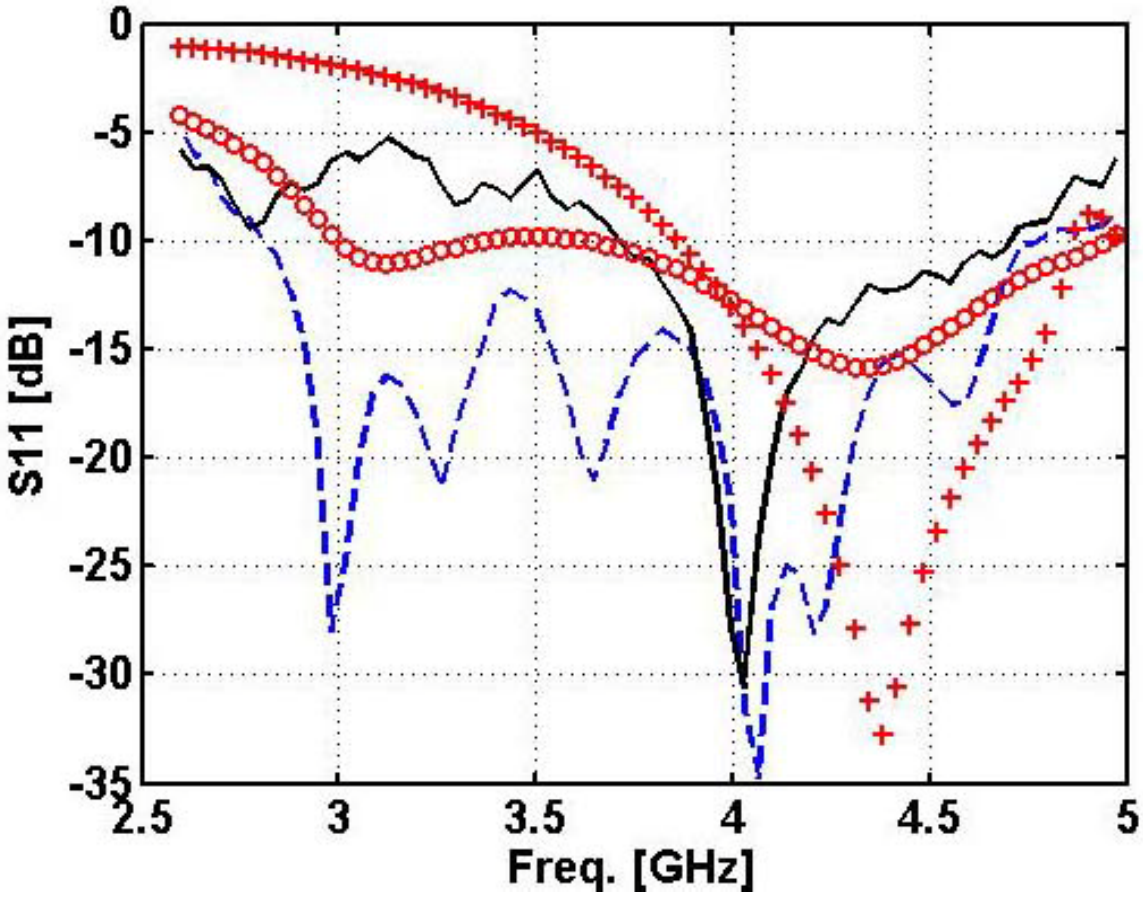

Figure 5-11. Reflection coefficient; Dashed: measured proposed antenna (ON-OFF or OFF-ON); Solid: measured proposed antenna (OFF-OFF); o: simulated proposed antenna (ON-OFF or OFF-ON); +: simulated proposed antenna (OFF-OFF)

The Standard Gain Antenna is shown. Figure 5-13 shows how the antenna under test (AUT) was mounted for radiation pattern measurement. In the figure, the reference antenna is shown.

Figure 5-14 shows the radiation patterns. The radiation patterns for both ON-OFF and OFF-ON are simulated and measured at 3, 3.5, 4, and 4.5 GHz. The simulated radiation patterns and the measured radiation patterns of reference antenna show good agreement with each other overall. However, there are discrepancies between the simulated and measured radiation patterns of proposed antenna which includes nulls in

the measured patterns. It might be contributed by the parasitic capacitance of the diode when it is switched off. This additional parasitic capacitance of about 0.25pF is not considered in HFSS simulation and might cause the change in radiation patterns. In addition, the DC bias wires of the circuit that are connected to the antenna can affect the radiation pattern. Still the measured radiation patterns of the proposed antenna with PIN diodes show clear beam steering patterns, i.e., at each measured frequency, the peak gain appears on the opposite side of the ON state diode as expected from the simulation. The diode performance is critical in beam steering because the imperfect isolation between the ON and OFF modes of the diode can damage the beam steering.

The differences in measured peak gains in dB between the reference antenna and the proposed antenna are -0.4, 0.9, 1, and 1.1 (Reference – Proposed) at 3, 3.5, 4, and 4.5GHz respectively. Average values of the two peak gains of ON-OFF and OFF-ON configurations are used. The proposed antenna shows less gain than the reference antenna except at 3 GHz. The lower gain is due to loss introduced by the diodes. Also, the loss due to diode increases slightly as the frequency increases.

In addition, compared to the broadband directional microstrip antenna [Park], an increase in gain is observed from the beam steering. Due to the different s11 ranges between the broadband directional microstrip antenna and the proposed antenna, gain only at 4.5GHz can be compared and the beam steering increased the peak gain from 4.5dB to 5.63 dB.

Table 5-1 compares the beam steering patterns shown in Figure 5-14 quantitatively. First, peak gain difference between the two regions is observed in an expected manner (i.e., higher peak gain is in 90º -180º region at ON-OFF mode and in

Table 5-1. Beam Steering Comparison of ON-OFF vs. OFF-ON at each frequency

Freq. (GHz) / Mode	Peak gain of 90º -180º region vs. 180º -270º region (Location, HPBW)	Average gain of 90º -180º region vs. 180º -270º region
3 /ON-OFF	3.38dB(at 100º,70º) vs. 0.47dB(at 184º,26º)	-1.5dB vs. -7.66dB
3 /OFF-ON	0.37dB(at 148º,30º) vs. 4.28dB(at 238º,30º)	-4.75dB vs. 0.49dB
3.5 /ON-OFF	4.65dB(at 92º,50º) vs. -1.56dB(at 204º,32º)	1.47dB vs. -10dB
3.5 /OFF-ON	1.11dB(at 172º,40º) vs. 4.48dB(at 256º,56º)	-8.9dB vs. 0.93dB
4 /ON-OFF	5.69dB(at 112º,44º) vs. 3.31dB(at 192º,22º)	-0.09dB vs. -2.81dB
4 /OFF-ON	-4dB(at 160º,16º) vs. 5.25dB(at 226º,20º)	-9.29dB vs. 0.81dB
4.5 /ON-OFF	5.63dB(at 162º,60º) vs. 4.18dB(at 208º,20º)	3.05dB vs. -3.87dB
4.5 /OFF-ON	3.18dB(at 142º,50º) vs. 5.99dB(at 238º,40º)	0.34dB vs. 0.62dB

180º -270º region at OFF-ON mode) at all of the measured frequencies. Second, peak gain location is not as symmetrical as the simulation but remains within the expected region. Third, HPBW of the steered beams with higher peak gains tends to be larger than the beams with lower peak gains as shown in the simulation. Last, the

average gains of the two regions are compared. Average gain was calculated by averaging all 45 points in each region. The region where the beam with higher peak gain is located shows higher average gain than the other region, as expected. Thus, more energy is directed towards the region where the beam with higher peak gain is located for each status.

5.6 Limitation of the Proposed Antenna

Although the beam steering is clearly shown as in Figure 5-14 and Table 5-1, there are some limitations with the proposed antenna. First, a simple beam steering or binary beam steering is possible with the current design. Second, there are nulls in the measured radiation pattern and discrepancies with the simulated radiation pattern. The nulls and the discrepancy are considered to be from wires that are connected to the antenna and poor diode performance, i.e., the OFF status of the diode is not completely OFF. Last, thus the antenna beam steering performance is dependent on the diode performance. These limitations need to be further investigated in both simulation and measurement.

5.7 Summary

A beam steering, broadband, single patch antenna is simulated, fabricated and measured. The proposed antenna requires no array for beam steering but requires only two additional diodes. This antenna operates from 2.8–4.8 GHz and shows electronic beam steering over that broadband range (sampled at 3, 3.5, 4, and 4.5 GHz). In addition to the horizontal beam steering, vertical beam steering is simulated. The wide frequency tuning range allows the radar system to be tuned for an optimum transmission frequency.

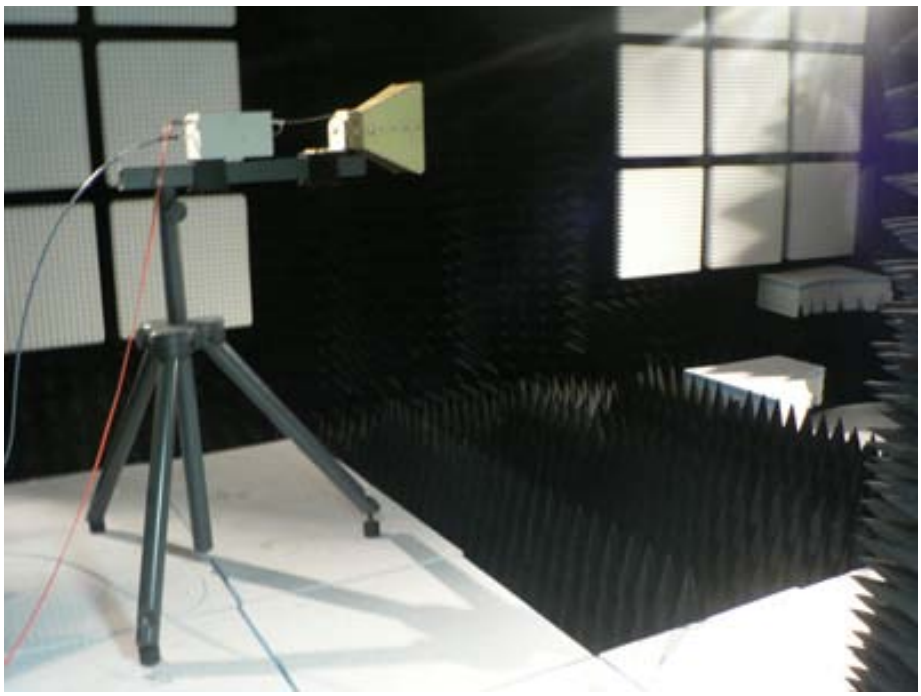

Figure 5-12. Inside of an anechoic chamber for the radiation pattern measurement shows standard gain antenna

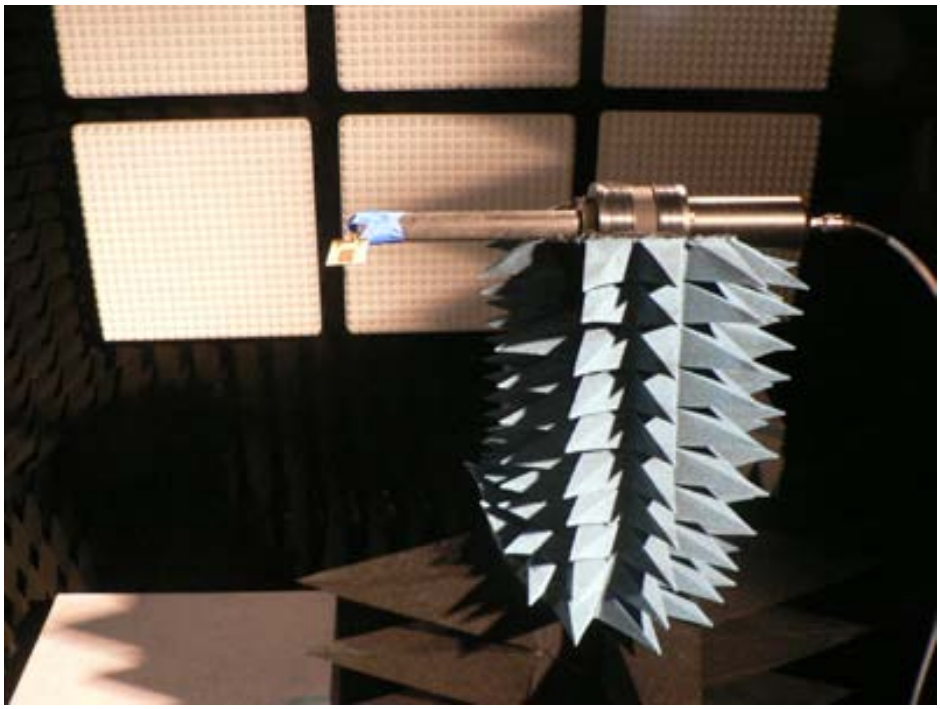

Figure 5-13. One of the ways of how the AUT was mounted.

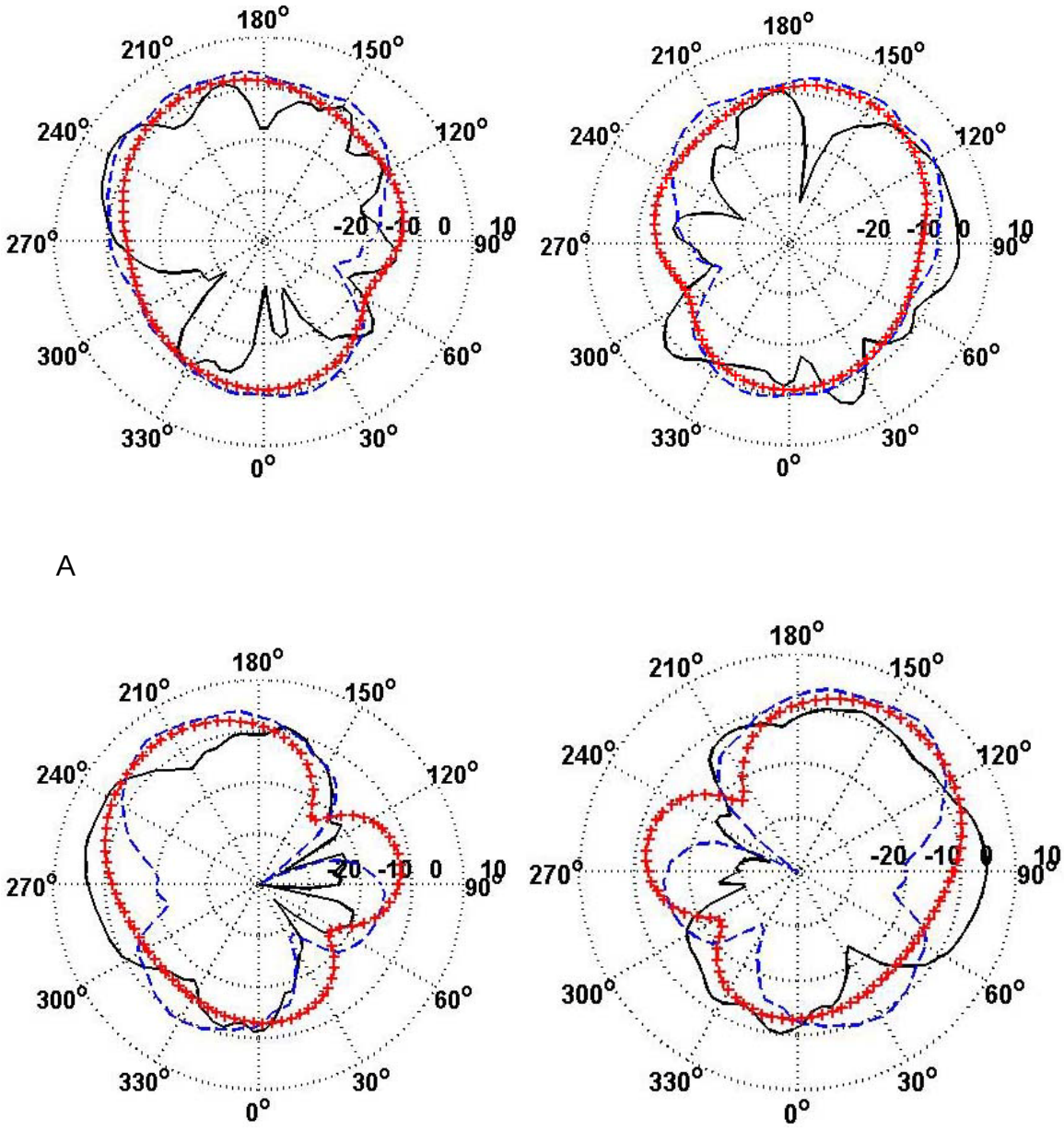

A

B

Figure 5-14. Comparison of measured radiation patterns of the proposed antenna, and reference antenna, and simulated radiation patterns of the proposed antenna (Solid black: measured proposed; Dashed blue: measured reference; ++ red: simulated reference) along Theta = 90 degree plane (X-Y plane). Radiation patterns at frequencies of (A) 3 GHz, (B) 3.5 GHz (C) 4 GHz, and (D) 4.5GHz are plotted. Left column is when the pair of diodes is in OFF-ON state. Right column is when the pair of diodes is in ON-OFF state. Antenna configuration with XYZ axes is shown in (E).

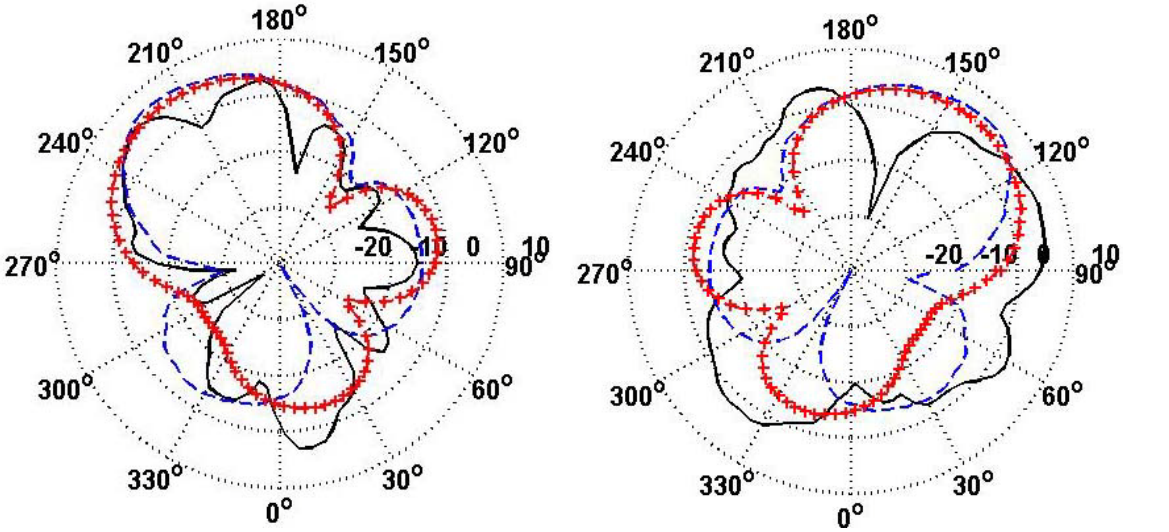

C

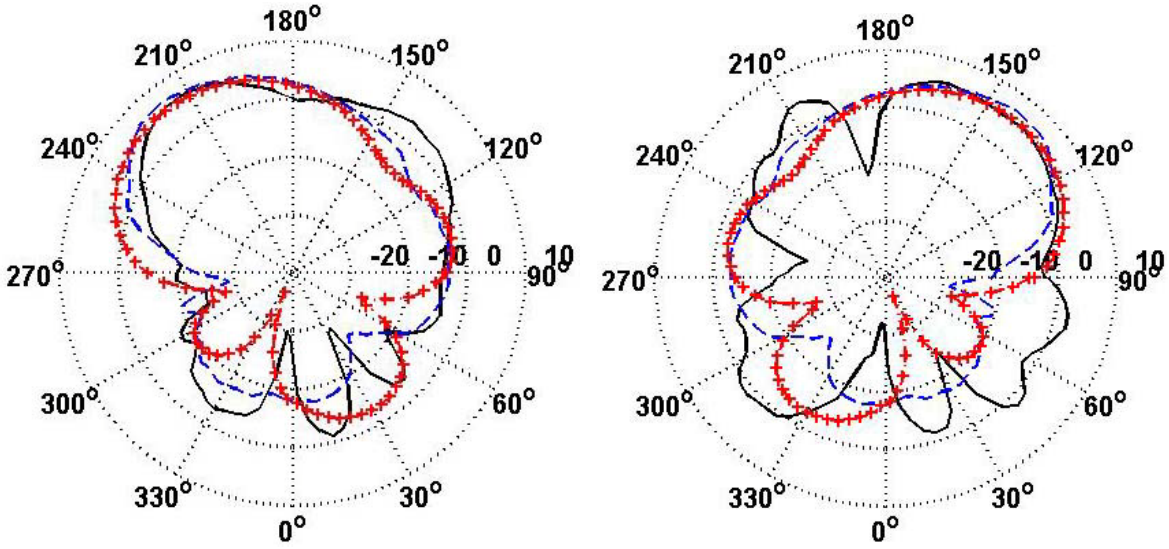

D

Figure 5-14. Continued

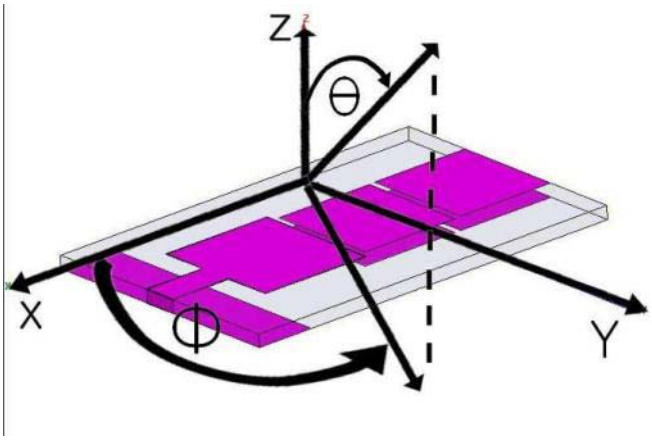

E

Figure 5-14. Continued

CHAPTER 6
SUMMARY

The non-contact vital sign radar detection system necessitated the development of the broadband, high gain antenna. The proposed design approach combines the advantage of the wideband antenna, the advantage of the parasitic patch for high gain, and the advantage of beam steering antennas within a single microstrip patch antenna. The proposed antenna requires no array for beam steering but requires only two additional diodes.

The broadband directional microstrip antenna was simulated, fabricated and measured. The partial ground plane improves broadband characteristics and the parasitic patches improve the gain. As a result, a 4.3–7 GHz broadband antenna with improved gain was designed and fabricated. Compared to a partial-ground-plane, single-patch, reference antenna, this broadband directional microstrip antenna shows desired directivity and improved gain performance. Its radiation pattern was designed for a vital sign radar detector mounted on the ceiling at corner locations. The radiation pattern also provides a better isolation between the transmitting and receiving antennas for this application. The design approach ensures that broadband performance can be achieved while improving the gain of the antenna.

In addition, effects of modifying the broadband directional microstrip antenna on the antenna characteristics such as reflection coefficient, radiation pattern, gain, or beam steering capability are investigated. The modification can include varying the width and/or length of the partial ground plane, adding stub(s) on the partial ground plane, varying the width, length, and/or location of the added stub, or varying the number, shape, gap, or location of the directors. It is important to evaluate the effects of

the modification on the antenna characteristics, since these effects may be exploited to improve the antenna performance.

Stub shape can affect s11 substantially, most of time it negatively affects the broadband characteristics. Beam pattern does not change substantially even though the stub shape is changed substantially. Most of the OFF/ON combination of the both stubs show beam steering, that is, the beam is away from the ON status stub. Even the ON stub connection is reduced, the current flowing through that connection is still stronger than the current flowing to OFF status stub through coupling. When the stub is modified greatly, the beam steering pattern can be inconsistent. In addition to horizontal beam steering using stubs, parasitic patches can be also used to steer beam horizontally. The advantage of the beam steering using the parasitic patch, instead of stub is that the parasitic patch does not affect the s11 significantly as stubs do. The disadvantage of beam steering using parasitic patch is that the beam steering is relatively weaker than the beam steering using stubs and the switching might be difficult to implement.

Different approaches were made for switching the antenna. Non-RF diode, non-surface mount type RF diode were tested on the fabricated antenna. Rough radiation pattern measurement was performed for a quick radiation pattern measurement after each s11 measurement before actual radiation pattern measurement in anechoic chamber. Mechanical switches such as relay were tested and the result was satisfactory but it is not suitable for this application. RF switch was tested but it didn't yield satisfactory results. Finally, when the surface mount type RF diode is used with patterned trace layer along with the applied reverse voltage to the OFF status diode, measurement data that resembles the simulation data are obtained.

Finally, a beam steering over broadband range is achieved with a single microstrip antenna. Specifically, a 2.8–4.8 GHz beam steering broadband microstrip antenna was designed, fabricated, and measured. Compared to the broadband directional microstrip antenna without stubs, the proposed broadband antenna shows lower broadband operating frequency, beam steering, and improved gain through the beam steering. The proposed antenna can steer beam in broadband range (sampled at 3, 3.5, 4, and 4.5 GHz) by switching PIN diodes that connect stubs and a partial ground plane. Its broadband beam steering is suitable for a vital sign radar application and applications where simple beam steering patterns are desired. The wide frequency tuning range allows the radar system to be tuned for an optimum transmission frequency. This antenna can be implemented in a radar sensor, which can be used for non-contact vital sign detection for security or healthcare applications.

LIST OF REFERENCES

[Li1] C. Li, “Doppler Phase Modulation Effect For Non-Contact Accurate Measurement Of Vital Signs And Other Periodic Movements,” Oral Proposal, 2008

[Balanis] C.A. Balanis, “Antenna Theory: Analysis and Design,” John Wiley & Sons, Inc., 1997, 2nd Edition, pp. 811-812

[Choi1] S. H. Choi, J. K. Park, S. K. Kim, and J. Y. Park, “A new ultra-wideband antenna for UWB applications,” Microwave and Optical Technology Letters, vol. 40, issue 5, pp. 399-401, Mar. 2004

[Choi2] J. Choi, K. Chung, and Y. Roh, “Parametric analysis of a band-rejection antenna for UWB application,” Microwave and Optical Technology Letters, vol. 47, issue 3, pp. 287-290, Nov. 2005

[Curto] S. Curto, M John, and M. Ammann, “Groundplane Dependent Performance of Printed Antenna for MB-OFDM-UWB,” Vehicular Technology Conference, pp. 352-356, April 2007

[Pozar1] Pozar, D.M, “Beam Transmission Of Ultra Short Waves: An Introduction To The Classic Paper By H. Yagi,” Proceedings of the IEEE, Volume 85, Issue 11, pp. 1857-1863, Nov. 1997

[Huang1] J. Huang, “Planar microstrip Yagi array antenna,” 1989 IEEE Antennas and Propagation Society International Symposium Digest, vol. 2, pp. 894-897, June 1989

[Huang2] J. Huang and A.C. Densmore, “Microstrip Yagi array antenna for mobile satellite vehicle application,” IEEE Transactions on Antennas and Propagation, vol. 39, issue 7, pp. 1024–1030, July 1991

[Kumar] G. Kumar, and K. C. Gupta, “Nonradiating edges and four edges gap-coupled multiple resonator broad-band microstrip antennas,” IEEE Transactions on Antennas and Propagation, vol. 33, issue 2, pp. 173 – 178, Feb. 1985

[Li2] C. Li and J. Lin, "Complex Signal Demodulation and Random Body Movement Cancellation Techniques for Non-contact Vital Sign Detection," IEEE MTT-S International Microwave Symposium Digest, pp. 567-570, Atlanta, June 2008

[Fusco] Fusco, V.F, “Mechanical beam scanning reflectarray,” IEEE Transactions on Antennas and Propagation, vol. 53, issue 11, pp. 3842 – 3844, Nov. 2005

[Andersson] Andersson, M, Goransson, B, Skarin, I, From, K., Cheng, S, Ojefors, E,Hallbjorner, P, Manholm, L,Rydberg, A, “Antennas with Fast Beam Steering for High Spectral Efficiency in Broadband Cellular Systems,” The 9th European Conference on Wireless Technology, pp. 12-15, Sep. 2006

[Rodenbeck] M. Li, Rodenbeck, C.T, Kai Chang, “Millimeter-wave dual-beam scanning microstrip patch antenna arrays fed by dielectric image lines,” IEEE Antennas and Propagation Society International Symposium, vol. 2, pp. 196 – 199, June 2002

[Preston] Preston, S.L, Thiel, D.V, Lu, J.W, O'Keefe, S.G, Bird, T.S, “Electronic beam steering using switched parasitic patch elements,” Electronics Letters, vol. 33, issue 1, pp. 7-8, Jan. 1997

[Yusuf1] Yusuf, Y, Xun Gong, “A Low-Cost Patch Antenna Phased Array With Analog Beam Steering Using Mutual Coupling and Reactive Loading,” Antennas and Wireless Propagation Letters, IEEE, vol. 7, pp. 81 – 84, 2008

[Yusuf2] Yusuf, Y, Xun Gong, “Beam-steerable patch antenna array using parasitic coupling and reactive loading,” Antennas and Propagation International Symposium, IEEE, pp. 4693-4696, June 2007

[Shynu] Shynu S. V, Gijo Augustin, C. K. Aanandan, P. Mohanan, K. Vasudevan, “A reconfigurable dual-frequency slot-loaded microstrip antenna controlled by pin diodes,” Microwave and Optical Technology Letters, vol. 44, issue 4, pp. 374-376, Feb. 2005

[Byun] S. B. Byun, J. A. Lee, J. H. Lim, T. Y. Yun, “Reconfigurable Ground-Slotted Patch Antenna Using PIN Diode Switching,” ETRI Journal, vol. 29, no. 6, pp. 832-834, Dec. 2007

[Lee] J. A. Lee, S. B. Byun, J. H. Lim, T. Y. Yun, “Reconfigurable antenna for wideband code division multiple access and Korean satellite digital multimedia broadcasting controlled by pin-diodes,” Microwave and Optical Technology Letters, vol. 49, issue 6, pp. 1334-1337, June 2007

[Nikolaou] Symeon Nikolaou, Bairavasubramanian, R, Lugo, C., Jr, Carrasquillo, I, Thompson, D.C, Ponchak, G.E, Papapolymerou, J, Tentzeris, M.M, “Pattern and frequency reconfigurable annular slot antenna using PIN diodes,” IEEE Transactions on Antennas and Propagation, vol. 54, issue 2, Part 1, pp. 439-448, Feb. 2006

[Mookiah] Mookiah, P, Piazza, D, Dandekar, K.R, “Reconfigurable spiral antenna array for pattern diversity in wideband MIMO communication systems,” Antennas and Propagation Society International Symposium, AP-S 2008. IEEE, pp. 1-4, July 2008

[Caverly] Caverly, R.H, Hoorfar, A, “Reconfigurable Hilbert antennas using high speed pin codes,” Radio and Wireless Symposium, 2009. pp. 151 – 154, Jan. 2009

[Derneryd] Derneryd, A, “A theoretical investigation of the rectangular microstrip antenna element,” IEEE Transactions on Antennas and Propagation, vol. 26, issue 4, pp. 532 – 535, July 1978

[Pozar2] Pozar, D, “Input impedance and mutual coupling of rectangular microstrip antennas,” IEEE Transactions on Antennas and Propagation, vol. 30, issue 6, pp. 1191 – 1196, Nov. 1982

[Covert] Covert, L.; Lin, J, “Simulation and measurement of a heatsink antenna: a dual-function structure,” IEEE Transactions on Antennas and Propagation, vol. 54, issue 4, pp. 1342 – 1349, Apr. 2006

[Park] Zivin Park, Changzhi Li, Jenshan Lin, “A Broadband Microstrip Antenna with Improved Gain for Non-Contact Vital Sign Radar Detection,” IEEE ANTENNAS AND WIRELESS PROPAGATION LETTERS Volume 8, pp. 939 – 942, 2009

BIOGRAPHICAL SKETCH

Zivin Park received his B.S. degree in electrical engineering from Seoul National University, Seoul, South Korea, in 1998. After graduation, he worked as a senior software engineer at Trigemm Infocomm in Seoul until 2001, developing voice response system for major telecommunication companies, banks, government in South Korea using Unix C Programming. He received his M.S. degree in electrical and computer engineering from University of Florida, Gainesville, FL, in 2003. His research topic was Fabrication and Characterization of Transparent ZnO Thin Film Transistor. He also researched on Deep Level Transient Spectroscopy (DLTS) on CIGS Solar Cell. He passed U.S. Patent Bar Exam in Dec. 2006 (Reg. No. 62851) and worked as a registered U.S. patent agent for a Intellectual Property law firm from 2006 to 2009, handling patent prosecutions in Electronics area. He received his Ph.D. degree in electrical and computer engineering from University of Florida, Gainesville, FL, in 2011. His doctorate research topic was designing patch antenna for non-contact Vital Sign Radar Detection, especially a Beam Steering Broadband Microstrip Antenna. His ZnO TFT research is published on Applied Physics Letter as a second author and his antenna research is published on IEEE Antennas and Wireless Propagation Letters as a first author twice.